The Dissertation Committee for Laura Paul Starkston
certifies that this is the approved version of the following dissertation:

Classifications and Applications of Symplectic Fillings of Seifert Fibered Spaces over S^2

Committee:

Robert E. Gompf, Supervisor

John Etnyre

Cameron Gordon

Çağrı Karakurt

John Luecke

Timothy Perutz

Classifications and Applications of Symplectic Fillings of Seifert Fibered Spaces over S^2

by

Laura Paul Starkston, B.A.

DISSERTATION

Presented to the Faculty of the Graduate School of

The University of Texas at Austin

in Partial Fulfillment

of the Requirements

for the Degree of

DOCTOR OF PHILOSOPHY

THE UNIVERSITY OF TEXAS AT AUSTIN

May 2015

Classifications and Applications of Symplectic Fillings of Seifert Fibered Spaces over S^2

Publication No. _____

Laura Paul Starkston, Ph.D.
The University of Texas at Austin, 2015

Supervisor: Robert E. Gompf

This dissertation focuses on classifications and examples of symplectic fillings of Seifert fibered spaces over S^2 with a canonical contact structure. Broad results are obtained describing how such fillings arise. In large families of examples, explicit and complete classifications are given. Examples of such fillings can be used to produce symplectic cut-and-paste operations. These operations are strict generalizations of the rational blow-down operations, and their relations to the rational blow-down are discussed. Reinterpretations of these cut-and-paste operations as monodromy substitutions are also explored.

Table of Contents

List of Figures

Chapter 1

Introduction

Symplectic forms provide additional geometric structure on a smooth manifold, while maintaining a reasonable level of flexibility to allow for topological cut and paste constructions. In certain cases, pseudoholomorphic curve tools can be used in symplectic manifolds (with or without boundary) to identify aspects of its topology, based on only a small amount of information about the submanifolds (e.g. [Eli90a], [Gro85], [McD90], [McD91]). In dimension four, we obtain particularly strong results, and the symplectic structure has key implications about the smooth structure. Therefore, symplectic manifolds make up an important subclass of all smooth manifolds.

To construct interesting examples of symplectic manifolds, one would like to be able to use a large range of cut-and-paste operations from the topologist's tool kit. Fortunately, many such operations can be performed, though care must be taken to ensure that the symplectic structures match up nicely along the pasting region. One way to ensure this, is to require one piece to have convex boundary and the other to have concave boundary (see section 2.1 for definitions). Then, if the contact manifolds on the two boundaries are contactomorphic, the pieces can be glued together to form a closed symplectic manifold.

There is a significant amount of work studying when there exists a symplectic 4-manifold with convex or concave boundary which is a particular contact manifold. It was

shown [EH02a], [Gay02], [AO02], and [Eli04] that all contact manifolds appear as the *concave* boundary of many different symplectic manifolds exhibiting a variety of topological properties. On the other hand, *convex fillings* are more rare, and in certain cases there are no symplectic manifolds inducing a given contact manifold convexly on its boundary: first shown for overtwisted contact structures by Eliashberg and Gromov [Eli90a] and later for tight examples by Etnyre and Honda [EH02b]. Results were completely established on the *existence* of a convex symplectic manifold whose boundary is a relatively simple manifold like S^3, a lens space, or a Seifert fibered space [Gom98], [LL11].

Stronger results on *classifications* of convex symplectic fillings of a given contact 3-manifold were only established for contact structures on S^3 [Eli90a], a particular canonical contact structure on lens spaces $L(p,q)$ [Lis08], all contact structures on the lens spaces $L(p,1)$ [PVHM10], and links of simple singularities [OO05]. The primary goal of this thesis is to explore the convex symplectic fillings of Seifert fibered spaces over S^2 with a canonical contact structure. A few additional results on classifications of symplectic fillings appeared during the preparation of this work (see [KL13], [Kal13], and [GL14]).

One particularly nice property of the canonical contact structures on Seifert fibered spaces is that they appear as the convex boundary of one standard filling, which is simply a small neighborhood of transversely intersecting symplectic surfaces (see section 2.2). Any two convex symplectic fillings of the same contact boundary look the same in a collared neighborhood of the boundary. Therefore if one of these fillings is found in a closed symplectic manifold, it can be exchanged for the other filling to create a new closed symplectic manifold. We can easily identify a standard convex filling of the contact manifolds of interest by finding the correct configuration of transversally intersecting symplectic surfaces. For

each alternate symplectic filling, we can build a potentially new closed symplectic 4-manifold by exchanging the neighborhood of surfaces with the alternate filling. The Seiberg-Witten invariants of the original closed manifold can be related to those of the newly constructed manifold, so properties of the smooth structure can be identified. Such constructions, resulting in exotic copies of $\mathbb{C}\mathrm{P}^2 \# N\,\overline{\mathbb{C}\mathrm{P}^2}$ for $N = 6, 7, 8$ were given by Karakurt and the author in [KS]. These constructions are modeled after the rational blow-down operation of Fintushel and Stern [FS97], which replaces a neighborhood of symplectic spheres with a lens space boundary, with an alternate symplectic filling which is a rational homology ball. This operation was generalized in [Par97] and [SSW08], and its formulation as a symplectic operation was established by Symington [Sym98], [Sym01].

A key property of Seifert fibered manifolds over S^2 with their canonical contact structures is that they are supported by *planar open book decompositions* (see section 2.3). This ensures that every convex symplectic filling is supported by a Lefschetz fibration filling the given open book decomposition (due to a theorem of Wendl [Wen10], see section 2.4). Each of these Lefschetz fibrations can be equivalently interpreted as a different factorization of the monodromy of the open book decomposition into positive Dehn twists. This monodromy substitution interpretation is often very practical for cut and paste applications of symplectic fillings.

The main ideas this thesis will present are as follows. Chapter 2 discusses the background definitions and theorems needed to set up the main problem. Chapter 3 proves the most general results about classifications of symplectic fillings of Seifert fibered spaces, using a generalization of the techniques used by Lisca for lens spaces [Lis08]. Chapter 4 gives explicit complete classifications for large families of examples. Chapter 5 explains certain

similarities and distinctions between rational blow-down operations and the cut-and-paste operations resulting from these new examples of symplectic fillings of Seifert fibered spaces. Chapter 6 explains how to translate the classifications obtained by the techniques of section 3 to monodromy substitutions.

Chapter 2

Background

2.1 Symplectic fillings

In this section, we will review the basic definitions of symplectic and contact manifolds, and discuss various types of symplectic fillings. The type of fillings which this thesis will focus on are minimal strong symplectic fillings.

Symplectic fillings are a particular case of symplectic manifolds with boundary. The *symplectic structure* on a manifold X (possibly with boundary) is a 2-form $\omega \in \Omega^2(X)$ which is non-degenerate (meaning for each $p \in X$ and each non-zero $V \in T_p(X)$ there exists $W \in T_p(X)$ such that $\omega_p(V, W) \neq 0$) and closed (meaning $d\omega = 0$). The standard example is when $X = \mathbb{R}^{2n}$ and $\omega = \sum_i dx_i \wedge dy_i$. Symplectic manifolds are necessarily even dimensional, because of the non-degeneracy condition. The odd dimensional counterparts of symplectic manifolds are contact manifolds.

A co-orientable *contact structure* on a $2n+1$ dimensional manifold Y is a hyperplane distribution ξ defined as the kernel of a 1-form $\alpha \in \Omega^1(Y)$ such that $d\alpha$ is non-degenerate on the hyperplane field $\xi := \ker \alpha$. Equivalently, $\alpha \wedge (d\alpha)^n \neq 0$. The 1-form α is called the contact form. The different choices of contact forms for a given contact structure differ by multiplication by positive functions. In dimension 3, ξ is a 2-dimensional plane field, and the condition $\alpha \wedge d\alpha \neq 0$ can be understood as a non-integrability condition on the hyperplanes

ξ: any surface which is tangent to ξ at a single point has tangency of degree one. Therefore no open subset of a surface has all of its tangent planes given by the contact planes.

For each contact structure, there is a unique *Reeb vector field*, R_α such that $\alpha(R) \equiv 1$ and $d\alpha(R, \cdot) \equiv 0$. The Reeb vector field depends on the 1-form α instead of on the contact structure $\xi = \ker(\alpha)$, but it exists for any contact form.

One reason contact and symplectic topology are often studied together is because contact manifolds give rise to symplectic manifolds and can appear as hypersurfaces in symplectic manifolds. This idea and the relations between symplectic and contact structures originated with Weinstein in [Wei79]. Further exposition is in [ABK$^+$94] and [Etn98], but we include the essential definitions and properties here.

Definition 2.1.1. The *symplectization* of a contact manifold $(Y, \xi = \ker(\alpha))$ is a symplectic manifold $(Y \times \mathbb{R}, \omega = d(e^t\alpha))$.

The form $d(e^t\alpha) = e^t(dt \wedge \alpha + d\alpha)$ is non-degenerate on $Y \times \mathbb{R}$ because the vectors in ξ pair non-degenerately in the $d\alpha$ piece, and ∂_t pairs positively with the Reeb vector field. It is closed since it is exact. This verifies that the symplectization is indeed a symplectic manifold. An important property of the symplectization is that it satisfies the following differential equation

$$\mathcal{L}_{\partial_t}\omega = \omega$$

where $\mathcal{L}$ denotes the Lie derivative. This follows from Cartan's formula $\mathcal{L}_V = d \circ \iota_V + \iota_V \circ d$ because

$$d \circ \iota_{\partial_t}(d(e^t\alpha)) + \iota_{\partial_t} \circ d(d(e^t\alpha)) = d \circ \iota_{\partial_t}(e^t(dt \wedge \alpha + d\alpha)) = d(e^t\alpha).$$

Vector fields V for which $\mathcal{L}_V\omega = \omega$ are called *Liouville vector fields*. These are often only defined over an open portion of a symplectic manifold, particularly in a neighborhood of a hypersurface. Note that the symplectic form is expanding as one flows along a Liouville vector field because ω is positively non-degenerate. In the symplectization we see this: as t increases, the form $d(e^t\alpha) = e^t(dt\wedge\alpha + d\alpha)$ scales exponentially by the constant e^t. Liouville vector fields are useful for identifying contact hypersurfaces in a symplectic manifold as shown in the following lemma.

Lemma 2.1.2. *Let (X,ω) be a $2n$ dimensional symplectic manifold and Y a hypersurface in X. Let V be a Liouville vector field defined in a neighborhood of Y and everywhere transverse to Y. Let $i : Y \to X$ be the inclusion map. Then $\alpha := i^*\iota_V\omega$ is a contact form on Y.*

Proof. We want to show $\alpha \wedge (d\alpha)^{n-1} \neq 0$.

Since V is a Liouville vector field $\mathcal{L}_V\omega = \omega$ so $(d\circ\iota_V + \iota_V\circ d)\omega = \omega$. Since ω is closed, this implies $d(\iota_V\omega) = \omega$. Therefore $d\alpha = i^*\omega$.

Since ω is non-degenerate and Y has co-dimension one, $d\alpha = i^*\omega$ has one dimensional kernel, generated by a vector field R. First we will show $\omega(V,R) \neq 0$. By definition of R, $\omega(U,R) = 0$ for every vector field U in TY. Since V is everywhere transverse to Y, every vector field on i^*TX can be written as $cV+U$ for some $U \in TY$. If we had $\omega(V,R) = 0$ at any point, ω would fail to be non-degenerate. Because $\omega(V,R) \neq 0$, R is not in $\ker\alpha = \ker(i^*\iota_V\omega)$ so it is transverse to $\xi := \ker\alpha$.

Next we show, $d\alpha$ is non-degenerate on ξ. A basis for ξ, together with R and V make up a frame for TX. By the non-degeneracy of ω we know that for every $p \in Y$ and $U_p \in \xi_p$,

there exist scalars c, d and a vector $U_p' \in \xi_p$ such that $\omega_p(U_p, U_p' + cV_p + dR_p) \neq 0$. However,

$$\omega_p(U_p, V_p) = -\iota_V \omega_p(U_p) = \alpha_p(U_p) = 0$$

since $\xi = \ker \alpha$. Furthermore

$$\omega_p(U_p, R_p) = i^*\omega_p(U_p, R_p) = d\alpha_p(U_p, R_p) = 0$$

since $R \in \ker(d\alpha)$. Therefore

$$d\alpha_p(U_p, U_p') = \omega_p(U_p, U_p') \neq 0.$$

□

Such a hypersurface Y is called a submanifold of *contact type*. The contact structure $\xi = \ker(\alpha)$ is called the *induced contact structure on* Y. Assuming everything is orientable, any two Liouville vector fields V and V' transverse to Y induce isotopic contact structures.

Lemma 2.1.3. *Suppose V and V' are Liouville vector fields which are both positively transverse to an oriented hypersurface Y. Let $\xi = \ker(i^*\iota_V\omega)$ and $\xi' = \ker(i^*\iota_{V'}\omega)$. Then ξ and ξ' are isotopic through contact structures.*

Note that by *Gray's theorem*, if there is a 1-parameter family of contact structures ξ_t, $0 \leq t \leq 1$ on a compact manifold M then the isotopy can be realized ambiently: namely there is a family of diffeomorphisms $\phi_t : M \to M$ such that $\phi_t^*(\xi_t) = \xi_0$. Therefore this isotopy of contact structures is in fact equivalent to an ambient isotopy of contact manifolds.

Proof. The vector field $V_t = (1-t)V + tV'$ is transverse to Y for all $0 \leq t \leq 1$. V_t is Liouville since $\mathcal{L}_{V_t}\omega = \mathcal{L}_{(1-t)V+tV'}\omega = (1-t)\mathcal{L}_V\omega + t\mathcal{L}_{V'}\omega = (1-t)\omega + t\omega = \omega$. Therefore $\alpha_t = i^*\iota_{V_t}\omega$ is a contact form for all $0 \leq t \leq 1$ interpolating between contact forms for ξ and ξ'. □

In fact, a neighborhood of a compact contact hypersurface is completely determined by the contact structure. The existence of the Liouville vector field allows us to identify this neighborhood with a neighborhood of the 0-section of the symplectization.

Lemma 2.1.4. *Suppose Y is a compact contact hypersurface in a symplectic manifold (X, ω) with a transverse Liouville vector field V inducing the contact form $\alpha = i^* \iota_V \omega$. Then there is a neighborhood of Y which is symplectomorphic to a neighborhood of $Y \times \{0\}$ in the symplectization of $(Y, \xi = \ker(\alpha))$, and the symplectomorphism restricts to the identity on Y.*

The idea is to match up the flow of the Liouville vector field with the $\mathbb{R}$ direction in the symplectization, and then isotope the symplectic structure along the contact hypersurface so that it matches that in the symplectization by lining up the Reeb vector fields in each. See [Etn98] for more details. Then the result follows from the following fundamental theorem in symplectic topology.

Theorem 2.1.5 (Moser-Weinstein)**.** *Let $N \subset M$ be a smooth compact submanifold. Let ω_0 and ω_1 be symplectic forms on M which agree on $TM|_N$. Then there exists a diffeomorphism $f : M \to M$ isotopic to the identity and fixing N pointwise such that $f^*\omega_1 = \omega_0$ in a neighborhood of N.*

When Y is the boundary of a symplectic manifold (X, ω), it can similarly appear as a hypersurface of contact type, but now it has a collared neighborhood which can be identified with a neighborhood of the 0-section in the half of the symplectization where $t \geq 0$ or $t \leq 0$. To determine which half, we need to consider the distinguished orientation Y inherits as

the boundary of X and comparing the outward normal to the direction of the transverse Liouville vector field. When the boundary looks like the the boundary of the half where $t \leq 0$ (the Liouville vector field points outward), we say the boundary is convex. When instead it looks like the boundary of the half of the symplectization where $t \geq 0$, we say the boundary is concave.

Definition 2.1.6. A symplectic manifold (W, ω) with boundary ∂W is a *strong symplectic filling* or *convex symplectic filling* of $(\partial W, \xi)$ if there is a Liouville vector field V defined in a neighborhood of ∂W which is everywhere transverse to ∂W and points outward such that $\xi = \ker(i^* \iota_V \omega)$. In this case we say (W, ω) has *convex boundary*.

Definition 2.1.7. A symplectic manifold (W', ω') with boundary $\partial W'$ has *concave boundary* if there is a Liouville vector field defined in a neighborhood of $\partial W'$ which is everywhere transverse to $\partial W'$ and points inward along the boundary. Such manifolds with concave boundary are often called *concave caps*.

The key property of symplectic manifolds with convex and concave boundary is that they can be glued together.

Theorem 2.1.8. *Suppose (M_i, ω_i) for $i = 1, 2$ are symplectic manifolds with compact boundary N_i, such that N_1 is convex and N_2 is concave. Let ξ_i denote the induced contact structures. If there is a contactomorphism $f : (N_1, \xi_1) \to (N_2, \xi_2)$ $f^* \xi_2 = \xi_1$, then $M_1 \cup_f M_2$ admits a symplectic structure.*

Moreover, sufficiently far away from the gluing area, the symplectic forms on the glued manifold agree with the original ω_i up to possible rescaling by a constant. The complete

proof of this theorem is in [Etn98], though the result was understood earlier by experts working on more specific gluings. The idea is to match up collared neighborhoods of the boundary inside the symplectizations. The only hitch is that the product structure on the symplectization and the position of the 0-section depends on the *contact form* α defined by the symplectic form and Liouville vector field, not just the *contact structure* ξ. The contactomorphism identifies the contact structures so the contact forms on the two pieces are related by a positive scalar function. We can identify a neighborhood of N_1 in M_1 with the lower half of a neighborhood of the 0-section of its symplectization as defined by its contact form α_1. We can then compare α_1 to the corresponding contact form α_2 on the other piece, and after possibly rescaling all of M_2, we can assume $\alpha_2 = g\alpha_1$ with $g > 1$. Then the collared neighborhood of (N_2, α_2) can be identified as a subset of $\{(t, y) \in \mathbb{R} \times Y : t \geq \log(g(y))\}$ in the symplectization defined by α_1. This places the concave piece strictly above the convex piece so they can be glued together along with the intermediate space in the symplectization: $\{(t, y) \in \mathbb{R} \times Y : 0 \leq t \leq \log(g(y))\}$.

While symplectic manifolds with convex boundary appear to be defined in a symmetric way to those with concave boundary, the reality is that manifolds with concave boundaries appear more often than convex boundaries. For example, every contact 3-manifold arises as the concave boundary of some symplectic 4-manifold, but not every contact 3-manifold has a convex symplectic filling. Moreover, the concave caps of a given contact 3-manifold often have significantly fewer topological restrictions than the convex fillings do. This makes classifying convex fillings both more manageable and more interesting than classifying concave caps. Moreover, convex fillings are related to other notions of fillings from complex and symplectic geometry as discussed in the following subsection.

2.1.1 Stronger and weaker versions of symplectic fillings

Notice that wherever a Liouville vector field is defined, the symplectic form is necessarily exact since $\omega = \mathcal{L}_V \omega = d(\iota_V \omega)$. A symplectic filling where the Liouville vector field extends over the entire manifold (W, ω) is called an *exact filling*. Obviously an exact filling is a strong symplectic filling, but the converse is not always true [Ghi05]. A stronger notion of filling is related to a type of complex manifold.

Definition 2.1.9. A *Stein manifold* is a properly embedded complex submanifold of some $(\mathbb{C}^N, i)$.

The relationship between Stein and symplectic manifolds is not immediately obvious. To see this, consider the radial function squared $\phi_0(z) = |z|^2$ on $\mathbb{C}^N$. It yields a symplectic form $\omega = -dd^{\mathbb{C}}\phi_0$ where $d^{\mathbb{C}}\phi_0(V) = d\phi(iV)$. Any function ϕ such that $-dd^{\mathbb{C}}\phi$ is symplectic where $d^{\mathbb{C}}\phi = d\phi \circ J$, is called strictly plurisubharmonic or J-convex. Grauert [Gra58] found that an equivalent definition for a Stein manifold is a complex manifold (X, J) which admits an exhausting (proper and bounded below) J-convex function.

Definition 2.1.10. Let (Y, ξ) be a contact manifold. A *Stein filling* of (Y, ξ) is a compact manifold W with boundary Y, such that there exists a Stein manifold (X, J) with an exhausting J-convex function ϕ such that $W = \phi^{-1}((-\infty, C])$ for some constant C, and $\xi = T(\partial W) \cap J(T(\partial W))$.

The natural symplectic form on a Stein filling is given by $\omega_\phi = -dd^{\mathbb{C}}\phi$ which is clearly exact and the gradient vector field for ϕ is Liouville and transverse to the boundary. Examples of exactly fillable contact manifolds which are not Stein fillable were discovered by Bowden [Bow12].

A weaker notion of symplectic fillings is simple to define when (W, ω) is a symplectic 4-manifold and $(\partial W, \xi)$ is a contact 3-manifold. In this case we have the following definition.

Definition 2.1.11. (W^4, ω) is a *weak symplectic filling* of $(\partial W^3, \xi)$ if ω is a positive area form on the contact planes ξ.

Strong symplectic fillings are weak symplectic fillings because for a strong filling, ω restricts to the contact planes as $d\alpha$ which is non-degenerate on ξ. Examples of weak fillings that are not strong symplectic fillings were first given by Eliashberg in [Eli96]. Generalizations of this notion to higher dimensions are discussed in [MNW13].

Remark 2.1.12. For the contact manifolds discussed in this thesis, the notions of weak, strong, exact, and Stein fillings will in fact all coincide (see section 2.4). The term *symplectic filling* will generally refer to a convex (strong) symplectic filling for the remainder of this thesis.

2.2 Seifert fibered spaces

The focus of this study will be on symplectic 4-manifolds with boundary given by a Seifert fibered 3-manifold. These manifolds have nice decompositions and are slight generalizations of circle bundles over surfaces. This section will review some equivalent definitions of Seifert fibered spaces from a topological perspective and discuss how they arise as the boundaries of certain plumbed 4-manifolds.

First, we give a constructive definition.

Definition 2.2.1. A *Seifert fibered space over* Σ (where Σ is a surface) is a 3-manifold obtained from a S^1 bundle over Σ by performing Dehn surgery on finitely many S^1 fibers,

such that none of the Dehn surgeries sends the meridian of the solid torus to the isotopy class of a fiber.

Performing Dehn surgery on a fiber means we cut out a neighborhood of that fiber, which is a solid torus, and reglue the solid torus by a diffeomorphism of the boundary torus. The diffeomorphism type of a manifold resulting from Dehn surgery on a given embedded circle is determined by the homology class the meridian of the solid torus is sent to under the gluing diffeomorphism. A topologically equivalent operation to performing the Dehn surgery is the following. Cut out a neighborhood of the embedded circle fiber and keep track of the rulings on the boundary torus by meridians μ, which bounded disks in the neighborhood we cut out, and longitudes λ specified by the direction of the nearby fibers (in general there is a choice of longitude, and this is a natural choice in this case). Choose a rational slope on the torus which represents the homology class the meridian would be sent to under the gluing map. Instead of gluing the solid torus back in via the gluing map, it is topologically equivalent to collapse each of the curves of the chosen rational slope down to a point. The image of the torus under this quotient corresponds under this equivalence to the core of the solid torus (the centers of the meridional disks). From this alternate perspective one can see that the following more abstract definition of a Seifert fibered space is equivalent to the constructive one.

Definition 2.2.2. A *Seifert fibered space over* Σ is a 3-manifold Y together with a map $\pi : Y \to \Sigma$ such that for every $p \in \Sigma$ there is a neighborhood U of p in Σ such that $\pi|_{\pi^{-1}(U)} : \pi^{-1}(U) \to U$ is diffeomorphic to an α/β solid torus fibration for some $\alpha/\beta \in \mathbb{Q}$.

An *α/β solid torus fibration* $p : S^1 \times D^2 \to D^2$ is a map from the solid torus to the disk, such that the preimage of the center of the disk is the core of the solid torus, and the

preimage of any point with radial coordinate $r > 0$ in D^2 is a curve of slope $\alpha\mu + \beta\lambda$ on the torus $S^1 \times S^1_r$.

Note that the 0 solid torus fibration is the trivial product fibration. The fibers which have an $\alpha/\beta \neq 0$ solid torus fibration are called the singular fibers. There are finitely many such fibers.

Now we will show how to draw surgery diagrams for Seifert fibered spaces. Then we will expand these rational surgery diagrams to integral surgery diagrams for the 3-manifolds, which display them as the boundaries of handlebody descriptions of 4-manifolds. See section 5.3 of [GS99] for excellent exposition on surgery and Kirby diagrams and the relations between them. The rational surgery diagrams can be built directly from definition 2.2.1. Start with the surgery diagram for a circle bundle over a surface as in figure 2.1. Note that by replacing the g pairs of 0-framed unknotted components by dotted circles, this becomes a handlebody diagram for a disk bundle filling the circle bundle. See [GS99] example 4.6.5 and section 6.1 for details. Next to obtain the Seifert fibered space, we want to do Dehn surgery on finitely many S^1 fibers. These fibers can be represented by curves which link once with the large e-framed component as in figure 2.2.

To change the rational surgery diagram of figure 2.2 into an integral surgery diagram, we can change each rationally framed component to an integrally framed component if we attach a chain of unknots with integral framings specified by a continued fraction expansion. If

$$q_i = z_i^1 - \cfrac{1}{z_i^2 - \cfrac{1}{\ddots - \frac{1}{z_i^n}}} \tag{2.2.1}$$

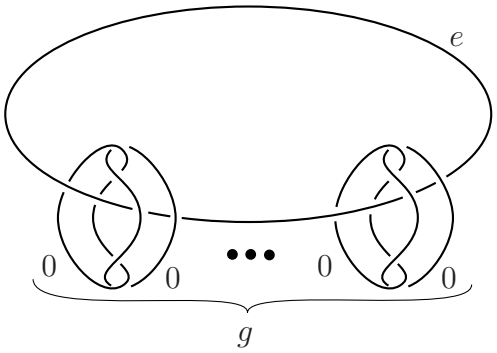

Figure 2.1: Surgery diagram for an S^1-bundle over a genus g surface of Euler number e.

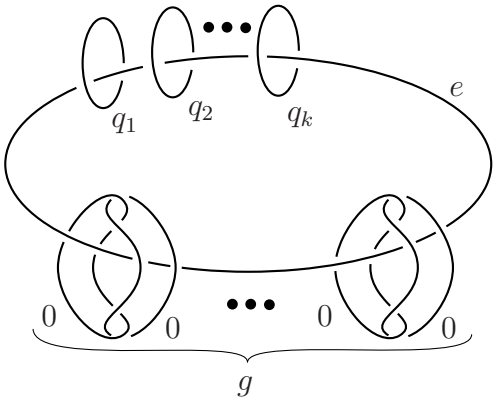

Figure 2.2: Surgery diagram for a Seifert fibered space over a genus g surface. $q_1, \cdots, q_k \in \mathbb{Q}$.

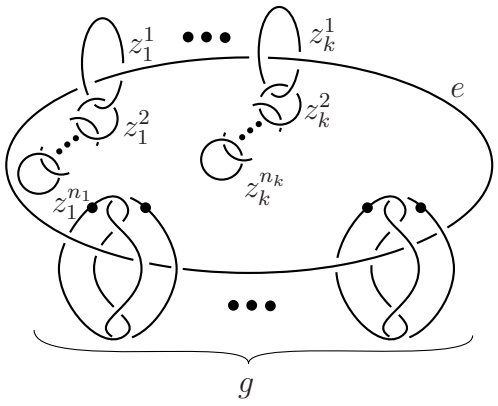

Figure 2.3: Kirby diagram for a plumbing whose boundary is a Seifert fibered space over a genus g surface, where all framings are integers.

then we can replace the q_i framed unknot with a chain of unknots with framings $z_i^1, \cdots, z_i^n \in \mathbb{Z}$ as in figure 2.3. The integral surgery diagram turns into the rational surgery diagram after a sequence of slam-dunks (see [GS99] section 5.3).

By replacing the g pairs of 0-framed circles by dotted circles representing 1-handles, the diagram of figure 2.3 represents a handlebody decomposition of a 4-manifold, which is a plumbing of disk bundles. Plumbings and their Kirby diagrams are explained in great detail in [GS99] sections 4.6.2 and 6.1, but we review the basics we will use here.

Given two disk bundles over surfaces, take a small disk in each surface and consider the trivial bundles over those disks. We can *plumb* the two bundles together by identifying these two trivial bundles over the two subdisks in a way that identifies the fibers of one bundle with the sections of the other and vice versa. The plumbing data is encoded in a marked graph where each vertex represents a disk bundle marked by its genus and Euler number (or just the Euler number if the genus is 0) and each edge corresponds to a plumbing between the bundles corresponding to the adjacent vertices as in figure 2.4.

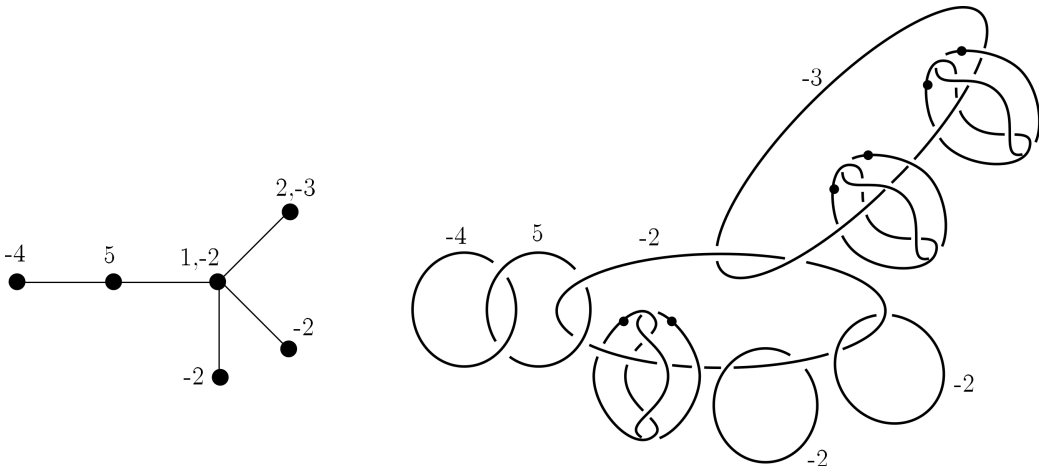

Figure 2.4: Plumbing graph and corresponding Kirby diagram

Disk bundles over spheres have simple handlebody decompositions given by a 0-handle and a 2-handle attached along an unknotted circle where the framing on the 2-handle determines the Euler number of the bundle. Disk bundles over higher genus g surfaces are similar but require $2g$ 1-handles. To get a handlebody for a plumbing of two such disk bundles, attach the 2-handles corresponding to each bundle along the same 0-handle such that the attaching circles link in a Hopf link. When the plumbing graph is a tree it does not matter whether the linking is done positively or negatively, but in general the edges of the graph can be labeled with a $+/-$ sign to specify this data.

The plumbings we will consider have graphs which are star-shaped trees, meaning there is one vertex (the *central vertex*) which can have valence > 2, from which linear arms emanate. When the genera for all bundles except possibly the one corresponding to the central vertex are 0, the boundary of such a plumbing is a Seifert fibered space as indicated in figure 2.3. We will focus on Seifert fibered spaces over S^2, so these bound star-shaped plumbings of disk bundles over spheres.

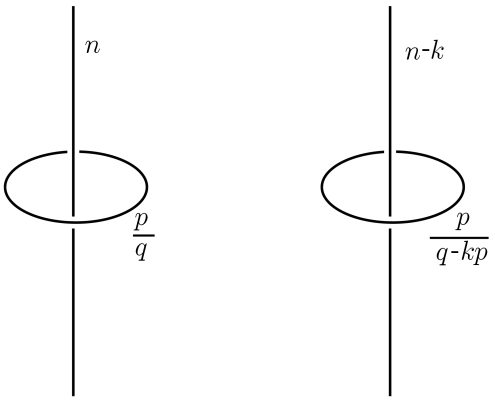

Figure 2.5: Rolfsen twist. $p, q, n, k \in \mathbb{Z}$.

The labeling on the rational surgery diagram depicted in figure 2.2 is not unique for a given Seifert fibered 3-manifold, and thus the corresponding plumbing which bounds the Seifert fibered manifold is not unique either. The ambiguity lies in the fact that we can perform *Rolfsen twists* to the surgery diagram in figure 2.2 along the components contributing the singular fibers. The Rolfsen twist is shown in figure 2.5. However, there is always a way to perform Rolfsen twists so that the rational surgery coefficients are strictly less than -1, and this provides a unique normalized surgery diagram. The values of $e, q_1 = \frac{\alpha_1}{\beta_1}, \cdots, q_k = \frac{\alpha_k}{\beta_k}$ in this normalized form provide the *Seifert invariants* of the space. The value of e in the normalized diagram is often referred to as e_0 and $\alpha_1, \cdots, \alpha_k$ are called the multiplicities of the singular fibers. Each of the rational numbers $q_1, \cdots, q_k < -1$ has a unique continued fraction expansion as in equation 2.2.1 made up of integers that are all at most -2. The plumbing whose Kirby diagram is given by expanding the surgery diagram with these continued fraction expansions will be the standard plumbing filling the Seifert fibered space.

2.3 Open books and Lefschetz fibrations

We would like a more topological way to interpret symplectic fillings of contact manifolds. This is possible for Stein fillings through Lefschetz fibrations.

Definition 2.3.1. A Lefschetz fibration on a compact, oriented 4-manifold X (possibly with boundary and co-dimension two corners) is a surjective smooth map to a compact, oriented surface (possibly with boundary) $f : X \to S$ which is a fiber bundle except around finitely many critical points on the interior. Near these critical points there must be local complex coordinates (z_1, z_2) which orient X such that f is given by $(z_1, z_2) \mapsto z_1^2 + z_2^2$ (the critical point occurs at $(0, 0)$). The co-dimension two corners are formed by the union of the boundary components of the regular fibers in $f^{-1}(\partial S)$, and can be smoothed.

In regular fibers above a small neighborhood of a critical value of a Lefschetz fibration, there is an isotopy class of simple closed curves which collapse to a point in the singular fiber. Such simple closed curves are called the *vanishing cycles* of the Lefschetz fibration. The topology of the 4-manifold is determined by the topology of the fibers, the critical values and their corresponding vanishing cycles.

We will only consider Lefschetz fibrations where the base surface is a disk D^2, and each regular fiber F is a surface with boundary. All such Lefschetz fibrations can be built from 0, 1, and 2-handles, where the 0 and 1 handles are used to build $F \times D^2$ and the 2-handles are attached along unknotted components, each lying in a fiber, and attached with framing -1 relative to the fiber.

Eliashberg proved that Stein fillings are characterized by having handlebody decompositions with certain properties [Eli90b] (expanded upon in dimension 4 by Gompf

[Gom98]). The handlebody decompositions for Lefschetz fibrations with boundary, which were mentioned above, have these properties as long as they are *allowable* (meaning all of the vanishing cycles are homologically essential curves in the fibers) and thus those manifolds support a Stein structure. It was shown in [LP01] and [AO02] that the converse holds: every Stein manifold admits the structure of an allowable Lefschetz fibration.

Now consider the restriction of the Lefschetz fibration structure to the boundary and corners of the manifold $Y = \partial X$. The boundary is made up of two pieces. The first piece comes from looking at the fibers above the boundary circle of the base disk. This is a fibration over the circle whose fibers are the same as the regular fibers of the Lefschetz fibration. The second piece comes from the union of the boundary components of all the fibers. For each boundary S^1 component of F this piece adds in a solid torus $S^1 \times D^2$. The intersection of these two pieces are tori coming from the corners of X. These corners can be smoothed via a standard corner model. The smoothing blurs the precise division between the two pieces, but the decomposition is well defined up to isotopy of the tori. We conclude that the complement of a disjoint union of solid tori in Y is a surface bundle over S^1, and the meridians of the solid tori are glued to sections of the fibration on its boundary. This is precisely the structure of an open book decomposition.

Definition 2.3.2. An *open book decomposition* of a 3-manifold Y is a link $B \subset Y$ and a fibration $\pi : Y \setminus B \to S^1$ whose fibers are Seifert surfaces for B. A fiber $\Sigma = \pi^{-1}(p)$ is called the *page* and the link B is called the *binding*.

The open book decomposition can be recovered from the page Σ and the monodromy ϕ of the fibration, since solid torus neighborhoods of the binding components are glued to

the fibration by a standard specified framing. The data (Σ, ϕ) is referred to as an *abstract open book*.

A standard example of an open book decomposition on S^3 has binding given by the Hopf link, and pages given by the S^1 family of annuli whose boundaries are all the chosen Hopf link. Each page is a union of the fibers of the Hopf fibration to S^2 above an interval in the base connecting the north and south poles of S^2, and these intervals come in an S^1 family.

Thurston and Winkelnkemper [TW75] showed that any open book decomposition gives rise to a contact structure, by taking planes which are almost tangent to the interior of the pages, and are positively transverse to the binding components (where the binding is oriented as the boundary of a page). We say that the open book decomposition *supports* the contact structure when it arises this way.

The open book decomposition on S^3 discussed above whose binding is the positive Hopf link (orienting the components as the boundary of the page to determine the sign of the linking), supports the standard tight contact structure on S^3, and the negative Hopf link open book supports an overtwisted contact structure on S^3.

Given two 3-manifolds with open book decompositions, their connected sum has an open book decomposition whose binding is a Murasugi sum of the bindings of the original open books, and whose pages are obtained by plumbing together the original pages as in figure 2.6. By taking the open book decomposition on S^3 mentioned above and connect summing in this way with any other open book on a 3-manifold Y, we get a new open book decomposition for $Y \# S^3 \cong Y$ called the *positive/negative stabilization* where we have

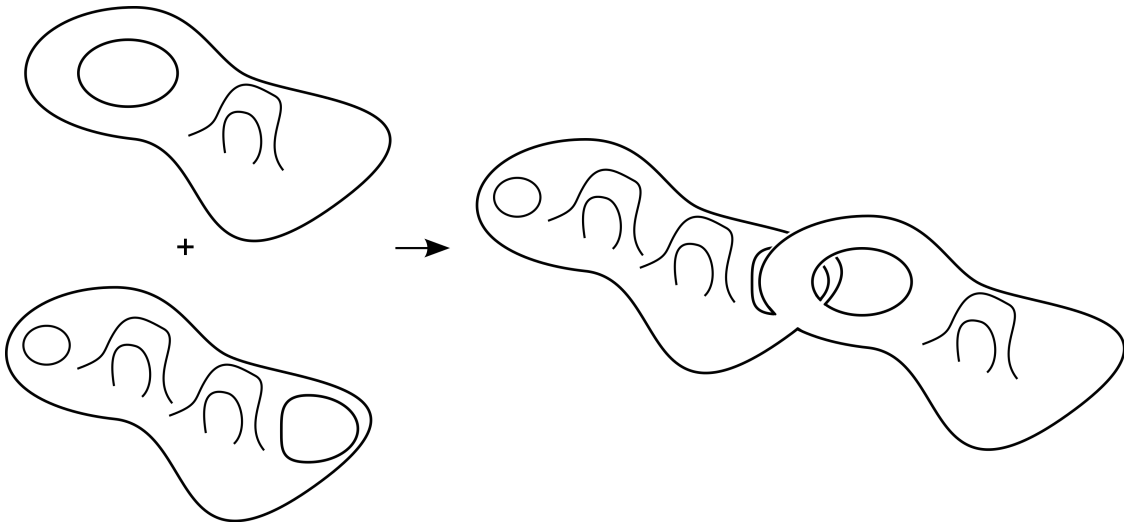

Figure 2.6: The page of a connect sum of open books.

attached a band to the pages of the open book on Y and performed a band sum on the binding. The contact manifold supported by the connected sum open book is equivalent to the connected sum of the originally supported contact manifolds. Because the positive Hopf open book on S^3 supports the standard tight contact structure, connect summing (Y, ξ) with (S^3, ξ_{std}) yields (Y, ξ), so positive stabilization does not change which contact structure the open book supports.

Giroux [Gir02] proved the converse of Thurston-Winkelnkemper's theorem, and established that contact structures on 3-manifolds up to contact isotopy are in one to one correspondence with open book decompositions up to positive stabilization.

We know from above that an allowable Lefschetz fibration admits a Stein structure. It is natural that the open book decomposition on the boundary of the Lefschetz fibration induces the same contact structure as the Stein structure. The details of this were verified in [Pla04].

A Lefschetz fibration determines the open book decomposition on its boundary, and it is useful to be able to describe that open book in terms of the fibers and vanishing cycles. The fibers of the Lefschetz fibration agree with the fibers of the open book decomposition, so it suffices to describe the monodromy of the open book. It can be shown that a Lefschetz fibration with a single vanishing cycle has a boundary open book whose monodromy is a single positive (right-handed) Dehn twist about the vanishing cycle. With multiple vanishing cycles, the boundary open book has monodromy given by a product of positive Dehn twists, one about each vanishing cycle. The conventions to keep track of the ordering of the Dehn twists in the cases relevant here are described below.

2.3.1 Conventions on monodromy factorizations and Lefschetz fibrations

A Lefschetz fibration naturally induces an open book decomposition on the boundary where the fibers of the open book are the same as the fibers of the Lefschetz fibration, and the monodromy is given by a product of positive (right-handed) Dehn twists about the vanishing cycles. Since mapping class groups of surfaces are non-abelian, the order of the vanishing cycles generally matters. For this reason, we will briefly mention the conventions that we will use throughout this thesis.

Suppose $c_1, \cdots, c_n$ are simple closed curves on the fiber. Denote by D_{c_i} a positive Dehn twist around c_i. The product $D_{c_1} D_{c_2} \cdots D_{c_n}$ means first Dehn twist along c_1, then c_2, and so on until finally along c_n. We will be particularly interested in the case where the fibers of the Lefschetz fibration and open book decomposition are *planar* (genus zero). In this case the fiber is a disk with holes, and we can place the holes along a circle concentric with the bounday of the disk. Labelling the holes $\{1, \cdots, m\}$ *counterclockwise*, we use the

notation $D_{i_1,\cdots,i_k}$ for $i_1,\cdots,i_k \in \{1,\cdots,m\}$ to indicate a positive Dehn twist about a curve which convexly contains the holes $i_1,\cdots,i_k$.

Any factorization of the monodromy of an open book decomposition into a product of positive Dehn twists corresponds to a Lefschetz fibration. When the fibers are disks with holes, we have the natural handlebody decomposition for this Lefschetz fibration where the holes are represented by dotted circles forming a trivial braid corresponding to 1-handles and the vanishing cycles correspond to 2-handles. We view the holed-disk fibers as orthogonal to the dotted circles, oriented so that the outward normal points downward. Then the monodromy factorization $D_{c_1}\cdots D_{c_n}$ corresponds to the Lefschetz fibration where the vanishing cycle c_1 appears at the top and c_n at the bottom (though these vanishing cycles lie on the upside-down disk). Flipping the entire diagram 180° around the horizontal axis in the page gives a handlebody decomposition where the vanishing cycle c_1 appears at the bottom and c_n appears at the top, but now these vanishing cycles are viewed as living on the disk without turning it upside-down. This is an alternate convention which has appeared in some of the literature. However, here we will use the convention where the disk fibers are oriented with a downward normal, and the vanishing cycles are ordered top to bottom.

Typically, to draw the handlebody, we will isotope the holes on the disk so that they all lie on the bottom half of the disk along a circle concentric to the boundary. An example, using the top to bottom convention where the outward normal to the disk points downward, is in figure 2.7.

In this case, a generating set of relations for the mapping class group can be easily described. The generators are given by Dehn twists about curves in the surface. Relations between these generators have three types. The first is that Dehn twists about disjoint

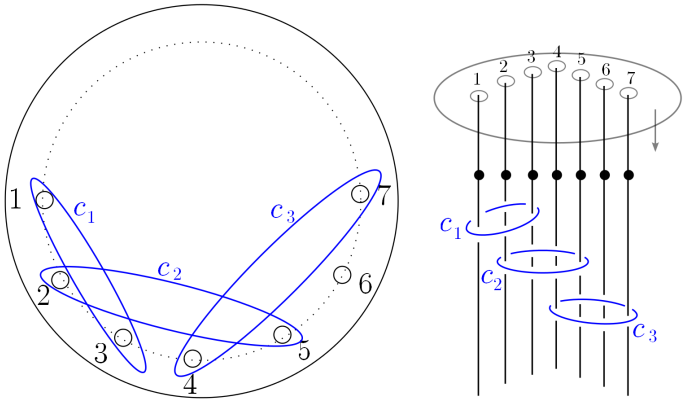

Figure 2.7: The Lefschetz fibration corresponding to the monodromy factorization $D_{1,3}D_{2,5}D_{4,7} = D_{c_1}D_{c_2}D_{c_3}$.

curves commute with each other. The second is the conjugacy relation: if $\phi = D_c$ then $D_c^{-1}D_{c'}D_c = D_{\phi(c')}$. The third is the *lantern relation*. To describe this relation on the disk with n holes, choose a standard model so the holes are placed on the vertices of a regular n-gon inside the disk. The lantern relations say that if A, B, and C are disjoint collections of holes so that the holes in A precede those of B which precede those of C going counterclockwise around the disk, then

$$D_A D_B D_C D_{A\cup B\cup C} = D_{A\cup B} D_{A\cup C} D_{B\cup C}. \tag{2.3.1}$$

By applying the lantern relation iteratively, one can obtain the following *daisy relations*. If $B_0, B_1, \cdots, B_m$ are subset of holes ordered counterclockwise around the disk, then

$$D_{B_0}^{m-1} D_{B_1} \cdots D_{B_m} D_{B_0\cup B_1\cup\cdots\cup B_m} = D_{B_0\cup B_1} D_{B_0\cup B_2} \cdots D_{B_0\cup B_m} D_{B_1\cup\cdots\cup B_m}. \tag{2.3.2}$$

Finally, by iteratively applying daisy relations, we find the following *generalized lantern*

relation. Here $B_1, \cdots, B_m$ are subsets of holes ordered counterclockwise around the disk.

$$D_{B_1}^{m-2} \cdots D_{B_m}^{m-2} D_{B_1 \cup \cdots \cup B_m} = (D_{B_1 \cup B_2} D_{B_1 \cup B_3} \cdots D_{B_1 \cup B_m})(D_{B_2 \cup B_3} \cdots D_{B_2 \cup B_m}) \cdots (D_{B_{m-1} \cup B_m}) \tag{2.3.3}$$

2.4 Open books on Seifert fibered spaces

Now we bring the previous three background sections together to discuss the main objects of study in this thesis: the canonical contact structures on Seifert fibered spaces over S^2 and their symplectic fillings. Recall from section 2.2 that such Seifert fibered spaces arise as the boundary of a plumbing of disk bundles over spheres according to a star-shaped graph, and under the normalization the Euler numbers on the non-central disk bundles are at most -2. The Euler number on the central disk bundle, e_0 is an invariant of the Seifert fibered space and can be any integer. These normalized plumbings are in one to one correspondence with Seifert fibered spaces. When $e_0 \leq -k$, Gay and Mark [GM13] showed that the plumbing supports a Lefschetz fibration which can be described explicitly in terms of the plumbing graph. The induced open book decomposition supports a contact structure on the boundary Seifert fibered space. Park and Stipsicz [PS14] showed this contact structure agrees with the *canonical contact structure* which was originally defined as the one given by the field of complex tangencies when realizing the Seifert fibered space as the link of an isolated normal surface singularity.

In fact Gay and Mark's construction is for a large class of plumbings of disk bundles over surfaces of any genus. Their set-up starts with a configuration of core symplectic surfaces $\mathcal{C} = C_1 \cup \cdots \cup C_n$ intersecting ω-orthogonally according to a negative definite plumbing graph Γ with no edges from a vertex to itself. A regular neighborhood of the union of these surfaces

is the plumbing. For each vertex v_j, let s_j be the sum of the valence of that vertex with the self-intersection number of the corresponding symplectic surface. Assume $s_j \leq 0$ for all vertices v_j (a.k.a. no bad vertices). Let Σ be the surface obtained from connect summing $|s_j|$ copies of D^2 to each C_j and then connect summing these surfaces together according to the graph. Let $\{c_1, \cdots, c_k\}$ be simple closed curves, with one around each connected sum neck, and τ the product of right handed Dehn twists around $c_1, \cdots, c_k$.

Theorem 2.4.1 (Gay and Mark [GM13] Theorem 1.1)**.** *Any neighborhood of $\mathcal{C}$ contains a neighborhood (Z, η) of $\mathcal{C}$ with strongly convex boundary, that admits a Lefschetz fibration $\pi : Z \to D^2$ having regular fiber Σ and exactly one singular fiber $\Sigma_0 = \pi^{-1}(0)$. The vanishing cycles are $c_1, \cdots, c_k$ and $\mathcal{C}$ is the union of the closed components of Σ_0. The induced contact structure ξ on ∂Z is supported by the induced open book (Σ, τ).*

Connect summing each surface with $|s_j|$ disks amounts to cutting $|s_j|$ holes in the surface. There is a vanishing cycle around each connected sum neck. Because all of these vanishing cycles lie disjointly in the surface describing the fiber of the Lefschetz fibration, we can deform the fibration so that all the critical points lie in a single fiber. Then, this critical fiber is made up of a union of the surfaces at the cores of the plumbings which intersect at a single point for each edge in the plumbing graph, along with some trivial disks that retract onto the surfaces. The number of Lefschetz critical points on each surface is designed to be the negation of its prescribed self-intersection number, because each Lefschetz critical point contributes -1 to this number.

In the case of the standard plumbings which fill Seifert fibered spaces over S^2, all the self-intersection numbers of the core spheres except possibly the central vertex are at

most -2 and their valencies are at most 2, so the only condition needed on these spaces for Gay and Mark's construction to go through is $e_0 \leq -k$. Furthermore all of the surfaces C_i are spheres, and connect summing a disk to a surface is equivalent to cutting a hole in the surface. Since the plumbing graphs are star-shaped, the final surface Σ will be a planar genus 0 surface with $\sum_i |s_i|$ boundary components.

In fact, Gay and Stipsicz showed earlier that any negative definite plumbing supports a convex symplectic structure in [GS09]. This implies that a slightly larger range of Seifert fibered spaces appears as the boundary of a strong symplectic filling, however it is not clear how to construct an open book supporting these contact structures. In practice, it is very useful to recognize a contact structure via a supporting open book decomposition. Furthermore, even if we found open book decompositions for these more general contact structures, it is likely they would no longer be planar.

Planar contact structures are particularly rigid, and the symplectic fillings of such contact manifolds satisfy very convenient properties as shown by Wendl.

Theorem 2.4.2 (Wendl [Wen10])**.** *Suppose (W, ω) is a strong symplectic filling of a planar contact manifold (M, ξ) with a given planar open book. Then (W, ω) is symplectically deformation equivalent to a Stein filling supported by a Lefschetz fibration which restricts to the given open book decomposition on its boundary. The Lefschetz fibration is allowable and thus supports a Stein structure if W is minimal.*

This was extended to weak symplectic fillings of planar contact structures in [NW11], thus in the planar case there is no distinction between weak, strong, and Stein fillings.

Chapter 3

Classification Methods

In this section we develop the main theory needed for classifying symplectic fillings of Seifert fibered spaces. Because of the methods used in the proof, we restrict to Seifert fibered spaces over S^2 which have Seifert invariant $e_0 \leq -k-1$ where e_0 and k are identified in figure 3.1. We will refer to such Seifert fibered spaces as *dually positive*, for reasons that will become clear shortly. Note that these plumbings satisfy the condition needed for Gay and Mark's theorem 2.4.1, so these Seifert fibered spaces have a canonical contact structure supported by a planar open book, and the plumbing gives a filling of this contact manifold.

The main argument here gives upper bounds (in terms of explicit diffeomorphism types) of strong symplectic fillings of dually positive Seifert fibered spaces with the canonical contact structure induced on the boundary of the plumbing ξ_{pl}. First, using a construction utilized by Stipsicz, Szabó and Wahl [SSW08], we will build the symplectic plumbing of spheres inside a closed symplectic manifold, such that the complement is also a symplectic plumbing of spheres, now with concave boundary. The dually positive condition will allow us to ensure that the concave piece contains a sphere of self-intersection number $+1$. Then we replace the convex plumbing of spheres by an arbitrary convex symplectic filling to form a closed symplectic manifold with the concave cap which still contains a sphere of self-intersection number $+1$ (analogous to Lisca's method to classify symplectic fillings of

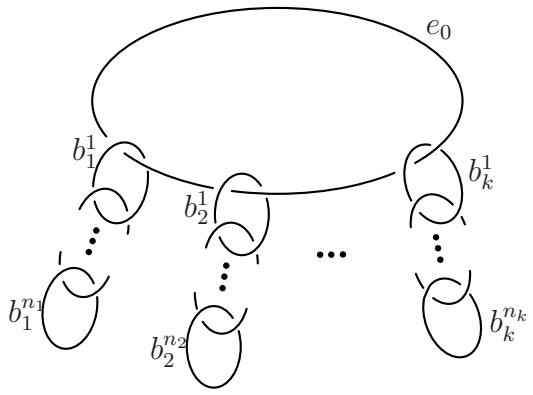

Figure 3.1: Surgery diagram for a Seifert fibered space with k singular fibers, $b_i^j \leq -2$. Equivalently a Kirby diagram for a plumbing bounding the Seifert fibered space.

$(L(p,q), \xi_{std})$). A theorem of McDuff implies that this closed manifold is a symplectic blow-up of $\mathbb{C}\mathrm{P}^2$ with its standard Kahler structure. To identify the topology of the unknown convex symplectic filling, it suffices to understand how the concave cap can symplectically embed into the blow-up of $\mathbb{C}\mathrm{P}^2$, since the convex filling must be its complement. Generalizing arguments of Lisca [Lis08], we obtain homological restrictions coming from the adjunction formula and intersection information of the spheres. Under certain conditions, we can show that the homology classes these spheres represent uniquely determines a symplectic embedding of their neighborhood into a blow up of $\mathbb{C}\mathrm{P}^2$. By deleting the possible embeddings of the concave cap from blow-ups of $\mathbb{C}\mathrm{P}^2$, we obtain the diffeomorphism types of all possible convex symplectic fillings of the given dually positive Seifert fibered space with contact structure ξ_{pl}.

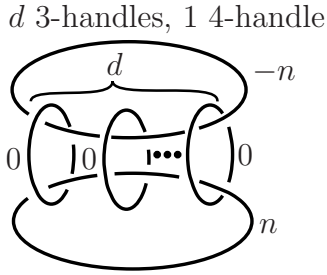

Figure 3.2: A handlebody diagram for the sphere bundle B_n. The relevant spheres (the zero section, infinity section, and d fibers) are represented by the cores of the 2-handles together with the pushed in Seifert surfaces for the attaching circles.

3.1 The dual graph construction

First we describe the dual graph construction of Stipsicz, Szabó, and Wahl [SSW08], which provides a symplectic embedding of the neighborhood of dually positive spheres into a blow-up of $\mathbb{C}\mathrm{P}^2$ whose complement is the concave cap we need.

The construction of the dual graph begins by looking at a complex ruled surface over $\mathbb{C}\mathrm{P}^1$. Topologically, this is an S^2 bundle over S^2. Each fiber will have self intersection number 0, and will intersect each section of the bundle in a single point. The zero and infinity sections have self-intersection numbers n and $-n$ respectively. It is convenient to have a handlebody diagram for the sphere bundle B_n, in which the 0-section, d distinct fibers, and the ∞-section are all visible. Such a diagram is given by figure 3.2.

To obtain the dual plumbing, we build the original plumbing inside a symplectic blow-up of B_n. We will allow blowups to be performed along the intersections of the various spheres in the picture. The proper transforms of these spheres will remain symplectic, and new exceptional spheres are symplectic submanifolds as well. At the beginning the spheres we keep track of are just the 0-section, the ∞-section, and the d fibers. As we blow-up, we

include the new exceptional spheres in the picture. Figure 3.3 shows an example, keeping track of both the standard short-hand notation to keep track of these blowups, as well as the corresponding handlebody diagrams. Note that each exceptional fiber will contain at least one sphere of self-intersection -1, which is the exceptional sphere from the most recent blow-up of that fiber. We perform the blow-ups so that if ignore these most recently introduced exceptional spheres, the remaining spheres we are tracking form two plumbing components, one component agrees with Γ and the other component gives the dual plumbing Γ'.

To see that the plumbings coming from Γ and Γ' glue together to give the blow-up of our original sphere bundle, imagine cutting the blown-up sphere bundle as shown above, along an equator of each regular fiber, and along the equator of the last exceptional sphere in each exceptional fiber, so that these equators all match up smoothly to form a 3-manifold. More precisely, we can find a Morse function ϕ on the blow-up of the ruled surface to $[0,1]$, whose values on the spheres for Γ are strictly less than $\frac{1}{2}$, and whose values on the spheres for Γ' are strictly greater than $\frac{1}{2}$. Then the 3-manifold we are interested in is $\phi^{-1}(1/2)$. Considering the singular fibration restricted to $\phi^{-1}([0,1/2])$, we see the generic fibers are disks which intersect once with the proper transform of the ∞-section (now the central sphere of Γ). The singular fibers contain the spheres in the arms of Γ, together with disks (the lower half of the last exceptional spheres), which intersect once with the last sphere in each arm. There is a deformation retract of $\phi^{-1}([0,1/2])$ to the spheres of Γ defined by taking a deformation retract of each disk to the point where it intersects a sphere of Γ. Therefore, $\phi^{-1}([0,1/2])$ is a regular neighborhood of the spheres of Γ, in other words a plumbing. The corresponding argument shows that $\phi^{-1}([1/2,1])$ is a plumbing for the dual graph Γ'. Note that each sphere in either graph is a symplectic submanifold since it is either one of the

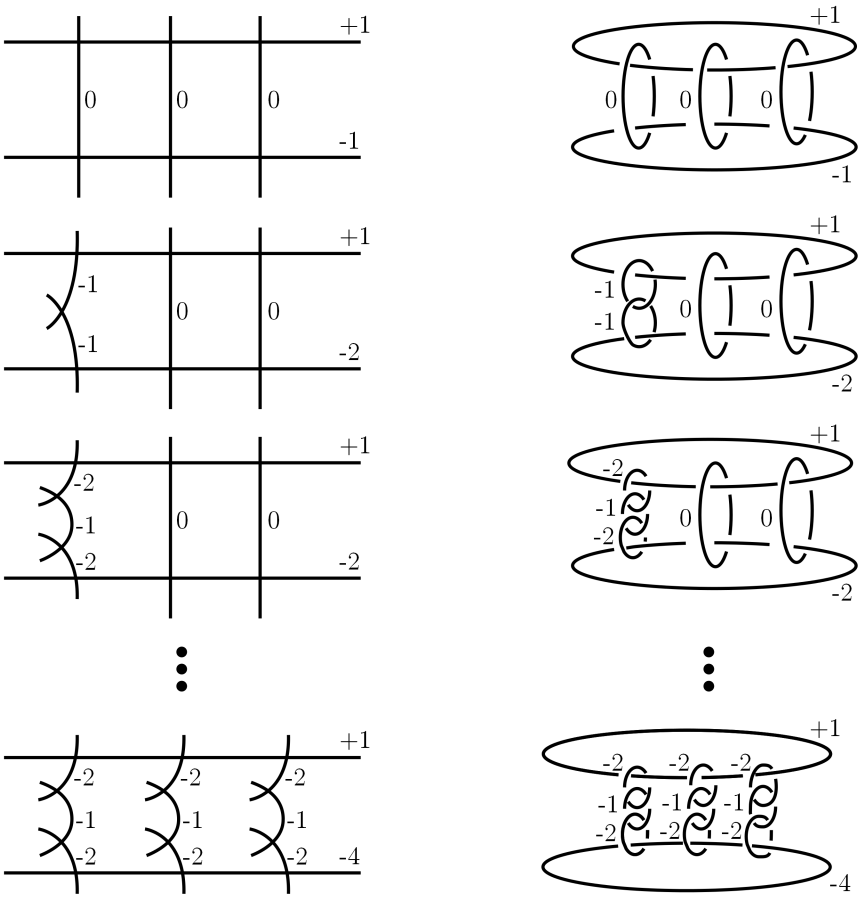

Figure 3.3: A sequence of blow-ups, keeping track of the spheres whose neighborhoods are plumbings. In the last stage we can see the star-shaped plumbing with 4 vertices, central vertex labeled with -4, and the three arms are labelled with -2, and its dual plumbing which is also star-shaped with 4 vertices, but the central vertex is labeled with $+1$ and three arms labeled with -2. The two plumbings are glued together along equators of the regular fibers and equators of the -1 spheres on the exceptional fibers.

distinguished sections, a fiber, an exceptional sphere, or the proper transform of one of these objects.

3.1.1 Dually Positive Graphs

The condition that a configuration of spheres is dually positive, ensures that one can build a dual configuration which is a star-shaped graph whose central vertex has self-intersection number $+1$. To see this, suppose the central vertex of the dually positive configuration has square $e_0 \leq -k-1$ where k is the number of arms in the original graph. Start with a sphere bundle with infinity section of self-intersection number -1, and zero section of self-intersection number $+1$, and keep track of $d = -e_0 - 1$ fibers (of self-intersection number 0). Blow up once at the intersections of each of the $-1 - e_0$ fibers with the (-1) infinity section. The proper transform of the zero section now has self-intersection number e_0, the exceptional spheres and proper transforms of the fibers have self-intersection number -1, and the zero section is unchanged so it still has self-intersection number $+1$. Next, in k of these singular fibers, blow-up at the intersection of the new exceptional sphere with the proper transforms of the original fiber. By continuing to blow up at points where an exceptional sphere of square -1 intersects an adjacent sphere, it is possible to build the dually positive graph emanating from the infinity section and ending just before the most recent exceptional -1 spheres in each fiber, without ever blowing up at a point on the zero section. Therefore the dual graph has central vertex with coefficient $+1$, and $-1 - e_0$ arms, whose vertices have all negative coefficients.

Note that when $e_0 < -k-1$, the dual graph contains $d = -e_0 - 1 > k$ arms, but only k of them are used to construct the singular fibers. Each of the remaining $-e_0 - 1 - k$ arms

shows up in the dual graphs construction as two -1 spheres, one of which is adjacent to the proper transform of the negative infinity section and will be cut in half to split the graph from the dual graph. The remaining -1 sphere (the proper transform of a regular fiber after one blow-up at its intersection with the 0-section) persists in the dual graph as a short arm.

Note that when $e_0 < -k-1$, there are other ways to produce a concave dual graph containing a $+1$ sphere, but the convention described here which only allows -1 spheres to appear in their own arms yields the strongest classification results.

3.2 McDuff's classification for closed symplectic manifolds

As explained in section 3.1.1, our condition that the configuration of spheres be dually positive ensures that the concave cap coming from the dual graph construction contains a sphere of self-intersection number $+1$. This condition is useful due to the following classification theorem.

Theorem 3.2.1 (McDuff [McD90])**.** *If (V^4, C^2, ω) is a minimal symplectic pair (namely $V \setminus C$ contains no exceptional curves), where C is a rational curve with self-intersection $C \cdot C = p \geq 0$, then (V, ω) is symplectomorphic either to $\mathbb{C}\mathrm{P}^2$ with its usual Kahler form or to a symplectic S^2 bundle over a compact surface M. Further, this symplectomorphism may be chosen so that it takes C either to a complex line or quadric in $\mathbb{C}\mathrm{P}^2$, or to a fiber of the S^2 bundle, or (if $M = S^2$) to a section of this bundle.*

In our case, this classification simplifies to a single manifold up to blowing up symplectically.

Corollary 3.2.2. *If (V^4, C^2, ω) is a minimal symplectic pair where C is a 2-sphere of self-intersection number $+1$ then (V, C, ω) is symplectomorphic to $(\mathbb{CP}^2, \mathbb{CP}^1, \omega_{std})$.*

By gluing any strong symplectic filling of a dually positive Seifert fibered space with contact structure ξ_{pl} to a neighborhood of its dual configuration, we obtain a symplectic pair (V, C, ω) satisfying all hypotheses of the theorem except minimality. After blowing down exceptional spheres in $V \setminus C$, it follows that such a convex filling embeds symplectically (up to rescaling the symplectic form) in a blow-up of $(\mathbb{CP}^2, \omega_{std})$ where the blow-ups are disjoint from the standard $\mathbb{CP}^1 \subseteq \mathbb{CP}^2$. The complement of the embedded convex filling is symplectomorphic to the corresponding plumbing of spheres described by the dual graph, and $+1$ sphere corresponding to the central vertex of the dual graph is identified with $\mathbb{CP}^1$.

3.3 Homological restrictions on embeddings of the cap

Denote by (X_M, ω_M) the closed symplectic manifold $\mathbb{CP}^2 \#M \overline{\mathbb{CP}^2}$ with symplectic form ω_M given by some symplectic blow up of the standard Kahler form on $\mathbb{CP}^2$. We would like to determine all possible symplectic embeddings of the positive dual graph plumbing of the concave cap. To understand possible embeddings, we first use some homological restrictions.

First fix a standard orthogonal basis $(\ell, e_1, \cdots, e_M)$ for $H_2(X_M; \mathbb{Z})$ where ℓ is represented by the complex projective line so $\ell^2 = +1$, and the e_m are represented by the exceptional spheres created in the blow-ups, so $e_m^2 = -1$, and $\ell \cdot e_m = e_m \cdot e_{m'} = 0$ for $m \neq m'$. Because these are represented by symplectic spheres, we can determine how the first Chern class of X_M evaluates on each of these homology classes via the adjunction

formula:

$$\langle c_1(X_M), \ell \rangle = \ell^2 + 2 = 3$$

$$\langle c_1(X_M), e_m \rangle = e_m^2 + 2 = 1$$

Now we would like to analyze what the spheres in the plumbing for the cap could represent in $H_2(X_M; \mathbb{Z})$ in terms of this basis. We will refer to the embedded sphere representing the central vertex as C_0, the symplectic spheres in the j^{th} arm of distance i from the center as C_i^j (so $C_1^1, \cdots, C_1^d$ are adjacent to the central vertex). We know that these spheres are also symplectic, so they must also satisfy the adjuction formula:

$$\langle c_1(X_M), [C_i^j] \rangle = [C_i^j]^2 + 2$$

Furthermore, we know that the sphere C_0 which has self-intersection number $+1$, is sent to the complex projective line so $[C_0] = \ell$. The intersection data implies spheres whose vertices are joined by an edge have homological intersection number $+1$, other distinct spheres have homological intersection number 0, and the square of the homology class represented by each sphere is given by the decoration on the graph (which is negative for all but C_0).

Now suppose that

$$[C_i^j] = a_0^{i,j} \ell + \sum_{m=1}^{M} a_m^{i,j} e_m$$

For $i = 1$ we have $1 = [C_1^j] \cdot [C_0] = [C_1^j] \cdot \ell$, so $a_0^{1,j} = 1$. Using the adjunction formula, and our knowledge of how $c_1(X_M)$ evaluates on the standard basis we get the following formula for the coefficients a_i^j:

$$3 + \sum_{i=1}^{M} a_m^{1,j} = 1 - \sum_{m=1}^{M} (a_m^{1,j})^2 + 2$$

so

$$\sum_{m=1}^{M}(a_m^{1,j})^2 + a_m^{1,j} = 0$$

Note that since $a_m^{1,j}$ are integers, we have $(a_m^{1,j})^2 + a_m^{1,j} \geq 0$ with equality if and only if $a_m^{1,j} \in \{0, -1\}$. Therefore $a_m^{1,j} \in \{0, -1\}$ for all $m \in \{1, \cdots, M\}$. Furthermore since

$$-n_{1,j} = [C_1^j]^2 = 1 - \sum_{m=1}^{M}(a_m^{1,j})^2,$$

there are precisely $n_{1,j} + 1$ values of m for which $a_m^{1,j}$ is -1. Thus we get the following result.

Lemma 3.3.1. *If C_1^j is a symplectic sphere in the dual graph configuration adjacent to the central vertex sphere, then its homology class has the form*

$$\ell - e_{m_1}^{1,j} - \cdots - e_{m_{n+1}}^{1,j}$$

For $i > 1$, we know that $0 = [C_i^j] \cdot [C_0] = [C_i^j] \cdot \ell$. Therefore $a_0^{i,j} = 0$ for all $i > 1$. In this case the adjuction formula yields the following formula:

$$\sum_{m=1}^{M} a_m^{i,j} = -\sum_{m=1}^{M}(a_m^{i,j})^2 + 2$$

so

$$\sum_{m=1}^{M}(a_m^{i,j})^2 + a_m^{i,j} = 2$$

Thus, all but one of the $a_m^{i,j}$'s is either 0 or 1, and exactly one $a_m^{i,j}$ is either 1 or -2 for for each $i > 1$. An inductive argument of Lisca [Lis08, Proposition 4.4] implies that $a_m^{i,j}$ can never be equal to -2, so there is always a unique $a_m^{i,j}$ equal to 1. Note that Lisca's statement refers to linear graphs of symplectic spheres embedded in a blow-up of $\mathbb{C}\mathrm{P}^2$, but each arm of the star-shaped graph (starting at the central vertex) is a linear graph satisfying the necessary hypotheses. Thus we conclude:

Lemma 3.3.2. *If C_i^j is a sphere in a symplectic embedding of the dual graph configuration, such that C_i^j does not correspond to a vertex adjacent to the central vertex ($i > 1$) then*

$$\left[C_i^j\right] = e_{m_0}^{i,j} - e_{m_1}^{i,j} - \cdots - e_{m_{n_{i,j}-1}}^{i,j}$$

We have further data given by the fact that $[C_1^j] \cdot [C_1^{j'}] = 0$ when $j \neq j' \in \{1, \cdots, d\}$:

$$\begin{aligned} 0 &= (\ell - e_{m_1^{1,j}} - \cdots - e_{m_{n_{1,j}+1}^{1,j}}) \cdot (\ell - e_{m_1^{1,j'}} - \cdots - e_{m_{n_{1,j'}+1}^{1,j'}}) \\ &= 1 - |\{m_1^{1,j}, \cdots, m_{n_{1,j}+1}^{1,j}\} \cap \{m_1^{1,j'}, \cdots, m_{n_{1,j'}+1}^{1,j'}\}| \end{aligned}$$

We conclude

Lemma 3.3.3. *For each distinct pair j, j', there is exactly one e_m which appears with coefficient -1 in both $[C_1^j]$ and $[C_1^{j'}]$.*

Further analysis of the intersection relations yields additional rules for the homology classes of the embedded symplectic spheres in the concave dual graph cap.

Lemma 3.3.4. *The class of the exceptional sphere which appears with coefficient $+1$ in $[C_2^j]$ appears with coefficient -1 in sphere $[C_1^j]$.*

Proof. Assuming the forms for the homology classes specified in lemmas 3.3.1 and 3.3.2 we get the following.

$$\begin{aligned} 1 = [C_2^j] \cdot [C_1^j] &= (e_{m_0} - e_{m_1} - \cdots - e_{m_n}) \cdot (h - e_{m_1'} - \cdots - e_{m_p'}) \\ &= |\{m_0\} \cap \{m_1', \ldots, m_p'\}| - |\{m_1, \ldots, m_n\} \cap \{m_1', \ldots, m_p'\}| \end{aligned}$$

□

Lemma 3.3.5. *For $i > 1$, either the exceptional class with coefficient $+1$ in $[C_i^j]$ appears with coefficient -1 in $[C_{i+1}^j]$ or the exceptional class with coefficient $+1$ in $[C_{i+1}^j]$ appears with coefficient -1 in $[C_i^j]$, or both. In particular, they do not share the same exceptional class with $+1$ coefficient. Furthermore, the exceptional classes which appear with coefficients -1 in $[C_i^j]$ are disjoint from those which appear with coefficient -1 in $[C_{i+1}^j]$ unless both conditions in the first sentence are satisfied, in which case they share exactly one exceptional class with -1 coefficient in common.*

Proof.

$$\begin{aligned} 1 &= [C_i^j] \cdot [C_{i+1}^j] \\ &= (e_{m_0} - e_{m_1} - \cdots - e_{m_n}) \cdot (e_{m'_0} - e_{m'_1} - \cdots - e_{m'_p}) \\ &= |\{m_0\} \cap \{m'_1, \ldots, m'_p\}| + |\{m'_0\} \cap \{m_1, \ldots, m_p\}| \\ &\quad -|\{m_0\} \cap \{m'_0\}| - |\{m_1, \ldots, m_n\} \cap \{m'_1, \ldots, m'_p\}| \end{aligned}$$

□

Lemma 3.3.6. *If e_x appears with coefficient $+1$ in $[C_i^j]$ then it does not appear with coefficient $+1$ in $[C_{i'}^{j'}]$ for any $(i', j') \neq (i, j)$.*

Proof. Suppose not. Then we obtain a contradiction as follows

$$\begin{aligned}
0 &\leq [C_i^j] \cdot [C_{i'}^{j'}] \\
&= (e_x - e_{m_1} - \cdots - e_{m_n}) \cdot (e_x - e_{m'_1} - \cdots - e_{m'_p}) \\
&= |\{x\} \cap \{m'_1, \ldots, m'_p\}| + |\{x\} \cap \{m_1, \ldots, m_n\}| - |\{x\} \cap \{x\}| - |\{m_1, \ldots, m_n\} \cap \{m'_1, \ldots, m'_p\}| \\
&= 0 + 0 - 1 - |\{m_1, \ldots, m_n\} \cap \{m'_1, \ldots, m'_p\}| \\
&< 0
\end{aligned}$$

□

Lemma 3.3.7. *If e_x appears with nonzero coefficient in distinct classes $[C_i^j]$ and $[C_{i'}^{j'}]$ and we do not have that $(i, j) = (i' \pm 1, j')$ or that $i, i' = 1$, then we have one or both of the following two possibilities.*

1. *the exceptional class with coefficient $+1$ in $[C_i^j]$ appears with coefficient -1 in $[C_{i'}^{j'}]$*
2. *the exceptional class with coefficient $+1$ in $[C_{i'}^{j'}]$ appears with coefficient -1 in $[C_i^j]$*

If only one of these possibilities holds then there is exactly one exceptional class which appears with coefficient -1 in both $[C_i^j]$ and $[C_{i'}^{j'}]$. If both (1) and (2) hold, then there are exactly two exceptional classes which appear with coefficient -1 in both.

Proof.

$$\begin{aligned} 0 &= [C_i^j] \cdot [C_{i'}^{j'}] \\ &= (e_{i_0} - e_{i_1} - \cdots - e_{i_n}) \cdot (e_{i'_0} - e_{i'_1} - \cdots - e_{i'_m}) \\ &= |\{i_0\} \cap \{i'_1, \ldots, i'_m\}| + |\{i'_0\} \cap \{i_1, \ldots, i_n\}| - |\{i_0\} \cap \{i'_0\}| - |\{i_1, \ldots, i_n\} \cap \{i'_1, \ldots, i'_n\}| \\ &= -|\{i_0\} \cap \{i'_0\}| - |\{i_1, \ldots, i_n\} \cap \{i'_1, \ldots, i'_n\}| \end{aligned}$$

□

If the graph for the convex filling we are considering has k arms, corresponding to the k singular fibers in the Seifert fibered space, then the coefficient on the central vertex of the graph, e_0 determines the relationship between k and d (the number of arms in the dual graph). As discussed in section 3.1.1, the number of arms in the dual graph is $d = -e_0 - 1$, and the dually positive assumption implies $k \leq -e_0 - 1$. When $d = -e_0 - 1$ is strictly larger than k, there are $d - k$ additional short arms each made up of a single symplectic sphere of self-intersection number -1. Therefore $[C_1^j] = \ell - e_{m_1^{1,j}} - e_{m_2^{1,j}}$ for $j \in \{k+1, \cdots, d\}$.

Lemma 3.3.8. *If $d = -e_0 - 1 > k + 1$ then the symplectic spheres $C_0, C_1^1, \cdots, C_1^d$ represent one of the following sets of homology classes in terms of the standard basis for*

$H_2(\mathbb{C}\mathrm{P}^2 \# M\,\overline{\mathbb{C}\mathrm{P}^2})$ (up to relabelling).

$$\begin{array}{lcl|lcl}
[C_0] & = & \ell & [C_0] & = & \ell \\
[C_1^1] & = & \ell - e_1 - e_{\cdot} - \cdots - e_{\cdot} & [C_1^1] & = & \ell - e_2 - \cdots - e_k - e_{k+1} - \cdots - e_d - e_{\cdot} - \cdots - e_{\cdot} \\
[C_1^2] & = & \ell - e_1 - e_{\cdot} - \cdots - e_{\cdot} & [C_1^2] & = & \ell - e_1 - e_2 - e_{\cdot} - \cdots - e_{\cdot} \\
 & \vdots & & & \vdots & \\
[C_1^k] & = & \ell - e_1 - e_{\cdot} - \cdots - e_{\cdot} & [C_1^k] & = & \ell - e_1 - e_k - e_{\cdot} - \cdots - e_{\cdot} \\
[C_1^{k+1}] & = & \ell - e_1 - e_{k+1} & [C_1^{k+1}] & = & \ell - e_1 - e_{k+1} \\
 & \vdots & & & \vdots & \\
[C_1^d] & = & \ell - e_1 - e_d & [C_1^d] & = & \ell - e_1 - e_d
\end{array}$$

Here $e_{\cdot}$ indicates that there can be additional distinct e_m's with coefficient -1 in these homology classes if the corresponding square is sufficiently negative. They should all be distinct from each other and distinct from all labeled e_m's.

Furthermore, if $d = k+1$ the above cases generalize to a family indexed by j, $0 \le j \le k$ (by a symmetry we may actually assume $j \le k/2$ and the two above cases correspond to $j = 0$ and $j = 1$ respectively).

$$\begin{array}{lcl}
[C_0] & = & \ell \\
[C_1^1] & = & \ell - e_1 - e_{m(1,j+1)} - e_{m(1,j+2)} \cdots - e_{m(1,k)} - e_{\cdot} - \cdots - e_{\cdot} \\
 & \vdots & \\
[C_1^j] & = & \ell - e_1 - e_{m(j,j+1)} - e_{m(j,j+2)} \cdots - e_{m(j,k)} - e_{\cdot} - \cdots - e_{\cdot} \\
[C_1^{j+1}] & = & \ell - e_2 - e_{m(1,j+1)} - e_{m(2,j+1)} - \cdots - e_{m(j,j+1)} - e_{\cdot} - \cdots - e_{\cdot} \\
 & \vdots & \\
[C_1^k] & = & \ell - e_2 - e_{m(1,k)} - e_{m(2,k)} - \cdots - e_{m(j,k)} - e_{\cdot} - \cdots - e_{\cdot} \\
[C_1^{k+1}] & = & \ell - e_1 - e_2
\end{array}$$

Here $m(a,b)$ are distinct for distinct pairs (a,b), and are distinct from $1, 2$.

Note that some of these options may not be possible in certain cases if the self-intersection numbers on the spheres in the dual graph configuration are not sufficiently negative.

Proof. First notice that there must be a common element e_m with coefficient -1 in all the classes $[C_1^{k+1}], \cdots, [C_1^d]$. This is trivial in the case that $k+1 = d$, and follows immediately from lemma 3.3.3 when $k+2 = d$. When $d > k+2$, lemma 3.3.3 implies that $[C_1^{k+1}]$ and $[C_1^{k+2}]$ share a unique element with coefficient -1 so without loss of generality $[C_1^{k+1}] = \ell - e_1 - e_2$ and $[C_1^{k+2}] = \ell - e_1 - e_3$. If $[C_1^{k+3}]$ does not have -1 coefficient for e_1 then lemma 3.3.3 implies $[C_1^{k+3}] = \ell - e_2 - e_3$, but then there is no way that $[C_1^1]$ can have e_m's with -1 coefficient for values of m in exactly one of $\{1,2\}$, exactly one of $\{1,3\}$, and exactly one of $\{2,3\}$ which is a contradiction. Since $[C_1^j]$ and $[C_1^{j'}]$ share exactly one element e_m with coefficient -1, we find that $[C_1^{k+1}] = \ell - e_1 - e_{k+1}, \cdots, [C_1^d] = \ell - e_1 - e_d$ for $e_{k+1}, \cdots, e_d$ all distinct.

Now consider the homology classes $[C_1^1], \cdots, [C_1^k]$. Each such class must either have -1 coefficient for e_1 or -1 coefficient for all of the classes $e_{k+1}, \cdots, e_d$ (not both). If $d > k+1$ then there can be at most one of the spheres $C_1^1, \cdots, C_1^k$, whose homology class has coefficient -1 for all the classes $e_{k+1}, \cdots, e_d$ since no two $[C_1^j]$ can share more than one e_i with coefficient -1. This proves the first part of the lemma.

When $d = k+1$ and $[C_1^{k+1}] = \ell - e_1 - e_2$, some of the classes $[C_1^1], \cdots, [C_1^k]$ must have coefficient -1 for e_1 and the rest must have coefficient -1 for e_2. Without loss of generality we assume the first j have -1 coefficient for e_1, and the rest have -1 coefficient for e_2. Then for each pair $(a,b) \in \{1, \cdots, j\} \times \{j+1, \cdots, k\}$ we must add another $e_{m(a,b)}$ which occurs with -1 coefficient in $[C_1^a]$ and $[C_1^b]$. If $m(a,b) = m(a',b')$ for $(a,b) \neq (a',b')$ then either $a \neq a'$ so $[C_1^a]$ and $[C_1^{a'}]$ both have coefficient -1 for both e_1 and $e_{m(a,b)}$ or $b \neq b'$ so $[C_b]$ and $[C_{b'}]$ both have coefficient -1 for e_2 and $e_{m(a,b)}$, but homology classes of distinct pairs of spheres can only share one common element with coefficient -1 so this is a contradiction. $\square$

3.4 Uniqueness of symplectic embedding for each homological embedding

Given a finite list of homology classes a symplectic embedding of the spheres of the dual graph into $\mathbb{C}\mathrm{P}^2 \# M\,\overline{\mathbb{C}\mathrm{P}^2}$ can represent, we would like to say that there are finitely many symplectic embeddings of the dual graph up to isotopy. There are two main steps to this process. The first is to follow the arguments of Lisca [Lis08] to carefully blow-down to $\mathbb{C}\mathrm{P}^2$, while keeping track of how this affects the embedded spheres of the dual graph. The second step is to analyze this blown-down embedding, and to try to understand the isotopy classes of a regular neighborhood of the blown-down dual graph in $\mathbb{C}\mathrm{P}^2$. The main conclusion of this section will be the following theorem.

Theorem 3.4.1. *Let Γ' be a star-shaped plumbing graph, such that the central vertex corresponds to a symplectic sphere C_0 of self-intersection number $+1$, a vertex which is the only one in its arm corresponds to a symplectic sphere C_1^j of self-intersection number ≤ -1, and all other vertices in the arms C_i^j correspond to symplectic spheres of self-intersection number ≤ -2. Suppose E and E' are symplectic embeddings of the corresponding concave symplectic plumbing into $\mathbb{C}\mathrm{P}^2 \# N\,\overline{\mathbb{C}\mathrm{P}^2}$ such that C_0 is sent to the complex projective line, the induced maps on second homology agree, and the following additional condition holds for the induced maps on second homology.*

($\star$) *For each j, the homology class of the sphere adjacent to the central sphere $E_*([C_1^j])$ has at most two exceptional classes e_i with the property that they appear with coefficient -1 in $E_*([C_1^j])$ and at least two other distinct classes $E_*([C_1^{j'}])$ and $E_*([C_1^{j''}])$.*

Then there is an isotopy from E to E' which extends to a regular neighborhood of the spheres.

This theorem will follow from the lemmas of the next two subsections.

Corollary 3.4.2. *When $e_0 < -k-1$ or $k \leq 6$, the isotopy class of an embedding of the concave cap of section 3.1 for the corresponding Seifert fibered space with k singular fibers is uniquely determined by the map induced by the embedding on second homology.*

The deduction of the corollary from the proposition follows from the homological analysis of section 3.3, particularly lemmas 3.3.3 and 3.3.8. The homological condition ($\star$) will be recast in section 3.4.2 in terms of configurations of line arrangements, and in this language it may be easier for the reader to see how this corollary follows. Therefore, we will discuss this deduction in section 3.4.2.

3.4.1 Blowing down

The following theorem was used by Lisca to solve this part of the problem when classifying symplectic fillings of lens spaces. In that case, the plumbing of spheres providing the concave cap is linear.

Theorem 3.4.3 (Lisca [Lis08] Theorem 4.2)**.** *Let ω_M be a symplectic form on $\mathbb{C}\mathrm{P}^2 \# M\,\overline{\mathbb{C}\mathrm{P}^2}$ obtained from the standard Kahler form by symplectic blow-ups. Let $\Gamma = C_0 \cup \cdots \cup C_j$ be a union of ω_M-orthogonal symplectic spheres, in the configuration of a linear graph, with self-intersection numbers $(1, 1-b_1, -b_2, \cdots, -b_j)$, such that C_0 is a complex line. Then there is a sequence of symplectic blow-downs*

$$(\mathbb{C}\mathrm{P}^2 \# M\,\overline{\mathbb{C}\mathrm{P}^2}, \omega_M) \to (\mathbb{C}\mathrm{P}^2 \# (M-1)\,\overline{\mathbb{C}\mathrm{P}^2}, \omega_{M-1}) \to \cdots \to (\mathbb{C}\mathrm{P}^2, \omega_0)$$

with ω_0 diffeomorphic to the standard Kahler form and such that Γ descends to two ω_M orthogonal symplectic spheres, each of self-intersection number 1.

In our situation, the dual graph is a star-shaped instead of linear. However, a star-shaped graph is simply the union of its k arms, each of which is a linear graph emanating from the central vertex. Therefore Lisca's theorem applies to each of the arms of the star-shaped dual configuration. We would like to keep track of all of these arms at once as we blow-down the manifold. Though we do not need a new argument here, a summary of Lisca's proof is included here to make it clear how it applies in the star-shaped case.

In our case, the dual configuration of spheres $\Gamma = C_0 \cup \cdots \cup C_m$ (in the shape of a star-shaped graph), is assumed to be symplectically embedded in $(\mathbb{C}\mathrm{P}^2 \#_M \overline{\mathbb{C}\mathrm{P}^2}, \omega_M)$. Here C_0 is identified with the complex projective line (by McDuff's theorem). First, choose an almost complex structure tamed by ω_M, for which the spheres $C_0, \cdots, C_m$ are all J-holomorphic. This allows us to have more control over intersections of spheres with any J-holomorphic sphere we blow down.

Relying on analysis of J-holomorphic curves by McDuff, Lisca proves a lemma (Lemma 4.5 in [Lis08]), which says that as long as $M > 0$, there exists a J-holomorphic sphere Σ such that $[\Sigma] \cdot [C_0] = 0$ and $[\Sigma]^2 = -1$. Furthermore, we can find Σ disjoint from Γ if and only if there is a symplectic sphere S of square -1 such that $[S] \cdot [C_j] = 0$ for $j = 0, 1, \cdots, m$. Note that Lisca stated this in the case that Γ is a linear plumbing, but the proof is unchanged for any configuration of symplectic spheres intersecting ω-orthogonally. Therefore, it is possible to blow down J-holomorphic spheres Σ until X_M is blown down to $\mathbb{C}\mathrm{P}^2$. Using the lemma, we can first blow down any Σ's disjoint from Γ, until there exists Σ for which $[\Sigma] \cdot [C_j] \neq 0$ for

some j. Because $C_0, \cdots, C_m$ are J-holomorphic, Σ must intersect them non-negatively. In our standard basis for $H_2(X_M; \mathbb{Z})$ as in the previous section, the fact that $[\Sigma] \cdot [C_0] = 0$ and $[\Sigma]^2 = -1$ implies $[\Sigma] = \pm e_i$. Given the analysis in the previous section of how to write $[C_j]$ in terms of this standard basis, we find that $[\Sigma] \cdot [C_j] \in \{-1, 0, 1\}$ for every $j = 0, \cdots, m$. Since Σ and C_j must intersect positively, either $\Sigma = C_j$ for some j, or $[\Sigma] \cdot [C_j] \in \{0, 1\}$ for all $j = 0, \cdots, m$. Lisca analyzes the relations between the e_i's showing up with non-zero coefficients in different $[C_j]$'s within a linear plumbing, and proves that blowing down Σ either reduces the length of the linear plumbing or reduces the absolute value of one of the self-intersection numbers of a C_j, $(j > 0)$, but the linear plumbing remains linear. This implies the conclusion of Lisca's theorem by induction.

In our case, we blow down a J-holomorphic sphere Σ, which may intersect any number of arms in the star-shaped graph. After blowing down, at least one arm is reduced in complexity, and each linear chain of symplectic spheres (originally these are the k arms) remains linear. It is possible that two of these linear chains intersect after a blow-down, so the graph would no longer be star-shaped. Because the existence of a J-holomorphic sphere to blow down, and the homological properties of the C_j do not depend on any assumptions about the non-intersection of the various arms, this does not prevent us from applying induction as in the linear case. We simply need to keep track of each linear chain separately, even as the chains intersect each other.

The conclusion is that each arm eventually descends to two symplectic spheres each of self-intersection number 1, one of which is the original C_0 (since all blow-downs were done disjointly from C_0). Therefore in total we have $d + 1$ symplectic spheres of self-intersection number 1 inside $(\mathbb{C}\mathrm{P}^2, \omega_{std})$.

We also have that our original J descends to an almost-complex structure J_0 on $\mathbb{C}\mathrm{P}^2$, which is tamed by $\omega_0(=\omega_{std})$, and the remaining $d+1$ spheres in the reduction of the dual graph are J_0 holomorphic. Because all of these spheres must represent the homology class ℓ and they are all J_0-holomorphic, each pair of spheres must intersect at a single point. Because the blow-downs were disjoint from C_0 and each of the other d spheres intersected C_0 in a different point initially, this remains true after blowing down. The other d spheres may intersect each other at multi-points if before blowing down, a group of them intersected a common exceptional sphere.

Note that the intersection configuration of these spheres (the data telling which collections of spheres have common multi-intersection points) is determined by the homological embedding data. If i of the d spheres adjacent to the central vertex sphere have a common exceptional class e_m appearing with coefficient -1 in their homology classes, then after blowing down, those i spheres will intersect at a common i-fold multi-intersection point. Thus we can extract the combinatorial data of the J_0-holomorphic line arrangement in the blow-down to $\mathbb{C}\mathrm{P}^2$ directly from the homology classes of the embedded spheres in $\mathbb{C}\mathrm{P}^2\#N\,\overline{\mathbb{C}\mathrm{P}^2}$ which intersect the central $+1$ sphere. Furthermore the homological embedding data determines which points to blow up at to get from the blown down configuration to the original configuration. The homological data also determines minimality of the filling appearing as the complement of the concave cap.

Lemma 3.4.4. *Let Γ' be a star-shaped plumbing graph, such that the central vertex corresponds to a symplectic sphere C_0 of self-intersection number $+1$, and all other vertices correspond to symplectic spheres C_i^j of negative self-intersection number. Let E be an embedding of the core symplectic spheres of Γ' into $\mathbb{C}\mathrm{P}^2\#N\,\overline{\mathbb{C}\mathrm{P}^2}$. Then the complement of a*

neighborhood of the image of E is minimal if and only if N is the smallest number of distinct exceptional classes appearing with non-zero coefficient in the homology classes represented by $\{E_*([C_i^j])\}_{i,j}$.

This lemma is a direct consequence of lemma 4.5 of Lisca's paper [Lis08] which says that there is such a disjoint exceptional (J-holomorphic) sphere if and only if there is an exceptional class which does not algebraically intersect any of the spheres (the pseudoholomorphic condition allows us to equate geometric and algebraic intersection numbers).

3.4.2 Uniqueness of the pair after blowing down

The goal of this section is to analyze possible smooth isotopy classes of a regular neighborhood of $d+1$ J_0-holomorphic spheres in $(\mathbb{C}\mathrm{P}^2, \omega_{std})$, each homologous to $\mathbb{C}\mathrm{P}^1 \subset \mathbb{C}\mathrm{P}^2$. We cannot assume that J_0 is the standard almost complex structure on $\mathbb{C}\mathrm{P}^2$ since we had to choose J originally so that each of the curves $C_0 \cdots C_m$ were J-holomorphic. However, because J_0 is tamed by ω_{std}, it is homotopic through almost complex structures tamed by ω_{std} to the standard almost complex structure J_{std}. This homotopy will allow us to isotope our J_0-holomorphic spheres to complex projective lines. Then we will analyze the space of complex projective lines which intersect according to the same combinatorial data.

Working with curves which are J-holomorphic for some J ensures that we need not worry about algebraically cancelling intersection points between curves since all intersections are positive. We want to control the way these $d+1$ spheres intersect, because a smooth isotopy of each of the $d+1$ spheres will extend to a smooth isotopy of a regular neighborhood of their union only when the way these spheres intersect is preserved.

First we would like to smoothly isotope our J_0 holomorphic spheres to complex projective lines, while keeping the intersection configuration fixed. A theorem of Gromov allows us to isotope each of the spheres through J_t-holomorphic curves to complex projective lines, but unfortunately we cannot always preserve the intersection configuration in sufficiently complicated configurations. However we will show that we can control this for configurations where no line passes through more than two multi-intersection points of multiplicity at least three.

These configurations will cover all of those we will obtain by blowing down dual graphs for dually positive Seifert fibered spaces with at most 6 singular fibers or with k singular fibers and $e_0 < -k-1$ (more complicated configurations can arise when $e_0 = -k-1$ and k is large) as in corollary 3.4.2. The reason this covers configurations when $e_0 < -k-1$ comes from the formula for the homology classes in lemma 3.3.8. The dual graph configuration contains one arm made up of a single sphere of square -1, and the homology class of this embedded sphere is $\ell - e_1 - e_2$ up to relabeling the exceptional classes. Every other sphere adjacent to the central vertex must have either e_1 or e_2 appearing with -1 coefficient in its homology class so e_1 and e_2 can correspond to multi-intersection points. No other exceptional classes can appear with non-zero coefficient in more than two of the homology classes of the spheres intersecting the central $+1$ sphere. Therefore there are at most two multi-intersection points of multiplicity greater than two, and if there are two such points then one of the lines of the configuration passes through both of them (the blow-down of the -1 sphere in the dual graph). These configurations appear in figure 3.4. When the number of singular fibers k is at most 6 and $e_0 = -k-1$, there are exactly $k \leq 6$ arms in the dual graph configuration. Thus this blows down to $k+1$ pseudoholomorphic lines, where one necessarily intersects the

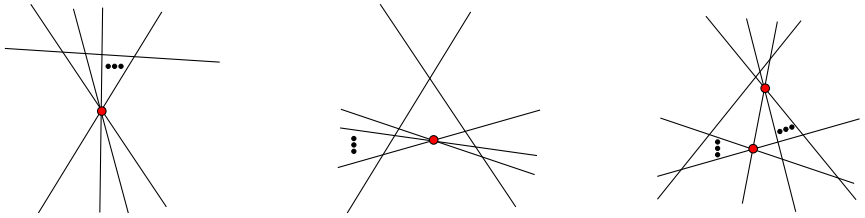

(a) One multi-point, one generic line

(b) One multi-point, two generic lines

(c) Two multi-points, one generic line

Figure 3.4: The combinatorial intersection configurations which can occur after blowing down an symplectic embedding of a star-shaped configuration of spheres, where the central sphere has square $+1$, and there is one arm consisting of a single sphere of square -1. These appear as concave caps for Seifert fibered spaces with $e_0 < -k - 1$.

others generically, so there are not enough lines to form a configuration where any one line passes through more than two multi-intersection points.

Lemma 3.4.5. *Let J be an almost complex structure on $\mathbb{C}\mathrm{P}^2$ tamed by the standard symplectic structure. Suppose $C^0, C^1, \cdots, C^d$ are J-holomorphic spheres embedded in $\mathbb{C}\mathrm{P}^2$ each representing the homology class of the complex projective line ℓ intersecting according to a combinatorial configuration such that no C^j passes through more than two multi-intersection points (points where at least three of the C^j have a common intersection). Then the spheres $C^0, C^1, \cdots, C^d$ can be isotoped to complex projective lines through pseudoholomorphic spheres such that the combinatorial intersection data of the C^j remains unchanged throughout the isotopy.*

Proof. Because J_0 and J_{std} are both tamed by ω_{std}, and the space of such J is contractible and thus connected, there exists a family of almost complex structures $\{J_t\}$ on $\mathbb{C}\mathrm{P}^2$ starting at J_0 and ending at $J_1 = J_{std}$. A theorem of Gromov [Gro85] states that for any J tamed by the standard symplectic structure on $\mathbb{C}\mathrm{P}^2$, any two points $v_1 \neq v_2 \in \mathbb{C}\mathrm{P}^2$ lie on a unique non-

singular rational (i.e. diffeomorphic to S^2) J-holomorphic curve homologous to $\mathbb{C}\mathrm{P}^1 \subset \mathbb{C}\mathrm{P}^2$. Therefore for each J_t in our homotopy, we can find a unique J_t-holomorphic sphere through two given points.

By fixing two points on each sphere and considering the family of J_t-holomorphic spheres through those two points, we get an isotopy $C_t^0, C_t^1, \cdots, C_t^d$ from the original embedded J-holomorphic spheres to complex projective lines. During this isotopy we can fix exactly two points on each sphere. If at a given intersection point, we choose to fix that point on every sphere passing through it, then that intersection is preserved (though potentially other spheres may pass through that point during the isotopy if they are not otherwise constrained). We will fix the multi-intersection points in this way. We are allowed to fix these intersections as long as there are no more than two on each sphere, which is the hypothesis in the proposition. Thus we can choose the isotopy so that at worst the intersection configuration becomes less generic. We will now discuss how to modify this isotopy to one which preserves the intersection configuration throughout.

The first phenomenon which we need to avoid, is that three of the multi-intersection points which we fix throughout the isotopy could become J_t-collinear for some $t > 0$, meaning that they all lie on the same J_t-holomorphic sphere in the homology class ℓ. Our initial assumption says that this does not occur for $t = 0$, so if it occurred for $t > 0$ this would allow C_t^i and C_t^j to coincide for $i \neq j$ in certain configurations and thus change the intersection configuration drastically. To ensure this does not occur, we will perform small isotopies at the beginning, to move these fixed multi-intersection points. We have fixed the family $\{J_t\}_{t\in[0,1]}$. Choose an ordering of the multi-intersection points in $\mathbb{C}\mathrm{P}^2$, $p_1, p_2, p_3, \cdots, p_z$. Leaving p_1 and p_2 fixed, consider the union of the J_t-holomorphic lines through p_1 and p_2 over all $0 \leq t \leq 1$.

This subset of $\mathbb{C}\mathrm{P}^2$ will have at least codimension one. Therefore, if p_3 lies in this subset, it can be perturbed slightly to p_3' so that it no longer is J_t-collinear with p_1 and p_2 for any t. Define an isotopy of the curves $C^0, C^1, \cdots, C^d$ by choosing a path $\gamma(s)$ from p_3 to p_3'. For each sphere C^j passing through p_3, if it passes through another p_i fix that point, and if not choose any other point on the sphere to fix. Then isotope C^j by defining C^j_s as the unique J_0-holomorphic sphere through the chosen fixed point and $\gamma(s)$. For each sphere that does not pass through p_3, fix it throughout this isotopy. By choosing the perturbation p_3' sufficiently close to p_3, we can ensure that the intersection configuration of $C^0, C^1, \cdots, C^d$ is unchanged during this small isotopy.

Now consider the space of J_t lines through p_1 and p_2, p_2 and p_3, and p_1 and p_3 varying with t. Again this subspace has at least codimension one, so p_4 can be perturbed to avoid this subspace and a corresponding isotopy of the C^j can be defined preserving the intersection configuration. Continue this process for each of the multi-intersection points. This shows that up to J_0-holomorphic isotopy, we can assume that no triple of the multi-points is J_t-collinear for any $t \in [0, 1]$.

Now, after any needed perturbations in the previous step, redefine the isotopy C^0_t, $C^1_t, \cdots, C^d_t$ by fixing two points on each of (the newly isotoped) $C^0, C^1, \cdots, C^d$, including all of the multi-intersection points and considering the unique J_t-holomorphic line through those two points. Consider any pair $C^j_t, C^{j'}_t$ which both pass through exactly two multi-intersection points. If they intersect at a fixed multi-point, their intersection remains fixed for all t. If they do not intersect at one of the fixed multi-intersection points, then their intersection will never occur at one of those fixed multi-intersection points because no three of those points ever lie on the same J_t-holomorphic line. Thus the only way the intersection configuration

can change is if one $C_t^{j_0}$ which passes through at most one fixed multi-intersection point passes through an intersection point of two or more spheres that it is not supposed to.

We will remove any such degeneracies by perturbing the relevant $C_t^{j_0}$'s one at a time. We can isotope each such $C_t^{j_0}$ through J_t-holomorphic spheres to avoid this phenomenon as follows. Suppose $C_t^{j_0}$ passes through the intersection of spheres $C_t^{j_1}, \cdots, C_t^{j_p}$ for $t \in \mathbf{T}$ when it shouldn't according to the original intersection configuration. Parameterize a neighborhood of this intersection point on $C_t^{j_1}$ by a small disk centered on the degenerated intersection point. Let $\eta^\theta(r)$ parameterize a ray from the center of the disk to a circle of radius ε and angle θ. Define $C_{t,r}^{j_0}$ to be the unique sphere through the point $\eta^{\theta_0}(r)$ and any multi-point that $C_0^{j_0}$ is supposed to pass through, or if $C_0^{j_0}$ does not pass through any multi-intersection point, some other fixed point on $C_t^{j_0}$ away from $C_t^{j_1}$. Defining $C_{t,r}^j = C_t^j$ for $j \neq j_0$, we get a 2-parameter family of configurations of spheres. The multi-intersection points are fixed for all r, t. By choosing the length of the ray ε sufficiently small, we can ensure that no new degeneracies of the configuration are introduced by the r-isotopy away from the degeneracy we are focusing on. Now for $r > 0$ and $t \in \mathbf{T}$, $C_{t,r}^{j_0}$ does not pass through $C_{t,r}^{j_1} \cap \cdots \cap C_{t,r}^{j_p}$ so the degeneracy is removed for the times of initial concern. However, it is possible that this degeneracy appears for $r > 0$ for other times $t \in I \setminus \mathbf{T}$ where a degeneracy did not previously exist. We indicate this schematically in figure 3.5, where the red indicates points (t, r) where the degeneracy occurs where $C_{t,r}^{j_0}$ passes through $C_{t,r}^{j_1} \cap \cdots \cap C_{t,r}^{j_p}$.

The key to finding an isotopy without these degeneracies is that we have an extra dimension to perturb in. Instead of requiring $C_{r,t}^{j_0}$ to pass through the point $\eta^{\theta_0}(r)$ on $C_t^{j_1}$ we can vary the angle θ. For each fixed t and corresponding almost complex structure J_t there is a unique point on $C_t^{j_1}$ which we are trying to make $C_t^{j_0}$ avoid: its intersection

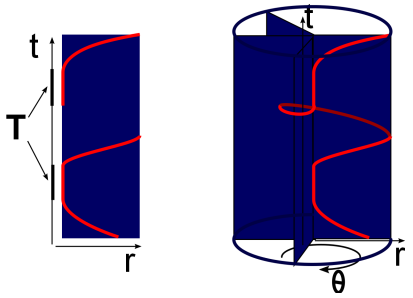

Figure 3.5: Schematic for an isotopy of a configuration and its potential to degenerate. By utilizing the angular dimension there is a path from $s = 0, t = 0$ to $t = 1$ which avoids the red degenerate points.

with $C_t^{j_2}, \cdots, C_t^{j_n}$. Therefore, if the degeneracy occurs at some (r_0, t_0) using the ray at angle θ_0, it will not occur at (r, t_0) for any r using a different angle θ'. Thus we remove the degeneracy by modifying this isotopy by replacing $\eta^{\theta_0}(r)$ by $\eta^{\theta_t}(r)$ where θ_t is an angle chosen as a function of t to avoid the degeneracy we are focusing on. The essential idea for this argument is that we can perturb the line in a real 2-dimensional space (because we are only trying to fix at most one multi-intersection point on the complex line) and the degeneracies we want to avoid are 0-dimensional, so we can find a 1-parameter family of configurations which avoid the degeneracies. We repeat this for other spheres contributing to degeneracies and eventually find an isotopy from the J_0-holomorphic configuration we started with (at $r = t = 0$) to a J_{std}-holomorphic (complex) configuration (at $t = 1$).

□

This tells us that, if there are no more than two multi-intersection points on any curve, all J-holomorphic configurations for J tamed by ω_{std} are isotopic. Now we would like to determine the number of isotopy classes of J-holomorphic configurations in given combinatorial arrangements of the types covered by lemma 3.4.5.

Lemma 3.4.6. *Fix an almost complex structure J on $\mathbb{C}\mathrm{P}^2$ tamed by the standard symplectic structure. Let $\mathcal{I}$ be a combinatorial intersection configuration of lines in which no line passes through more than two multipoints. Then the space of J-holomorphic lines with combinatorial intersection configuration $\mathcal{I}$ is path-connected and non-empty.*

Proof. It is well known that through any two points in $\mathbb{C}\mathrm{P}^2$ there is a unique complex projective line. The same is true for J-holomorphic spheres in the homology class of a complex projective line by Gromov [Gro85]. Each multi-intersection point in the configuration $\mathcal{I}$ (where at least three lines pass through the same point), must be placed somewhere in $\mathbb{C}\mathrm{P}^2$. The multi-intersection points must be placed at different positions and no three of them should be co-linear. The space of such points is parameterized by $(\mathbb{C}\mathrm{P}^2)^{\times M} \setminus (\Delta \cup \Lambda)$ where Δ indicates the fat diagonal consisting of points $(x_1, \cdots, x_M)$ where $x_i = x_j$ for some $i \neq j$, and Λ consists of the set of points $(x_1, \cdots, x_M)$ where x_i, x_j, x_k are J-collinear for distinct $i, j, k \in \{1, \cdots, M\}$. As discussed in the previous lemma, Δ and Λ have co-dimension ≥ 2 in $(\mathbb{C}\mathrm{P}^2)^{\times M}$ so $(\mathbb{C}\mathrm{P}^2)^{\times M} \setminus (\Delta \cup \Lambda)$ is a connected, non-empty, non-compact manifold of dimension $4M > 0$. We can parameterize the space of J-holomorphic lines with combinatorial intersection $\mathcal{I}$ where the multi-intersection points occur at a fixed $(\alpha_1, \cdots, \alpha_M) \in (\mathbb{C}\mathrm{P}^2)^{\times M} \setminus (\Delta \cup \Lambda)$ as follows. We will build up the configuration space by placing the lines one by one and adding an additional product factor to the configuration space for each line. For any line in the configuration which passes through two multi-intersection points, its position is completely determined by J and the points α_i and α_j in $\mathbb{C}\mathrm{P}^2$ which it is required to pass through. Thus the configuration space for placing each of these J-holomorphic lines is a single point (so they are trivial product factors in the configuration space). For J-holomorphic lines which pass through only one multi-intersection point α_i, the space of possibilities for such

a line is path-connected and (real) 2-dimensional, and there is a 0-dimensional subspace which must be removed corresponding to the lines which pass through α_i and some other α_j. This can be more precisely parameterized by the points on any chosen J-holomorphic lines which is disjoint from α_i, minus the points on that line which are J-collinear with α_i and some other α_j. For J-holomorphic lines which pass through no multi-intersection points, there is a path-connected real 4-dimensional space of possibilities parameterized by pairs of points on a chosen pair of J-holomorphic lines disjoint from the α_i, with a 2-dimensional subspace removed consisting of pairs of points which are J-collinear with some α_i. The product of these path-connected non-empty factors will again be path-connected and non-empty. From this product we must remove some further subspaces corresponding to configurations where two of the lines (which pass through 0 or 1 multi-intersection point) coincide, or intersect non-generically at a point that is not an α_i. Similarly to the previous lemma, these subspaces have co-dimension at least 2, so removing them does not change the connectedness or non-emptyness of the configuration space. Thus the configuration space $\mathcal{M}_{\mathcal{I},J}$ of J-holomorphic lines intersecting according to $\mathcal{I}$ maps to $(\mathbb{C}\mathrm{P}^2)^{\times M} \setminus (\Delta \cup \Lambda)$ by specifying the multi-intersection points, and the fiber above each $(\alpha_1, \cdots, \alpha_M)$ is connected and non-empty. We conclude that $\mathcal{M}_{\mathcal{I},J}$ is connected and non-empty as claimed. □

Remark: In contrast, if we considered a configuration where some of the lines passed through three or more multi-points, the fact that such a line exists puts a constraint on the variables determining the earlier lines. In the standard complex case, these yield polynomial relations on the homogeneous coordinates of the points determining the lines. With sufficiently many lines, one can construct intersection configurations for which the space of complex projective lines in that configuration is disconnected or empty. It is interesting to

study whether the combinatorial arrangements that can be realized by complex projective lines are the same as those which can be realized by J-holomorphic versions for other almost complex structures.

3.5 Finite classification results

We conclude this chapter by bringing these results together to deduce a finite classification theorem.

Theorem 3.5.1. *If Y is a Seifert fibered space with k singular fibers and either*

1. *$e_0 = -k - 1$ and $k \leq 6$, or*
2. *$e_0 \leq -k - 2$*

then (Y, ξ_{pl}) has finitely many minimal strong symplectic fillings up to diffeomorphism. Loose upper bounds can be computed directly from the Seifert invariants.

Proof. From sections 3.1 and 3.2 we deduced that for a given such Y, there is a chosen concave plumbing of spheres, and strong symplectic fillings of Seifert fibered spaces all arise as the complement of a symplectic embedding of this concave plumbing into $\mathbb{C}\mathrm{P}^2 \# N\, \overline{\mathbb{C}\mathrm{P}^2}$ for some N. The fillings are minimal precisely when N is the smallest number of exceptional classes appearing with non-zero coefficient in the homology class of some sphere of the concave plumbing. By section 3.4 and specifically corollary 3.4.2 we conclude that for each induced map on second homology, there is a unique smooth isotopy class of embeddings of the concave plumbing. Therefore the theorem follows from an upper bound on the number of possible distinct induced maps on second homology.

By lemmas 3.3.1 and 3.3.2, the homology classes of the C_i^j in terms of the standard basis for $H_2(\mathbb{C}\mathrm{P}^2 \# N\,\overline{\mathbb{C}\mathrm{P}^2})$ have the forms

$$[C_1^j] = \ell - e_{m_1}^{1,j} - \cdots - e_{m_{n_{1,j}+1}}^{1,j}$$

and for $i > 1$

$$\left[C_i^j\right] = e_{m_0}^{i,j} - e_{m_1}^{i,j} - \cdots - e_{m_{n_{i,j}-1}}^{i,j}$$

so up to symmetry of relabelling the exceptional classes, the only possible differences between homological embeddings are determined by which exceptional classes appear with non-zero coefficient in which collections of sphere classes. To obtain precise bounds, there is a combinatorial problem to solve subject to restrictions determined by the intersection data of the spheres (lemmas 3.3.3, 3.3.5, 3.3.6, and 3.3.7), but we can easily get a very loose upper bound on the number of possibilities. If $S = \sum_{i,j}(n_{i,j}+1)$, then there are less than S different exceptional classes which have non-zero coefficient in any $[C_j]$. Thus there are less than S^S arrangements of these e_i into the slots above, thus giving an upper bound on the number of induced maps on second homology. □

Chapter 4

Explicit classifications and examples

In this chapter we will provide classifications and examples of symplectic fillings for many families of Seifert fibered spaces. We will start with a very explicit simple example and work out all of the details carefully in this case. Later examples will follow similar methods so some of the intermediate steps will be abbreviated. To understand these examples explicitly and to discover Lefschetz fibrations supporting these fillings, we will make significant use of handlebody diagrams and Kirby calculus tools. A reader unfamiliar with these tools should certainly spend some time with part 2 of the book by Gompf and Stipsicz [GS99].

4.1 Simplest Examples

Because the number of symplectic fillings is determined by possible ways of writing the homology classes of the spheres in the dual graph, one can obtain a simple family of examples by insisting that the dual graph is star-shaped with three arms, and each arm has length one as in figure 4.1b. These are the dual graphs of three armed graphs with central vertex decorated by -4 and all other vertices decorated by -2. These graphs depend on three positive integer parameters n_1, n_2, and n_3 which determine the lengths of the arms as in figure 4.1a, and are the negations on the coefficients of the spheres in the arms of the dual graph. We work through the classification of convex fillings for this example in full detail to

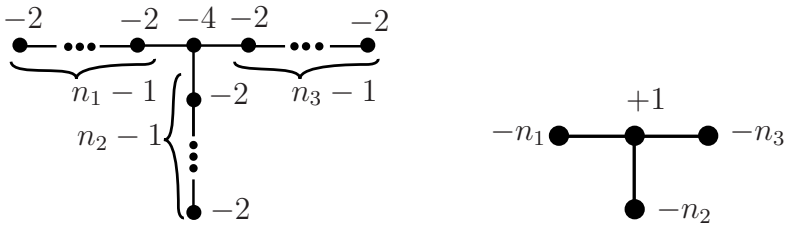

(a) Graphs (b) Dual Graphs

Figure 4.1: The graphs and dual graphs representing a simple family of plumbings.

make it clear how to obtain the possible diffeomorphism types of symplectic fillings from the homological restrictions. In this simple example we will label the three spheres in the three arms of the dual graph C_1, C_2, and C_3.

Now we need to determine the possible ways to write $[C_0], [C_1], [C_2], [C_3]$ in terms of the standard basis $(\ell, e_1, \cdots, e_M)$ for $H_2(X_M; \mathbb{Z})$. By lemma 3.3.1, we know that they must have the form

$$\begin{aligned}
[C_0] &= \ell \\
[C_1] &= \ell - e_{i_1^1} - \cdots - e_{i^1_{n_1+1}} \\
[C_2] &= \ell - e_{i_1^2} - \cdots - e_{i^2_{n_2+1}} \\
[C_3] &= \ell - e_{i_1^3} - \cdots - e_{i^3_{n_3+1}}
\end{aligned}$$

and by lemma 3.3.3, $|\{i_1^j, \cdots, i^j_{n_j+1}\} \cap \{i_1^{j'}, \cdots, i^{j'}_{n_{j'}+1}\}| = 1$ for $j \neq j' \in \{1, 2, 3\}$. There are exactly two different ways three sets can have each pairwise intersection be a unique element. The first is that they all share a single element in common, and the second is that each of the three pairs has a different common element. Up to relabeling, the two possibilities are as follows.

Case A			Case B		
$[C_0]$	$=$	ℓ	$[C_0]$	$=$	ℓ
$[C_1]$	$=$	$\ell - e_1 - e_1^1 - \cdots - e_{n_1}^1$	$[C_1]$	$=$	$\ell - e_1 - e_2 - e_1^1 - \cdots - e_{n_1-1}^1$
$[C_2]$	$=$	$\ell - e_1 - e_1^2 - \cdots - e_{n_2}^2$	$[C_2]$	$=$	$\ell - e_1 - e_3 - e_1^2 - \cdots - e_{n_2-1}^2$
$[C_3]$	$=$	$\ell - e_1 - e_1^3 - \cdots - e_{n_3}^3$	$[C_3]$	$=$	$\ell - e_2 - e_3 - e_1^3 - \cdots - e_{n_3-1}^3$

Note here all of the e_i^j are all distinct from each other and from the e_m's.

Now we can see how each of these translates into an embedding of the dual configuration. After blowing down all exceptional spheres, the proper transform of the image of the dual graph spheres under the embedding will be four symplectic spheres homologous to $\mathbb{C}\mathrm{P}^1$, and by lemma 3.4.5 we may assume that they are four complex projective lines. In case A, e_1 appears in $[C_1], [C_2]$ and $[C_3]$ with non-zero coefficient, so when we blow up the sphere representing e_1, it will be at a point of intersection of three of the original $+1$ spheres. The remaining blow-ups are done on a point of a single one of these three spheres, so that the resulting proper transforms have sufficiently negative self-intersection numbers.

In a Kirby diagram, the original four complex projective lines are represented by four $+1$ framed unknots with a single positive twist as in figure 4.2a. In order to ensure this is a diagram for $\mathbb{C}\mathrm{P}^2$, we cancel the extra three 2-handles with three 3-handles, and close off the manifold with a 4-handle. The first blow-up in case A introduces a new -1 framed unknot which links three of the four original link components, untwists these three components, and reduces the framing coefficients on each by 1. The remaining blow-ups in case A introduce more -1 framed unknots which link once with one of the three untwisted original link components and reduce the corresponding framing coefficient by 1. The resulting diagram is shown in figure 4.2b.

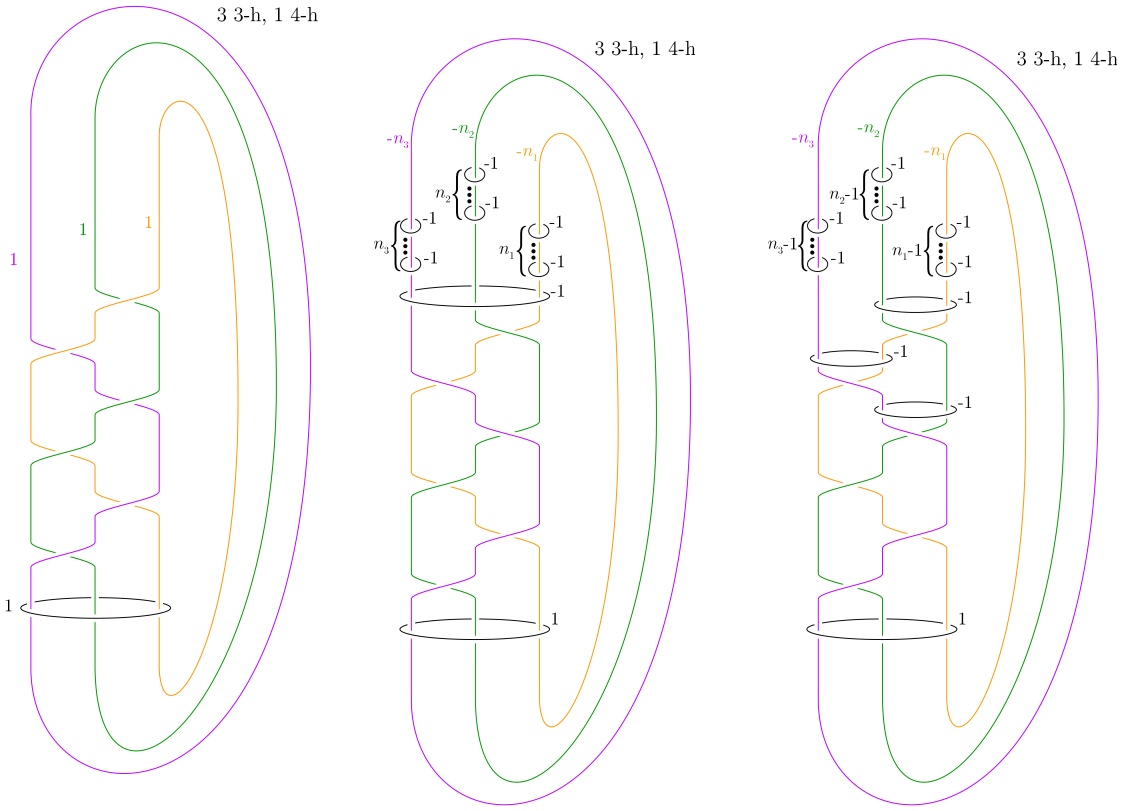

(a) Diagram for $\mathbb{C}P^2$ with four +1 spheres.

(b) Blow up in case A.

(c) Blow up in case B.

Figure 4.2

Similarly in case B, the blow-ups corresponding to e_1, e_2, e_3 are done at intersections of the three pairs C_1, C_2, and C_3, and the other blow-ups are done at points on only one of their proper transforms. In the Kirby diagram, these are visible in figure 4.2c.

The concave dual plumbing spheres are is visible in each of the diagrams for a blow-up of $\mathbb{C}\mathrm{P}^2$ as the union of the cores of four 2-handles together with their Seifert surfaces pushed into the 0-handle. We wish to find the diffeomorphism types of the complements of these embeddings, since these are the potential symplectic fillings.

Because the union of the Seifert surfaces of the four attaching circles for C_0, C_1, C_2, C_3 is connected, their complement in the 0-handle retracts to a subset of the boundary of the 0-handle. Therefore the complement of the dual configuration is given by deleting the 0-handle and the four 2-handles corresponding to C_0, C_1, C_2, C_3. It is easier to understand the diffeomorphism type of the resulting manifold with boundary by turning the manifold upside down so the boundary appears on the top instead of on the bottom. Since both possible diagrams (figures 4.2b and 4.2c) have three 3-handles, the resulting upside-down handlebody in the complement of the dual configuration will have three 1-handles, together with 2-handles corresponding to all the extra 2-handles in the diagram which are not part of the dual configuration, coming from the blow-ups. The boundary of the 0-handle and 1-handles is $\#_3 S^2 \times S^1$. This appears as a surgery diagram given by the mirror image of the original diagram with surgery coefficients the negations of the framings. Surgery coefficients are put in brackets, $\langle \cdot \rangle$. An attaching circle of an upside down 2-handle will be a 0-framed meridian of the surgery circle corresponding to the attaching circle of the original 2-handle (see [GS99] for more details on turning handlebodies upsidedown). In order to get the diagram into a more standard form, we perform diffeomorphisms on the boundary between

the 1-handlebody and the 2-handles until the boundary looks standard (like 0-surgery on the three component unlink). Once the boundary of the 1-handlebody looks standard, we can replace each zero surgered unlink component with a dotted circle representing a 1-handle. The corresponding diagrams are in figures 4.3a and 4.3c. Further handleslides and 1-2 handle cancellations yield figure 4.3d.

Notice that the diagram in figure 4.3d is the original plumbing of spheres, which we know has a standard symplectic structure with convex boundary inducing ξ_{pl} by theorem 2.4.1.

In the embedding in figure 4.2c determined by case B, we find a different possible diffeomorphism type for a symplectic filling. The complement of the dual configuration turned upsidedown is given by figure 4.4a. Figures 4.4b, 4.4c, and 4.4d are obtained by surgery and handle moves.

Note that the resulting manifold in figure 4.4d for case B can be obtained from the resulting manifold in figure 4.3d by a rational blow-down of the -4 framed sphere (the 1-handle and the black 2-handle form a rational homology ball). Because the symplectic structure on the manifold in figure 4.3d, has the -4-framed sphere as a symplectic submanifold, by an observation of Gompf [Gom95] we can cut out this -4-framed sphere and replace it with the rational homology ball as in figure 4.4d such that the symplectic structure extends over the rational homology ball. Note that this does not change the symplectic structure in a neighborhood of the boundary of the plumbing of spheres in figure 4.3d, so the boundary remains convex and induces the same contact structure ξ_{pl}.

Alternatively we can arrange this diagram to be a Stein handlebody. If we arrange

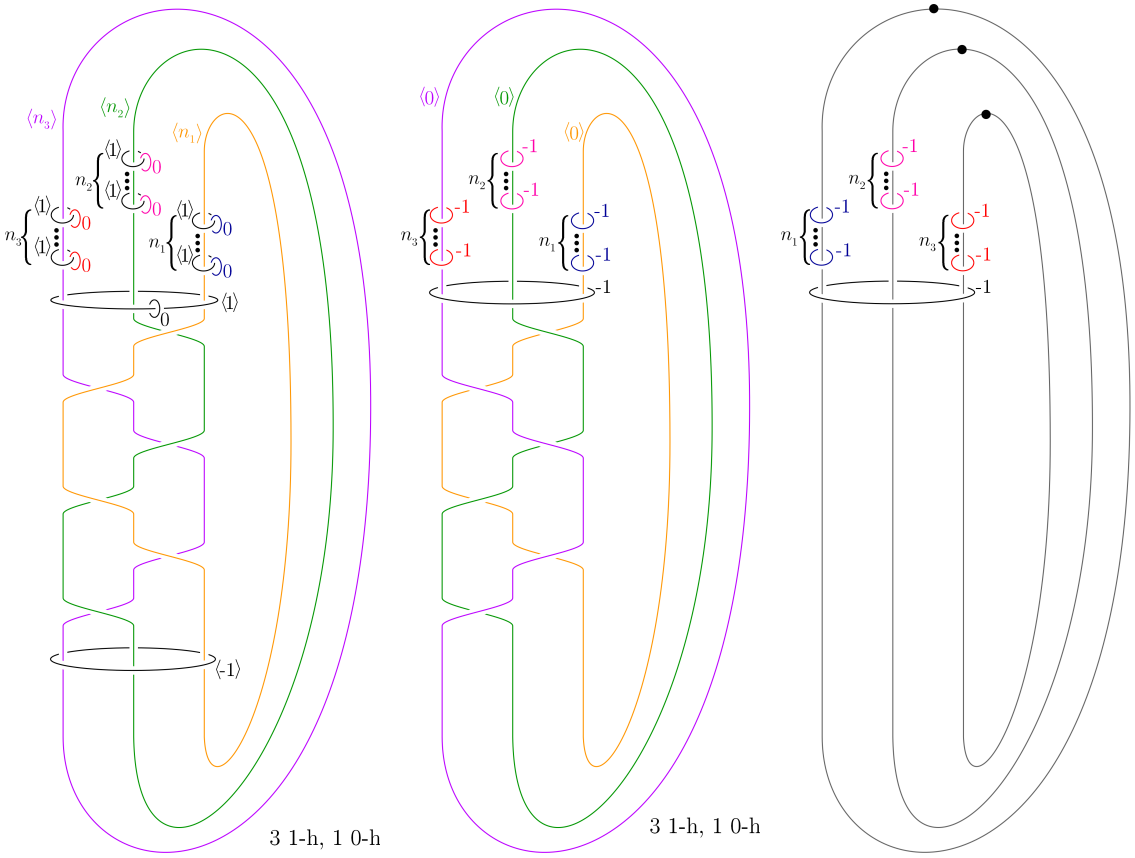

(a) Upsidedown complement of dual configuration in case A

(b) Moves on surgery diagram

(c) Simplified and using dotted circle notation

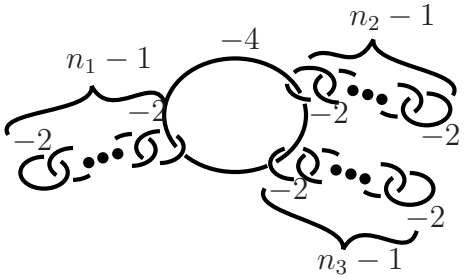

(d) Handleslides and cancellations

Figure 4.3: The diffeomorphism type of the possible symplectic filling from case A.

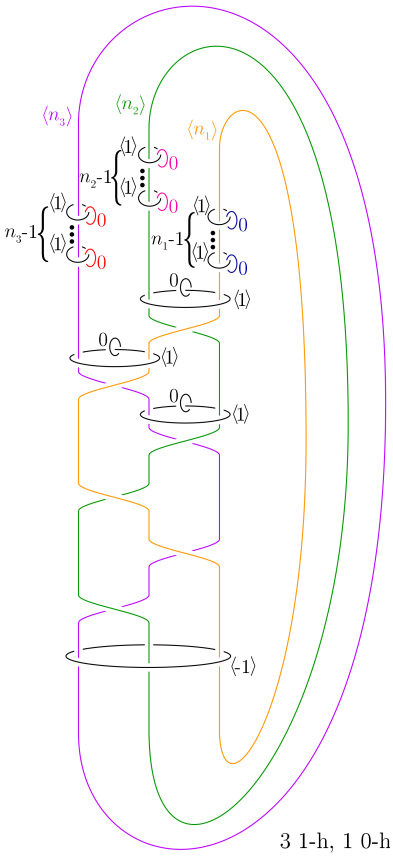

(a) Upsidedown complement of dual configuration in Case B

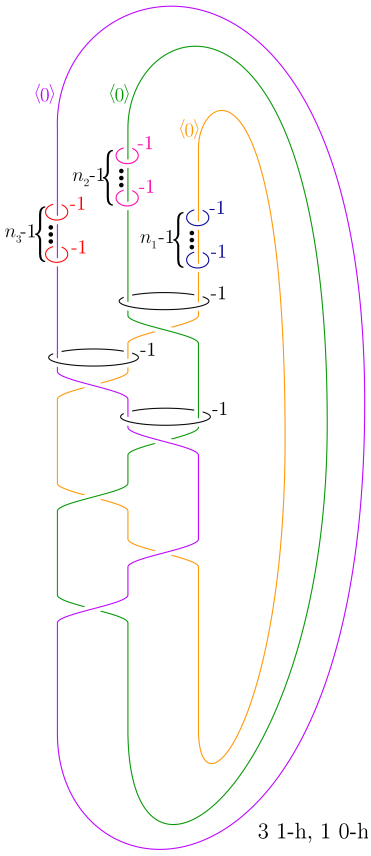

(b) Moves on surgery diagram

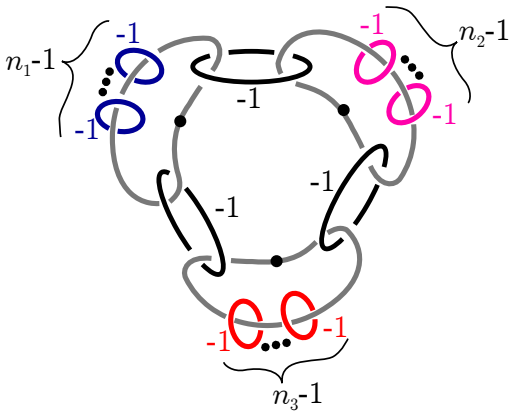

(c) Dotted circle notation

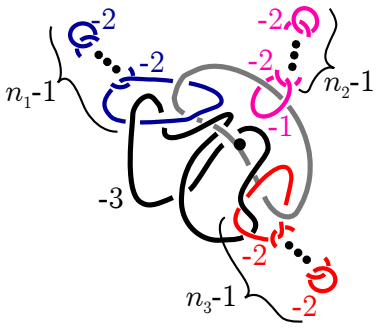

(d) Handle cancellation

Figure 4.4: The diffeomorphism type of the possible symplectic filling from case B.

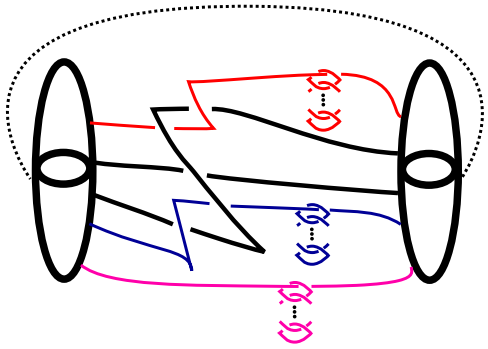

Figure 4.5: Stein handlebody for figure 4.4d. Framings on 2-handles are given by 1 less than the Thurston-Bennequin number of the attaching circle.

that the Kirby diagram is in a standard form such that all the 2-handles are contained in a rectangular box, the two attaching balls for each of the 1-handles are aligned on opposite sides of the box, and the 2-handles are attached along Legendrian tangles inside the box such that the framing coefficient is given by 1 less than the Thurston-Bennequin number of the attaching circle then there exists a Stein structure on this 4-manifold (by [Eli90b], [Gom98]). Replacing the dotted circle in figure 4.4d with two attaching balls, and keeping track of framings carefully, after isotopies we can achieve a diagram where the 2-handles are attached along Legendrian knots with framing coefficients given by $tb - 1$ in figure 4.5. To verify that the contact structure is correct, we look at the classification of contact structures on these Seifert fibered spaces. In these cases, there are three distinct contact structures which are distinguished from each other by their Euler class. We can compute the Euler class of the induced contact structure on the boundary of a Stein manifold in a standard way involving rotation numbers of the attaching circles (see [Gom98]). To check this matches the Euler class of the contact manifold we started with, track $PD(e(\xi))$ through a diffeomorphism taking this diagram representing the 3-manifold to the standard one as the boundary of a

star-shaped plumbing of spheres.

A third way to see the convex symplectic structure on this manifold is to view it as a Lefschetz fibration over a disk. By rotating the projection plane of the diagram in figure 4.4b by 90° (look at the diagram in figure 4.4b from the left side of the page), and then using dotted circle notation, we get figure 4.7a. We claim this diagram represents Lefschetz fibrations which induces an open book decomposition on its boundary that support the contact structure ξ_{pl}. The Lefschetz fibration will have base D^2 and regular fibers 3-hold disks, $D_3 = D^2 \setminus \{N(p_1), N(p_2), N(p_3)\}$ where $\{N(p_i)\}$ are disjoint neighborhoods of points contained in the interior of D^2. We obtain a handlebody diagram for $D^2 \times D_3$ from the 3 disjoint parallel dotted circles, because one can think of a dotted circle as the removal of a 2-handle from the interior of the 0-handle. If we view the 0-handle as $D^2 \times D^2$, we can view the dotted circles as removing a neighborhood of $D^2 \times \{p_i\}$. Then we attach the -1 framed 2-handles along the boundary of $D^2 \times D_3$. We can see a trivial open book decomposition with pages D_3 on $\partial(D^2 \times D_3) = S^1 \times D_3 \cup D^2 \times [\partial\, D^2 \sqcup \partial\, N(p_1) \sqcup N(p_2) \sqcup \partial\, N(p_3)]$. Note that each attaching circles of a 2-handles lies in a page of this trivial open book and the Seifert framing in the handlebody diagram agrees with the page framing coming from this open book decomposition. Therefore the framing on the 2-handles is -1 relative to the page framing, so the attaching circles are vanishing cycles in a Lefschetz fibration.

It is useful to understand the open book decomposition supporting ξ_{pl} given to us by theorem 2.4.1. The construction of Gay and Mark tells us that the pages of the open book are given by the surface obtained by connect summing $|s_j|$ copies of D^2 to each sphere C_j in our graph, and then connect summing these surfaces according to the plumbing graph. In our case, the central sphere C_0 has $s_0 = -4+3 = -1$, the spheres in the arms but not on the

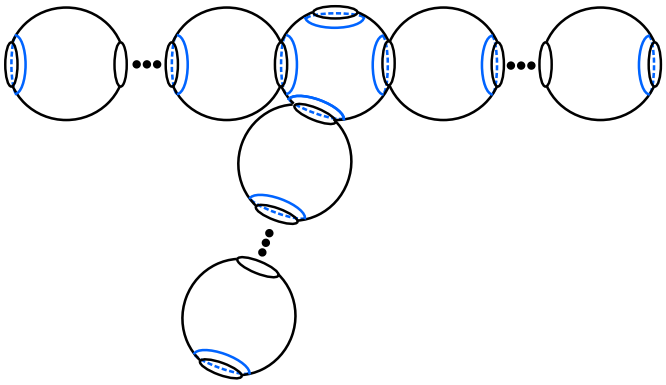

Figure 4.6: A page of the open book decomposition supporting ξ_{pl} given by [GM13]. A product of Dehn twists about the blue curves gives the monodromy.

ends have $s_j = -2 + 2 = 0$, and the spheres on the ends have $s_j = -2 + 1 = -1$. Therefore the pages are surfaces as in figure 4.6. The monodromy is given by a product of positive Dehn twists about the simple closed curves around each connect sum neck, shown as the blue curves in figure 4.6. Note that the order of these Dehn twists does not matter, because the curves are all disjoint from each other so the corresponding Dehn twists commute in the mapping class group.

On the other hand, our Lefschetz fibration induces an open book decomposition on its boundary whose pages are disks with three holes and whose monodromy is a product of positive Dehn twists about the vanishing cycles ordered as in figure **??**. This monodromy is equivalent by a lantern relation to positive Dehn twists about the curves in figure 4.7c, which is equivalent to the open book decomposition determined by figure 4.6 which we know supports ξ_{pl}. Therefore our filling has the structure of a Lefschetz fibration which induces an open book decomposition on its boundary that supports the contact structure ξ_{pl} we are interested in.

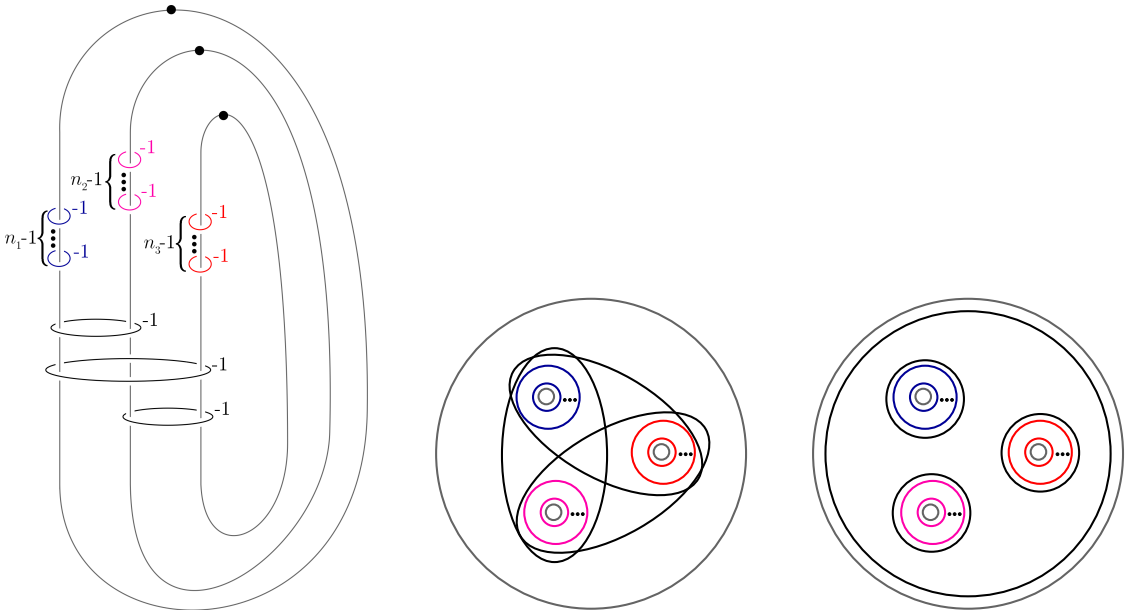

(a) Lefschetz fibration (b) Open book decomposition (c) Equivalent open book

Figure 4.7: The Lefschetz fibration is visible in this handlebody description of the second symplectic filling, and the open book decomposition induced on the boundary has monodromy given by a product of positive Dehn twists about the curves pictured here.

Since the vanishing cycles in this Lefschetz fibration are homologically essential, this 4-manifold supports a Stein structure, inducing ξ_{pl} on the boundary. The Stein structure induces a convex symplectic structure on this filling.

We can conclude from this detailed analysis multiple ways of seeing the following classification for this case.

Theorem 4.1.1. *If (Y, ξ_{pl}) is the convex boundary of a dually positive plumbing of spheres, where the star-shaped graph has exactly three arms, the central vertex has self-intersection coefficient -4, and each arm has arbitrary length, but each sphere in any arm has self-intersection coefficient -2 then (Y, ξ_{pl}) has exactly two minimal strong symplectic fillings up to diffeomorphism, given by the original symplectic plumbing and the manifold obtained by rationally blowing down the central -4 sphere.*

4.2 A family with $e_0 \leq -k-3$

We can provide a complete classification for a similar family to our simplest family in the case where e_0 is sufficiently negative.

Theorem 4.2.1. *If (Y, ξ_{pl}) is the boundary of a dually positive plumbing of spheres with k arms, where the coefficient on the central vertex is $e_0 \leq -k-3$, and the coefficients on the spheres in the arms are all -2, then all diffeomorphism types of minimal strong symplectic fillings are obtained from the original plumbing of spheres by a rational blow-down of the central vertex sphere together with $-e_0 - 4$ spheres of square -2 in one of the arms.*

Proof. When the central vertex on our graph is labeled by $e_0 \leq -k-3$ where k is the number of arms in our graph, the dual graph will have $d = -e_0 - 1$ arms, where $d-k$ of these arms

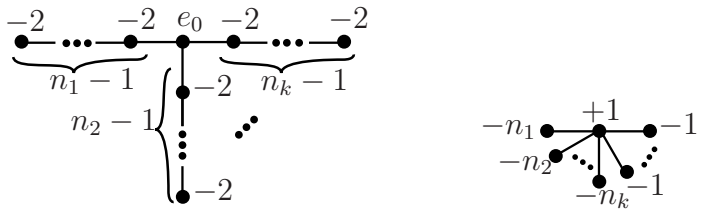

(a) Graphs (b) Dual graphs

Figure 4.8: A simple family of graphs and their dual graphs ($e_0 \leq -k-3$ and $n_1, n_2, \cdots, n_k \geq 2$).

are made up of a single symplectic sphere of square -1. If we assume all the arms of the dual graph have length one, the possible homology classes each dual graph sphere can represent is completely determined by lemma 3.3.8. The graphs that these correspond to have central vertex with coefficient e_0 and k arms, each made up of some number of spheres of square -2 as in figure 4.8.

When $\max\{n_1, \cdots, n_k\} < d-2 = -e_0 - 3$, only one of the homology representations in lemma 3.3.8 is possible and this corresponds to the diffeomorphism type of the original plumbing of disk bundles over spheres. When $\max\{n_1, \cdots, n_k\} \geq d-2 = -e_0 - 3$, we have other diffeomorphism types obtained from the original plumbing of disk bundles over spheres by a rational blow-down of a linear subgraph consisting of the central vertex and the next $-e_0 - 4$ spheres of square -2 in one of the arms. Such rational blow-downs were shown to be symplectic operations by Symington in [Sym98]. Since we can perform this operation on the interior of the filling, this will not change the convex symplectic structure near the boundary. Therefore we can realize all these diffeomorphism types as convex symplectic fillings. The handlebody diagrams of these embeddings, and the Lefschetz fibrations on their complements are described in section 6.2.2. □

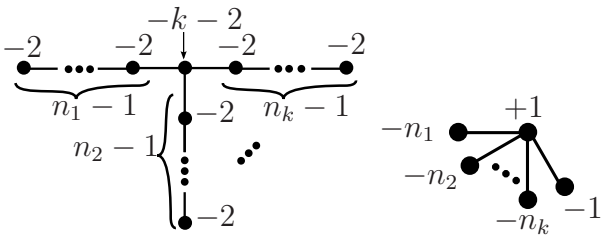

(a) Graphs (b) Dual graphs

Figure 4.9: Graphs and dual graphs for a family where $e_0 = -k-2$.

4.3 New fillings in the case $e_0 = -k-2$

The previous section considered families of dual graphs which include an arm with a single -1 sphere where all of the complementary fillings are obtained by already well understood operations: the Fintushel-Stern rational blow-downs. Here we consider the case when $e_0 = -k-2$ to utilize the final and most interesting homological arrangements specified in lemma 3.3.8. The corresponding fillings are genuinely new, which will be discussed in greater detail in section 5. The graphs and dual graphs we consider here are shown in figure 4.9.

As in the case where $e_0 \leq -k-3$, each corresponding Seifert fibered space has one convex filling given by the plumbing according to the graph of figure 4.9a, and others given by a rational blow-down of the linear chain consisting of the central sphere of square $-k-2$ and $k-2$ spheres of square -2 from the i^{th} arm, assuming that arm has length at least $k-2$ (equivalently $n_i \geq k-1$). When $e_0 \leq -k-3$ these were the only symplectic fillings, but when $e_0 = -k-2$, we have additional fillings coming from the last possibility in lemma 3.3.8, assuming certain other inequalities on the n_i. We recall the homological possibilities

from lemma 3.3.8 here for easy reference:

$$\begin{array}{lcl}
[C_0] & = & \ell \\
[C_1^1] & = & \ell - e_1 - e_{m(1,j+1)} - e_{m(1,j+2)} \cdots - e_{m(1,k)} - e_\cdot - \cdots - e_\cdot \\
 & \vdots & \\
\left[C_1^j\right] & = & \ell - e_1 - e_{m(j,j+1)} - e_{m(j,j+2)} \cdots - e_{m(j,k)} - e_\cdot - \cdots - e_\cdot \\
\left[C_1^{j+1}\right] & = & \ell - e_2 - e_{m(1,j+1)} - e_{m(2,j+1)} - \cdots - e_{m(j,j+1)} - e_\cdot - \cdots - e_\cdot \\
 & \vdots & \\
\left[C_1^k\right] & = & \ell - e_2 - e_{m(1,k)} - e_{m(2,k)} - \cdots - e_{m(j,k)} - e_\cdot - \cdots - e_\cdot \\
\left[C_1^{k+1}\right] & = & \ell - e_1 - e_2
\end{array}$$

Here $m(a,b)$ are distinct for distinct pairs (a,b), and are distinct from $1,2$. Thus the inequalities that must be satisfied for the n_i (up to reordering the arms) for these possibilities indexed by j are $n_1, \cdots, n_j \geq k-j$ and $n_{j+1}, \cdots, n_k \geq j$. Note that the degenerate case $j=0$ (or symmetrically $j=k$) gives the homological embedding corresponding to the convex plumbing and $j=1$ (or symmetrically $j=k-1$) gives the rational blow-down case that appeared previously, but we get new possibilities for $1 < j < k-1$. Note that the n_i can satisfy the inequalities for some values of j but not others and the number of distinct symplectic fillings will be affected by this.

Theorem 4.3.1. *If (Y, ξ_{pl}) is the convex boundary of a symplectic plumbing according to the graph of figure 4.9a, then every minimal symplectic filling of (Y, ξ_{pl}) is diffeomorphic to one of the manifolds given by a Lefschetz fibration of the form shown in figure 4.11 for some $0 \leq j \leq k$ after any permutation of the arms such that $n_1, \cdots, n_j \geq k-j$ and $n_{j+1}, \cdots, n_k \geq j$.*

The work needed to obtain upper bounds on the number of fillings follows immediately from lemma 3.3.8 and corollary 3.4.2. The ideas used in section 4.1 to construct smooth embeddings of the spheres of the dual graph for each homological embedding via a

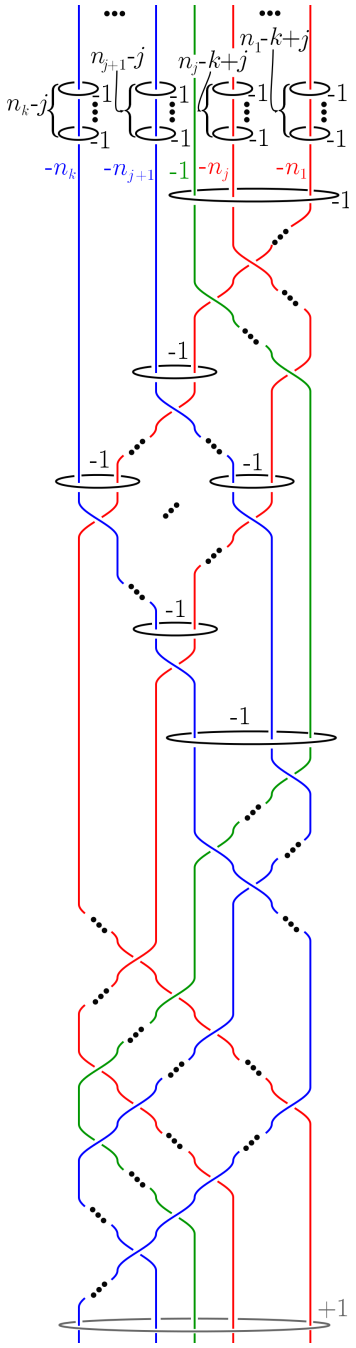

(a) Embedding of dual plumbing.

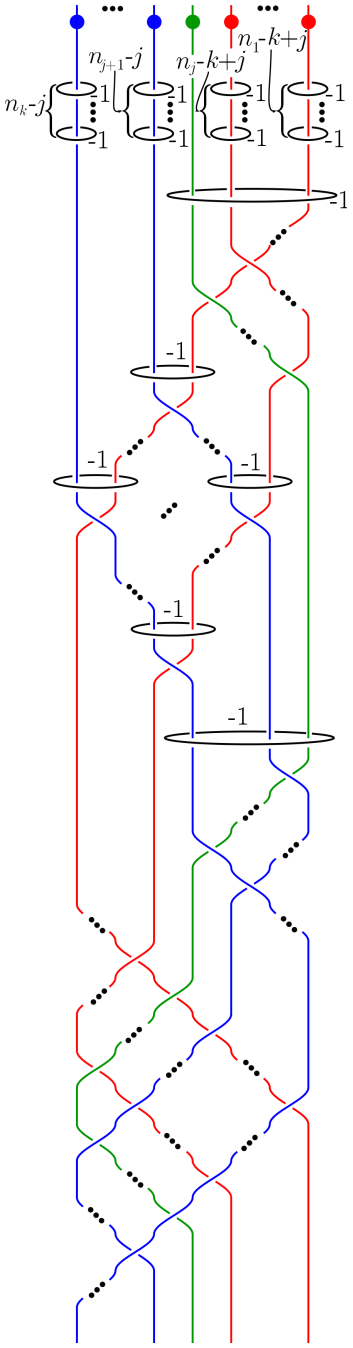

(b) Complement of dual plumbing upsidedown with simplified surgery diagram.

Figure 4.10

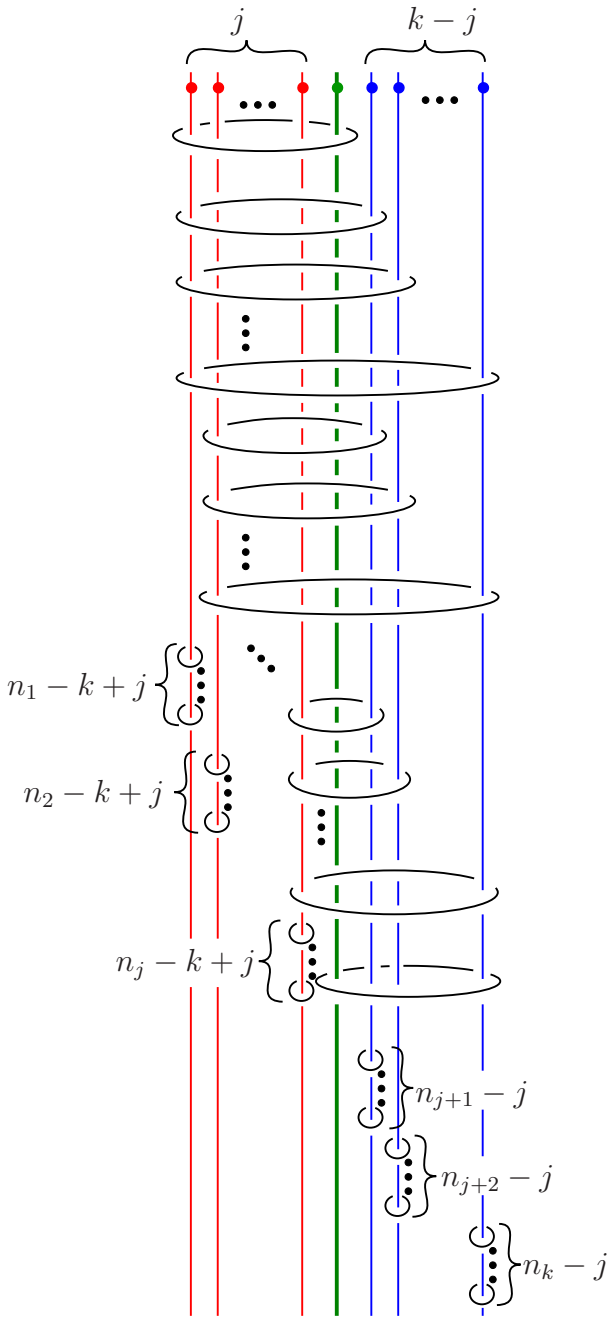

Figure 4.11: Lefschetz fibrations for fillings of (Y, ξ_{pl}), ranging through $0 \leq j \leq k$.

handlebody diagram can be repeated for these examples. Blowing up a $k+1$ stranded braid consisting of a single full positive twist as specified by the homological data gives the embeddings shown in figure 4.10a, and turning these embeddings upsidedown, and then simplifying the surgery diagram yields figure 4.10b. Rotating the projection plane of the diagram by 90° so that we look at the diagram of figure 4.10b from the left side of the page yields the Lefschetz fibration diagrams of figure 4.11. Therefore it suffices to show that the contact structure induced on the boundaries of the Lefschetz fibrations of figure 4.11 is indeed ξ_{pl}. This is implied by the following lemma when $m = j$ and $n = k - j$.

Let $\Sigma_{0,m+1+n}$ denote the disk with $m + 1 + n$ holes centered on the vertices of a regular polygon. Let the holes be labelled counterclockwise as $A_1, \cdots A_m, B, C_1, \cdots, C_n$. Let $D_{S_1,\cdots,S_k}$ denote a positive (right-handed) Dehn twist about a curve which convexly encloses the holes labelled $S_1, \cdots, S_k$.

Lemma 4.3.2. *The following two products of positive Dehn twists are equal in the mapping class group of* $\Sigma_{0,m+1+n}$

$$\phi_{m,n} = D_{A_1,\cdots,A_m,B,C_1,\cdots,C_n} D_{A_1}^n \cdots D_{A_m}^n D_B D_{C_1}^m \cdots D_{C_n}^m$$

$$\psi_{m,n} = D_{A_1,\cdots,A_m,B}(D_{A_1C_1} \cdots D_{A_1C_n}) \cdots (D_{A_mC_1} \cdots D_{A_mC_n}) D_{B,C_1,\cdots,C_n}$$

Proof. We will utilize the generalized lantern relation

$$D_{1,\cdots,k} D_1^{k-2} \cdots D_k^{k-2} = D_{1,2} D_{1,3} \cdots D_{1,k} D_{2,3} \cdots D_{2,k} \cdots D_{k-2,k-1} D_{k-2,k} D_{k-1,k}$$

which can be obtained by repeatedly applying the standard lantern relation:

$$D_{1,2,3}D_1D_2D_3 = D_{1,2}D_{1,3}D_{2,3}.$$

Applying this relation to the factorization for $\phi_{m,n}$, we get a new factorization (not positive) given by

$$D_{A_1}^{-m+1}\cdots D_{A_m}^{-m+1}D_B^{-m-n+2}D_{C_1}^{-n+1}\cdots D_{C_n}^{-n+1}(D_{A_1,A_2}\cdots D_{A_1,A_m})D_{A_1,B}(D_{A_1,C_1},\cdots D_{A_1,C_n})$$

$$(D_{A_2,A_3}\cdots D_{A_2,A_m})D_{A_2,B}(D_{A_2,C_1},\cdots D_{A_2,C_n})\cdots(D_{A_{m-1},A_m})D_{A_{m-1},B}(D_{A_{m-1},C_1},\cdots D_{A_{m-1},C_n})$$

$$D_{A_m,B}(D_{A_m,C_1}\cdots D_{A_m,C_n})(D_{B,C_1}\cdots D_{B,C_n})(D_{C_1,C_2}\cdots D_{C_1,C_n})\cdots(D_{C_{n-2}C_{n-1}}D_{C_{n-2},C_n})D_{C_{n-1},C_n}$$

On the other hand, applying the generalized lantern relation twice on the factorization for $\psi_{m,n}$ to split the twists $D_{A_1,\cdots,A_m,B}$ and $D_{B,C_1,\cdots,C_n}$ shows that $\psi_{m,n}$ is equal to the product:

$$D_{A_1}^{-m+1}\cdots D_{A_m}^{-m+1}D_B^{-m+1}(D_{A_1,A_2}\cdots D_{A_1,A_m})D_{A_1,B}(D_{A_2,A_3}\cdots D_{A_2,A_m})D_{A_2,B}\cdots(D_{A_{m-1},A_m})D_{A_{m-1},B}$$

$$D_{A_m,B}(D_{A_1,C_1}\cdots D_{A_1,C_n})(D_{A_2,C_1}\cdots D_{A_2,C_n})\cdots(D_{A_{m-1},C_1}\cdots D_{A_{m-1},C_n})(D_{A_m,C_1}\cdots D_{A_m,C_n})$$

$$D_B^{-n+1}D_{C_1}^{-n+1}\cdots D_{C_n}^{-n+1}(D_{B,C_1}\cdots D_{B,C_n})(D_{C_1,C_2}\cdots D_{C_1,C_n})\cdots(D_{C_{n-2},C_{n-1}}D_{C_{n-2},C_n})D_{C_{n-1},C_n}$$

Comparing these two factorizations, we see that they differ only by commuting Dehn twists about curves which are disjoint. Specifically, all the twists about boundary parallel curves commute with anything, and the products of the form $(D_{A_i,C_1}\cdots D_{A_i,C_n})$ commute with Dehn twists about curves convexly enclosing any collection of the holes $\{A_{i+1},\cdots,A_m,B\}$. □

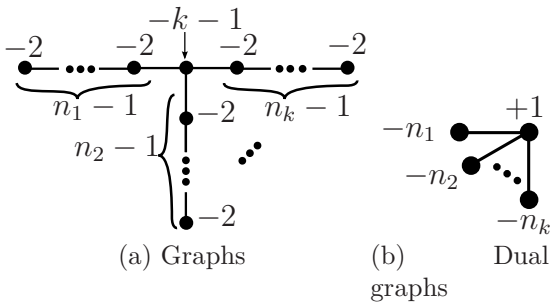

(a) Graphs (b) Dual graphs

Figure 4.12: Graphs and dual graphs for a family where $e_0 = -k-1$.

4.4 Classifications when $e_0 = -k-1$ and $k \leq 6$

Now we consider examples where $e_0 = -k-1$ where k is the number of arms and the spheres in the arms all have square -2 as in figure 4.12a. In this case, unless $k \leq 6$, we cannot ensure we have produced complete classifications using corollary 3.4.2. When $k = 3$, this case was covered in section 4.1. Therefore, in this section we provide complete classifications for this family when $k = 4, 5, 6$, yielding some new examples of fillings.

The dual graphs for this family of examples have the form shown in figure 4.12b, namely the arms all have length one with a single sphere of square $-n_j \leq -2$. Therefore the possible homological embeddings are dictated by lemma 3.3.3. When $k \leq 6$, there is a unique diffeomorphism class of minimal symplectic fillings for each homological embedding of the dual graph. The homology class of C_0 is always ℓ, so it suffices to specify the homology classes of C_1^j for $j \in \{1, \cdots, k\}$.

Note that if the n_j are not sufficiently large, it may not be possible to realize all possible homology configurations. It suffices to assume $n_j \geq k-2$ for all $j \in \{1, \cdots, k\}$ to homologically obtain all possible combinations allowed by lemma 3.3.3, but for $k > 6$ the homological possibilities may not be realizable by J-holomorphic configurations of J-

complex lines. When the n_j are not all at least $k-2$, there are fewer possible fillings and the classification can be easily deduced by studying the homological possibilities which are allowed by the given n_j.

A symplectic embedding of the dual graph spheres representing the homology classes specified by $\mathcal{E}_n^k$ will reduce after blowing-down to a configuration of projective lines with intersection data specified by $\mathcal{I}_n^k$ shown in figures 4.13 and 4.17. Each of the homological embeddings can be realized as smooth and symplectic embeddings visible in the Kirby diagrams of figures 4.14, 4.15, 4.16, 4.18, 4.19, and 4.20. By cutting out the spheres of the dual graphs in each of these embeddings, we obtain manifolds with a Lefschetz fibration structure in the same way this occurred in the simple examples of section 4.1.

When $k = 4$, there are three distinct possibilities up to reordering the arms and relabeling the exceptional classes.

	$\mathcal{E}_1^4$	$\mathcal{E}_2^4$
$[C_1^1] =$	$\ell - e_1 - e_. - \cdots - e_.$	$\ell - e_1 - e_2 - e_. - \cdots - e_.$
$[C_1^2] =$	$\ell - e_1 - e_. - \cdots - e_.$	$\ell - e_1 - e_3 - e_. - \cdots - e_.$
$[C_1^3] =$	$\ell - e_1 - e_. - \cdots - e_.$	$\ell - e_1 - e_4 - e_. - \cdots - e_.$
$[C_1^4] =$	$\ell - e_1 - e_. - \cdots - e_.$	$\ell - e_2 - e_3 - e_4 - e_. - \cdots - e_.$

	$\mathcal{E}_3^4$
$[C_1^1] =$	$\ell - e_1 - e_2 - e_3 - e_. - \cdots - e_.$
$[C_1^2] =$	$\ell - e_1 - e_4 - e_5 - e_. - \cdots - e_.$
$[C_1^3] =$	$\ell - e_2 - e_4 - e_6 - e_. - \cdots - e_.$
$[C_1^4] =$	$\ell - e_3 - e_5 - e_6 - e_. - \cdots - e_.$

The Lefschetz fibrations obtained by cutting out these embedded dual spheres for the $k = 4$ case have fibers which are four holed disks. We will label the holes counter-clockwise by $1, 2, 3, 4$. The ordered vanishing cycles correspond to a positive factorization

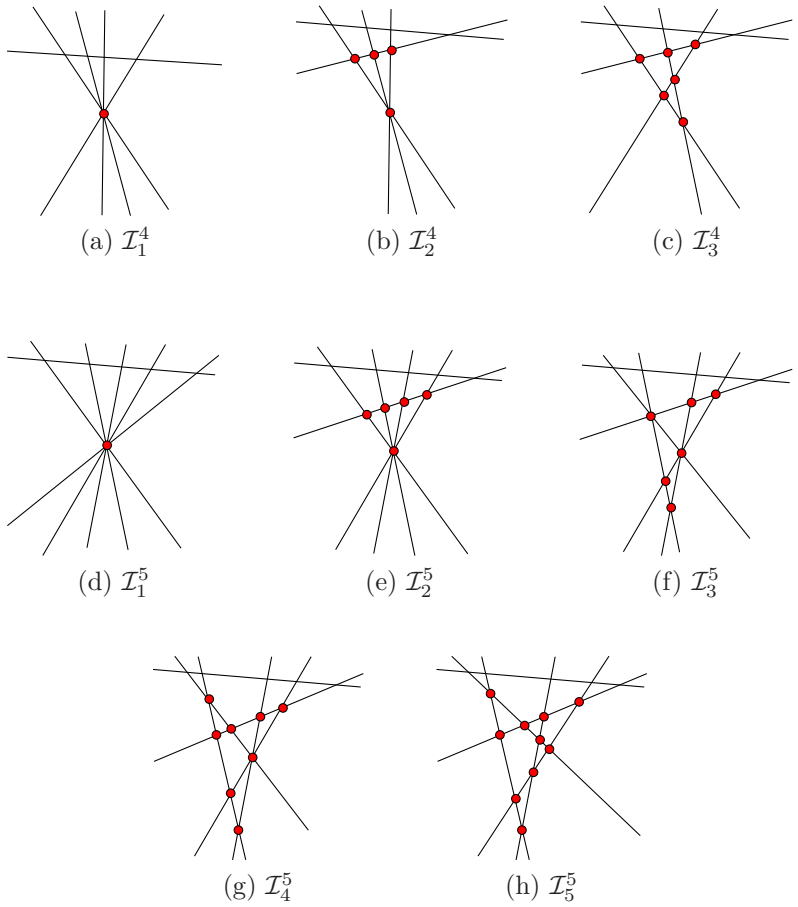

(a) $\mathcal{I}_1^4$ (b) $\mathcal{I}_2^4$ (c) $\mathcal{I}_3^4$

(d) $\mathcal{I}_1^5$ (e) $\mathcal{I}_2^5$ (f) $\mathcal{I}_3^5$

(g) $\mathcal{I}_4^5$ (h) $\mathcal{I}_5^5$

Figure 4.13: Each configuration $\mathcal{I}_n^k$ represents $k+1$ complex projective lines $C_0, C_1, \cdots, C_k$. C_0 always intersects each of the other lines in a distinct double point. The diagrams represent how other intersections can coincide at multi-intersection points corresponding to the blow-downs of the homological embedding of the dual graph described by $\mathcal{E}_n^k$. The possible configurations for $k = 4, 5$ are shown here.

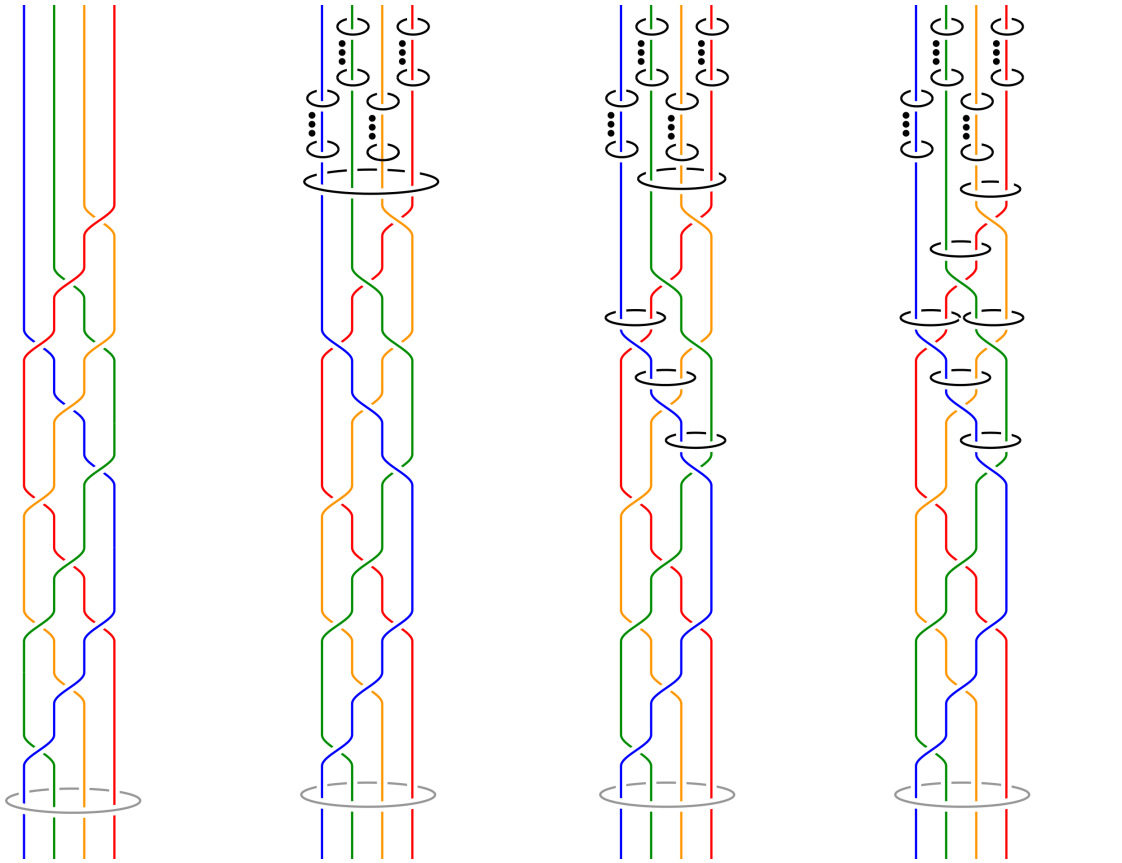

(a) $+1$, $+1$, $+1$, $+1$, $+1$

(b) $\mathcal{E}^4_1$: $+1$, $-n_1$, $-n_2$, $-n_3$, $-n_4$, -1

(c) $\mathcal{E}^4_2$: $+1$, $-n_1$, $-n_2$, $-n_3$, $-n_4$, -1

(d) $\mathcal{E}^4_3$: $+1$, $-n_1$, $-n_2$, $-n_3$, $-n_4$, -1

Figure 4.14: After closing up each braid, each figure shows the attaching circles for the 2-handles of handlebody diagrams with *four* 3-handles and a single 4-handle. The framings are specified below each diagram with color coordination. The left-most figure is a diagram for $\mathbb{C}\mathrm{P}^2$, and the others are blow-ups of $\mathbb{C}\mathrm{P}^2$ in which the dual sphere embeddings are exhibited. The equators of the exceptional spheres are shown in black, and the number of these circles which link a single colored circle is determined by the framings: a total of n_j+1 black circles link the colored circle with framing $-n_j$.

of the monodromy for the standard open book supporting the canonical contact structure. In each case the complement of the embedding $\mathcal{E}_1^k$ is the Lefschetz fibration on the convex plumbing described by Gay and Mark's theorem 2.4.1. The factorizations for the Lefschetz fibrations corresponding to the fillings appearing as the complements of all the embeddings are specified below.

$$\mathcal{E}_1^4 \Big| D_1^{n_1} D_2^{n_2} D_3^{n_3} D_4^{n_4} D_{1,2,3,4}$$

$$\mathcal{E}_2^4 \Big| D_1^{n_1-1} D_2^{n_2-1} D_3^{n_3-1} D_4^{n_4-2} D_{1,2,3} D_{1,4} D_{2,4} D_{3,4}$$

$$\mathcal{E}_3^4 \Big| D_1^{n_1-2} D_2^{n_2-2} D_3^{n_3-2} D_4^{n_4-2} D_{1,2} D_{1,3} D_{1,4} D_{2,3} D_{2,4} D_{3,4}$$

It is not hard to show that these factorizations are all equal in the mapping class group. The second factorization is related to the first by a daisy relation, and the third is related to the second by a lantern relation (along with some commutation of Dehn twists about disjoint curves).

When $k = 5$, there are five distinct possibilities up to reordering the arms and exceptional classes.

	$\mathcal{E}_1^5$	$\mathcal{E}_2^5$
$[C_1^1] =$	$\ell - e_1 - e_\cdot - \cdots - e_\cdot$	$\ell - e_1 - e_2 - e_\cdot - \cdots - e_\cdot$
$[C_1^2] =$	$\ell - e_1 - e_\cdot - \cdots - e_\cdot$	$\ell - e_1 - e_3 - e_\cdot - \cdots - e_\cdot$
$[C_1^3] =$	$\ell - e_1 - e_\cdot - \cdots - e_\cdot$	$\ell - e_1 - e_4 - e_\cdot - \cdots - e_\cdot$
$[C_1^4] =$	$\ell - e_1 - e_\cdot - \cdots - e_\cdot$	$\ell - e_1 - e_5 - e_\cdot - \cdots - e_\cdot$
$[C_1^5] =$	$\ell - e_1 - e_\cdot - \cdots - e_\cdot$	$\ell - e_2 - e_3 - e_4 - e_5 - e_\cdot - \cdots - e_\cdot$

	$\mathcal{E}_3^5$
$[C_1^1] =$	$\ell - e_1 - e_3 - e_4 - e_\cdot - \cdots - e_\cdot$
$[C_1^2] =$	$\ell - e_1 - e_5 - e_6 - e_\cdot - \cdots - e_\cdot$
$[C_1^3] =$	$\ell - e_1 - e_2 - e_\cdot - \cdots - e_\cdot$
$[C_1^4] =$	$\ell - e_2 - e_3 - e_5 - e_\cdot - \cdots - e_\cdot$
$[C_1^5] =$	$\ell - e_2 - e_4 - e_6 - e_\cdot - \cdots - e_\cdot$

	$\mathcal{E}_4^5$	$\mathcal{E}_5^5$
$[C_1^1] =$	$\ell - e_1 - e_2 - e_5 - e_. - \cdots - e_.$	$\ell - e_1 - e_2 - e_3 - e_4 - e_. - \cdots - e_.$
$[C_1^2] =$	$\ell - e_1 - e_3 - e_6 - e_. - \cdots - e_.$	$\ell - e_1 - e_5 - e_6 - e_7 - e_. - \cdots - e_.$
$[C_1^3] =$	$\ell - e_1 - e_4 - e_7 - e_. - \cdots - e_.$	$\ell - e_2 - e_5 - e_8 - e_9 - e_. - \cdots - e_.$
$[C_1^4] =$	$\ell - e_2 - e_3 - e_4 - e_8 - e_. - \cdots - e_.$	$\ell - e_3 - e_6 - e_8 - e_{10} - e_. - \cdots - e_.$
$[C_1^5] =$	$\ell - e_5 - e_6 - e_7 - e_8 - e_. - \cdots - e_.$	$\ell - e_4 - e_7 - e_9 - e_{10} - e_. - \cdots - e_.$

The Lefschetz fibrations obtained by cutting out these embedded dual spheres for the $k = 5$ case have fibers which are five holed disks, with holes labeled counter-clockwise $1, 2, 3, 4, 5$. The factorizations for the Lefschetz fibrations are:

$$\mathcal{E}_1^5 \Big| D_1^{n_1} D_2^{n_2} D_3^{n_3} D_4^{n_4} D_5^{n_5} D_{1,2,3,4,5}$$

$$\mathcal{E}_2^5 \Big| D_1^{n_1-1} D_2^{n_2-1} D_3^{n_3-1} D_4^{n_4-1} D_5^{n_5-3} D_{1,2,3,4} D_{1,5} D_{2,5} D_{3,5} D_{4,5}$$

$$\mathcal{E}_3^5 \Big| D_1^{n_1-2} D_2^{n_2-2} D_3^{n_3-1} D_4^{n_4-2} D_5^{n_5-2} D_{1,2,3} D_{1,4} D_{1,5} D_{2,4} D_{2,5} D_{3,4,5}$$

$$\mathcal{E}_4^5 \Big| D_1^{n_1-2} D_2^{n_2-2} D_3^{n_3-2} D_4^{n_4-3} D_5^{n_5-3} D_{1,2,3} D_{1,4} D_{1,5} D_{2,4} D_{2,5} D_{3,4} D_{3,5} D_{4,5}$$

$$\mathcal{E}_5^5 \Big| D_1^{n_1-3} D_2^{n_2-3} D_3^{n_3-3} D_4^{n_4-3} D_5^{n_5-3} D_{1,2} D_{1,3} D_{1,4} D_{1,5} D_{2,3} D_{2,4} D_{2,5} D_{3,4} D_{3,5} D_{4,5}$$

These factorizations are all equal in the mapping class group. The second factorization is related to the first by a daisy relation with four petals, the fourth is related to the second by a daisy relation with three petals, and the fifth is related to the fourth by a lantern relation. The third is related to the fourth by a lantern relation.

When $k = 6$, there are nine distinct possibilities up to reordering the arms and

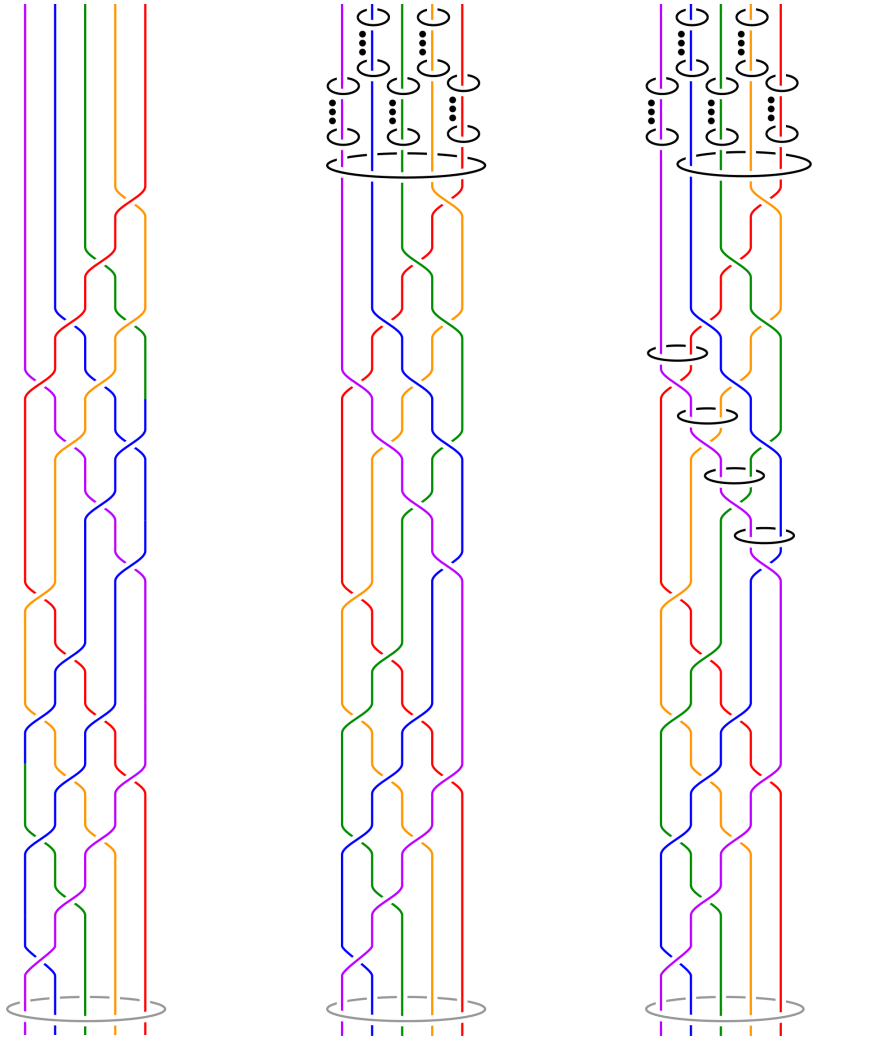

(a) $+1$, $+1$, $+1$, $+1$, $+1$, $+1$

(b) $\mathcal{E}^5_1$: $+1$, $-n_1$, $-n_2$, $-n_3$, $-n_4$, $-n_5$, -1

(c) $\mathcal{E}^5_2$: $+1$, $-n_1$, $-n_2$, $-n_3$, $-n_4$, -1

Figure 4.15: After closing up each braid, each figure shows the attaching circles for the 2-handles of handlebody diagrams with *five* 3-handles and a single 4-handle. The left-most figure is a diagram for $\mathbb{C}\mathrm{P}^2$, and the others are blow-ups of $\mathbb{C}\mathrm{P}^2$ in which the dual sphere embeddings are exhibited.

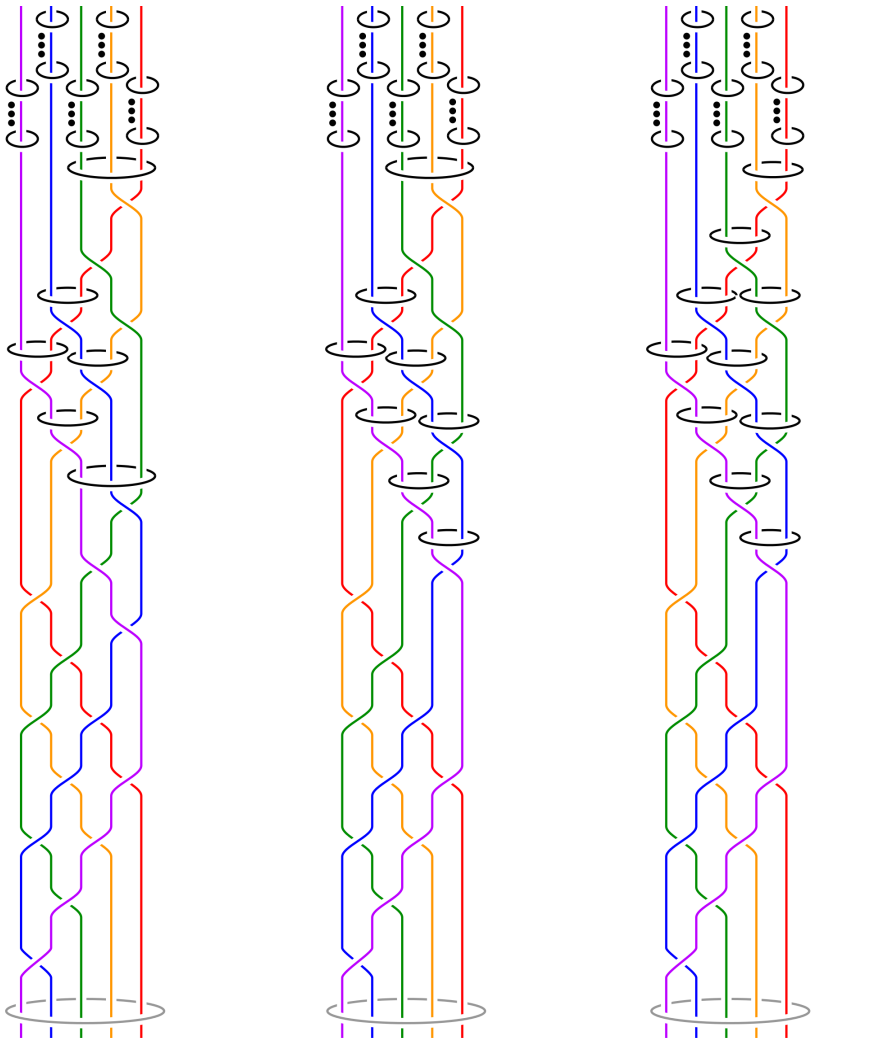

Figure 4.16: After closing up each braid, each figure shows the attaching circles for the 2-handles of handlebody diagrams with *five* 3-handles and a single 4-handle. The left-most figure is a diagram for $\mathbb{C}\mathrm{P}^2$, and the others are blow-ups of $\mathbb{C}\mathrm{P}^2$ in which the dual sphere embeddings are exhibited.

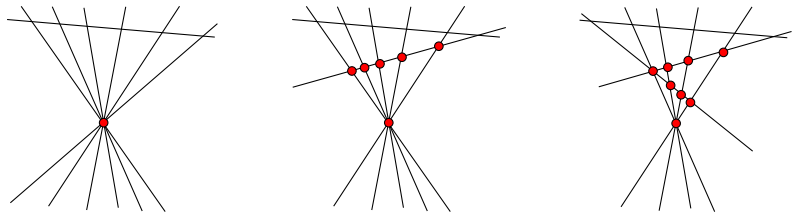

(a) $\mathcal{I}_1^6$ (b) $\mathcal{I}_2^6$ (c) $\mathcal{I}_3^6$

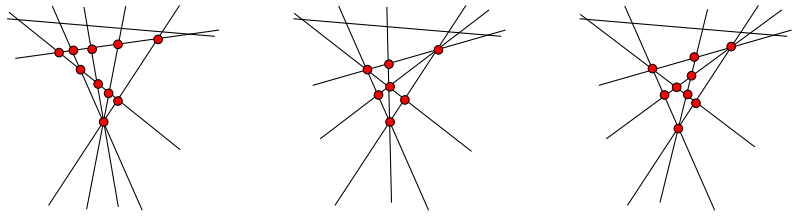

(d) $\mathcal{I}_4^6$ (e) $\mathcal{I}_5^6$ (f) $\mathcal{I}_6^6$

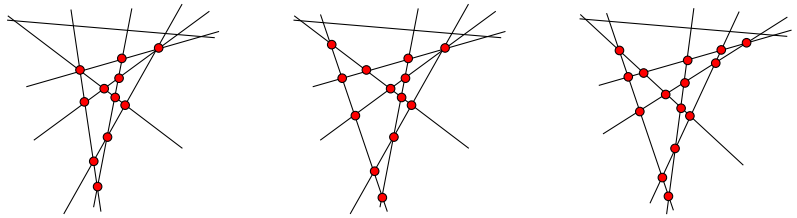

(g) $\mathcal{I}_7^6$ (h) $\mathcal{I}_8^6$ (i) $\mathcal{I}_9^6$

Figure 4.17: Each configuration $\mathcal{I}_n^k$ represents $k+1$ complex projective lines $C_0, C_1, \cdots, C_k$. C_0 always intersects each of the other lines in a distinct double point. The diagrams represent how other intersections can coincide at multi-intersection points corresponding to the blow-downs of the homological embedding of the dual graph described by $\mathcal{E}_n^k$. The possible configurations for $k = 6$ are shown here.

exceptional classes.

	$\mathcal{E}_1^6$	$\mathcal{E}_2^6$
$[C_1^1] =$	$\ell - e_1 - e. - \cdots - e.$	$\ell - e_1 - e_2 - e. - \cdots - e.$
$[C_1^2] =$	$\ell - e_1 - e. - \cdots - e.$	$\ell - e_1 - e_3 - e. - \cdots - e.$
$[C_1^3] =$	$\ell - e_1 - e. - \cdots - e.$	$\ell - e_1 - e_4 - e. - \cdots - e.$
$[C_1^4] =$	$\ell - e_1 - e. - \cdots - e.$	$\ell - e_1 - e_5 - e. - \cdots - e.$
$[C_1^5] =$	$\ell - e_1 - e. - \cdots - e.$	$\ell - e_1 - e_6 - e. - \cdots - e.$
$[C_1^6] =$	$\ell - e_1 - e. - \cdots - e.$	$\ell - e_2 - e_3 - e_4 - e_5 - e_6 - e. - \cdots - e.$

	$\mathcal{E}_3^6$	$\mathcal{E}_4^6$
$[C_1^1] =$	$\ell - e_1 - e_3 - e_4 - e. - \cdots - e.$	$h - e_1 - e_2 - e_3 - e. - \cdots - e.$
$[C_1^2] =$	$\ell - e_1 - e_5 - e_6 - e. - \cdots - e.$	$h - e_1 - e_4 - e_5 - e. - \cdots - e.$
$[C_1^3] =$	$\ell - e_1 - e_7 - e_8 - e. - \cdots - e.$	$h - e_1 - e_6 - e_7 - e. - \cdots - e.$
$[C_1^4] =$	$\ell - e_1 - e_2 - e. - \cdots - e.$	$h - e_1 - e_8 - e_9 - e. - \cdots - e.$
$[C_1^5] =$	$\ell - e_2 - e_3 - e_5 - e_7 - e. - \cdots - e.$	$h - e_2 - e_4 - e_6 - e_8 - e. - \cdots - e.$
$[C_1^6] =$	$\ell - e_2 - e_4 - e_6 - e_8 - e. - \cdots - e.$	$h - e_3 - e_5 - e_7 - e_9 - e. - \cdots - e.$

	$\mathcal{E}_5^6$	$\mathcal{E}_6^6$
$[C_1^1] =$	$\ell - e_1 - e_3 - e_5 - e. - \cdots - e.$	$h - e_1 - e_3 - e_4 - e. - \cdots - e.$
$[C_1^2] =$	$\ell - e_1 - e_4 - e_6 - e. - \cdots - e.$	$h - e_1 - e_5 - e_6 - e_7 - e. - \cdots - e.$
$[C_1^3] =$	$\ell - e_1 - e_2 - e_7 - e. - \cdots - e.$	$h - e_1 - e_2 - e_8 - e. - \cdots - e.$
$[C_1^4] =$	$\ell - e_2 - e_4 - e_5 - e. - \cdots - e.$	$h - e_2 - e_4 - e_5 - e_9 - e. - \cdots - e.$
$[C_1^5] =$	$\ell - e_2 - e_3 - e_6 - e. - \cdots - e.$	$h - e_2 - e_3 - e_6 - e. - \cdots - e.$
$[C_1^6] =$	$\ell - e_3 - e_4 - e_7 - e. - \cdots - e.$	$h - e_3 - e_7 - e_8 - e_9 - e. - \cdots - e.$

	$\mathcal{E}_7^6$
$[C_1^1] =$	$\ell - e_1 - e_2 - e_3 - e. - \cdots - e.$
$[C_1^2] =$	$\ell - e_1 - e_4 - e_5 - e_6 - e. - \cdots - e.$
$[C_1^3] =$	$\ell - e_1 - e_7 - e_8 - e_9 - e. - \cdots - e.$
$[C_1^4] =$	$\ell - e_3 - e_4 - e_7 - e_{10} - e_{11} - e. - \cdots - e.$
$[C_1^5] =$	$\ell - e_2 - e_5 - e_8 - e_{10} - e. - \cdots - e.$
$[C_1^6] =$	$\ell - e_2 - e_6 - e_9 - e_{11} - e. - \cdots - e.$

	$\mathcal{E}_8^6$
$[C_1^1] =$	$h - e_1 - e_2 - e_3 - e_4 - e_. - \cdots - e_.$
$[C_1^2] =$	$h - e_1 - e_5 - e_6 - e_7 - e_. - \cdots - e_.$
$[C_1^3] =$	$h - e_1 - e_8 - e_9 - e_{10} - e_. - \cdots - e_.$
$[C_1^4] =$	$h - e_2 - e_5 - e_8 - e_{11} - e_{12} - e_. - \cdots - e_.$
$[C_1^5] =$	$h - e_3 - e_6 - e_9 - e_{11} - e_{13} - e_. - \cdots - e_.$
$[C_1^6] =$	$h - e_4 - e_7 - e_{10} - e_{12} - e_{13} - e_. - \cdots - e_.$

	$\mathcal{E}_9^6$
$[C_1^1] =$	$h - e_1 - e_2 - e_3 - e_4 - e_5 - e_. - \cdots - e_.$
$[C_1^2] =$	$h - e_1 - e_6 - e_7 - e_8 - e_9 - e_. - \cdots - e_.$
$[C_1^3] =$	$h - e_2 - e_6 - e_{10} - e_{11} - e_{12} - e_. - \cdots - e_.$
$[C_1^4] =$	$h - e_3 - e_7 - e_{10} - e_{13} - e_{14} - e_. - \cdots - e_.$
$[C_1^5] =$	$h - e_4 - e_8 - e_{11} - e_{13} - e_{15} - e_. - \cdots - e_.$
$[C_1^6] =$	$h - e_5 - e_9 - e_{12} - e_{14} - e_{15} - e_. - \cdots - e_.$

The Lefschetz fibrations obtained by cutting out these embedded dual spheres for the $k = 6$ case have fibers which are six holed disks, with holes labeled counter-clockwise $1, 2, 3, 4, 5, 6$. The factorizations for the Lefschetz fibrations are found from the embeddings as was done in the simple case of section 4.1. The most complicated case is for the embedding $\mathcal{E}_5^6$ and given Lefschetz fibration on the complement of the shown embedding is produced explicitly in section 6.2.

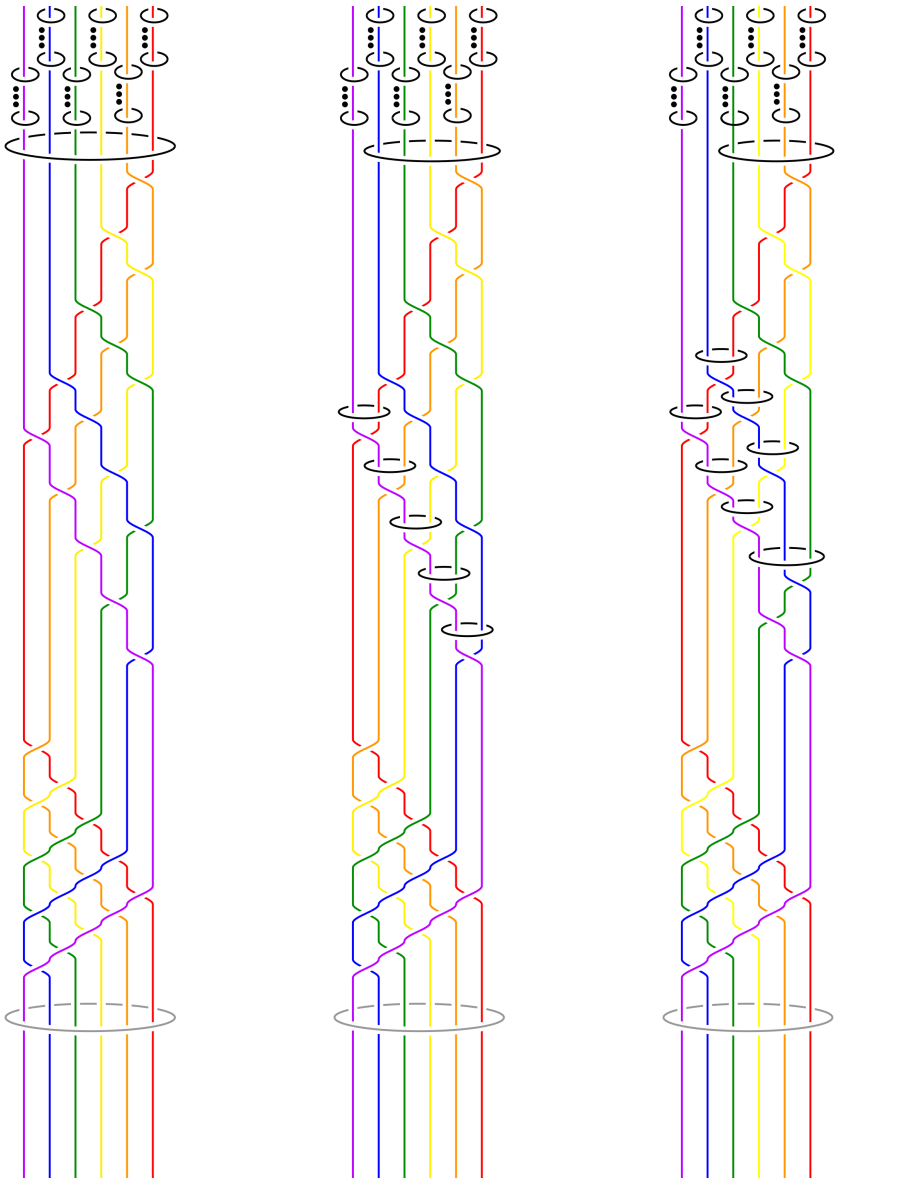

(a) $\mathcal{E}^6_1$: $+1$, $-n_1$, $-n_2$, $-n_3$, $-n_4$, $-n_5$, $-n_6$, -1

(b) $\mathcal{E}^6_2$: $+1$, $-n_1$, $-n_2$, $-n_3$, $-n_4$, $-n_5$, $-n_6$, -1

(c) $\mathcal{E}^6_3$: $+1$, $-n_1$, $-n_2$, $-n_3$, $-n_4$, $-n_5$, $-n_6$, -1

Figure 4.18: After closing up each braid, each figure shows the attaching circles for the 2-handles of handlebody diagrams with *six* 3-handles and a single 4-handle. The left-most figure is a diagram for $\mathbb{C}\mathrm{P}^2$, and the others are blow-ups of $\mathbb{C}\mathrm{P}^2$ in which the dual sphere embeddings are exhibited.

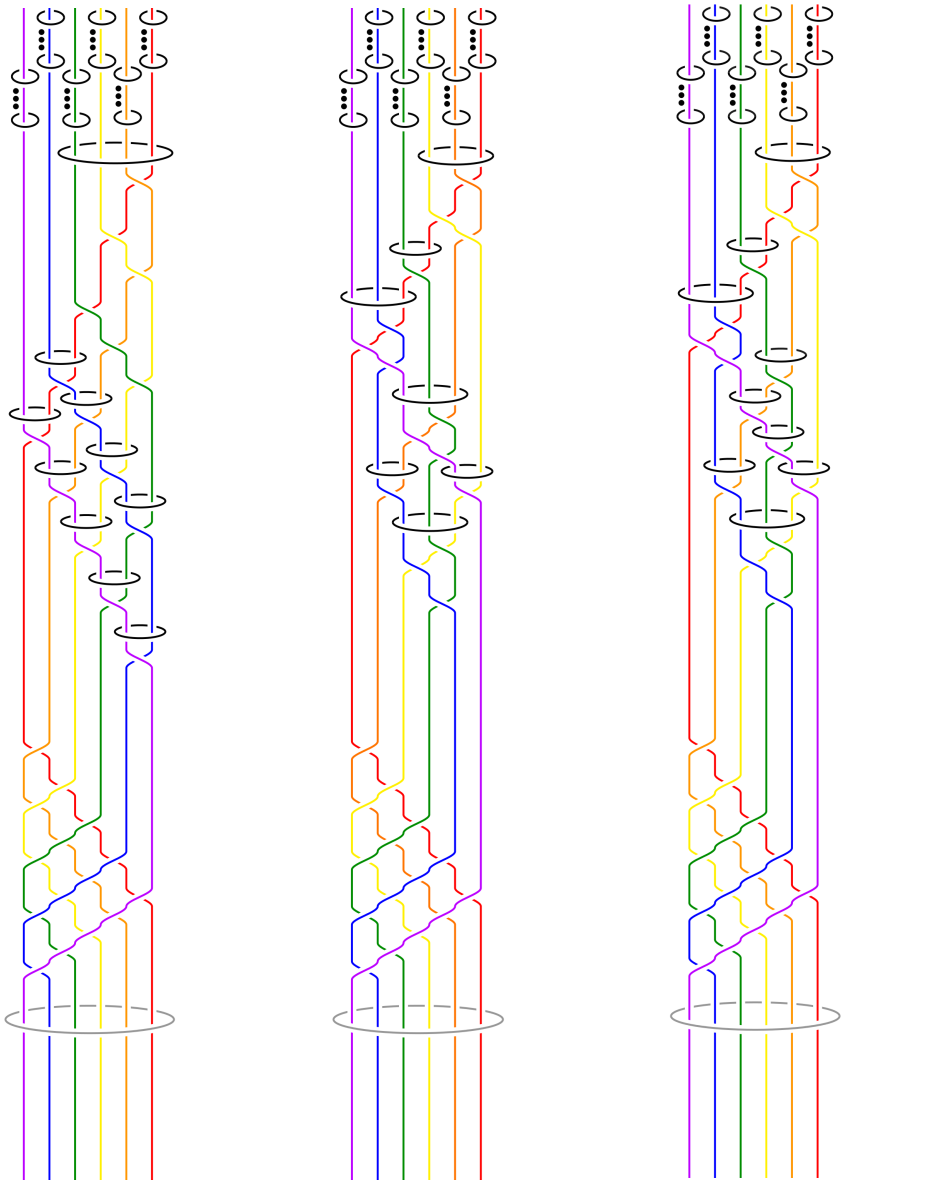

(a) $\mathcal{E}^6_4$: $+1$, $-n_1$, $-n_2$, $-n_3$, $-n_4$, $-n_5$, $-n_6$, -1

(b) $\mathcal{E}^6_5$: $+1$, $-n_1$, $-n_2$, $-n_3$, $-n_4$, $-n_5$, $-n_6$, -1

(c) $\mathcal{E}^6_6$: $+1$, $-n_1$, $-n_2$, $-n_3$, $-n_4$, $-n_5$, $-n_6$, -1

Figure 4.19: After closing up each braid, each figure shows the attaching circles for the 2-handles of handlebody diagrams with *six* 3-handles and a single 4-handle. The left-most figure is a diagram for $\mathbb{C}\mathrm{P}^2$, and the others are blow-ups of $\mathbb{C}\mathrm{P}^2$ in which the dual sphere embeddings are exhibited.

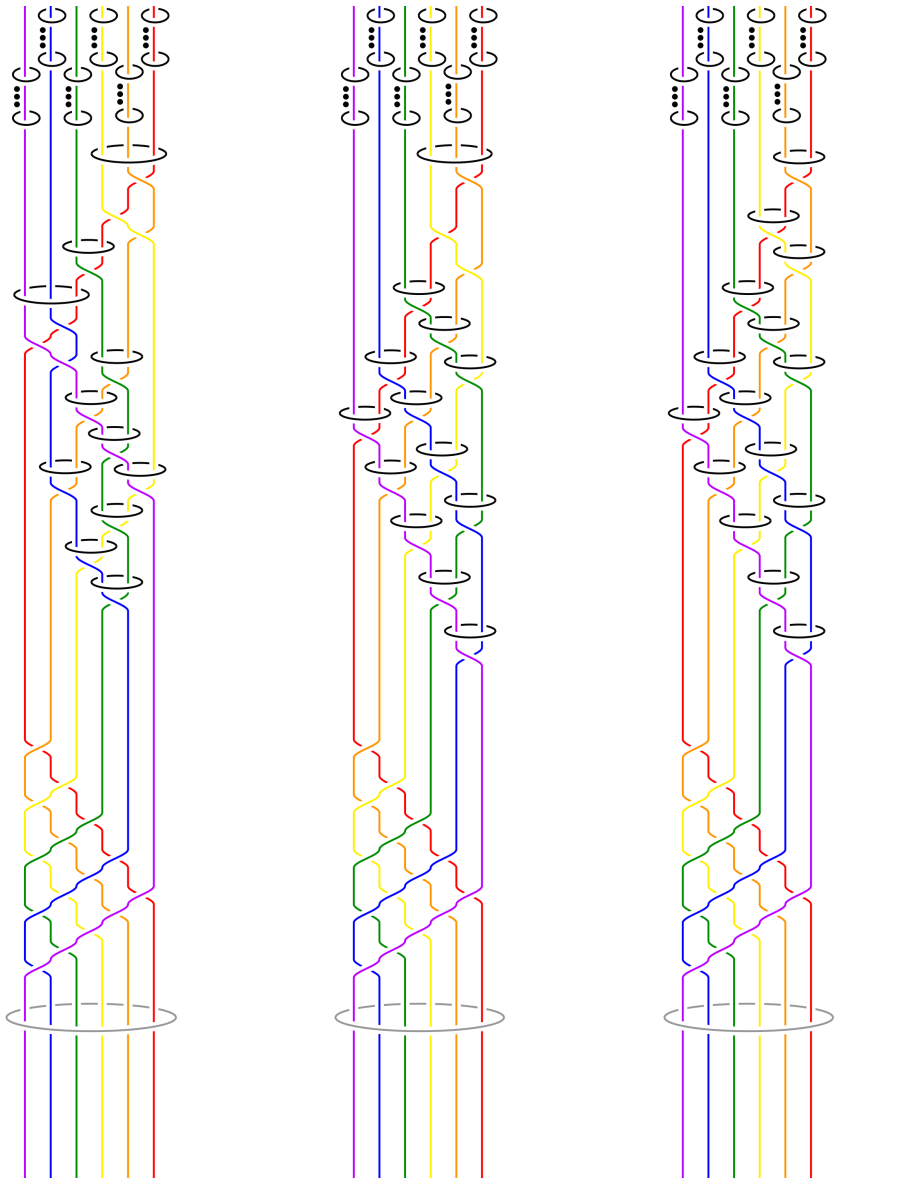

(a) $\mathcal{E}^6_7$: $+1$, $-n_1$, $-n_2$, $-n_3$, $-n_4$, $-n_5$, $-n_6$, -1

(b) $\mathcal{E}^6_8$: $+1$, $-n_1$, $-n_2$, $-n_3$, $-n_4$, $-n_5$, $-n_6$, -1

(c) $\mathcal{E}^6_9$: $+1$, $-n_1$, $-n_2$, $-n_3$, $-n_4$, $-n_5$, $-n_6$, -1

Figure 4.20: After closing up each braid, each figure shows the attaching circles for the 2-handles of handlebody diagrams with *six* 3-handles and a single 4-handle. The left-most figure is a diagram for $\mathbb{C}\mathrm{P}^2$, and the others are blow-ups of $\mathbb{C}\mathrm{P}^2$ in which the dual sphere embeddings are exhibited.

$\mathcal{E}_1^6 \mid D_1^{n_1} D_2^{n_2} D_3^{n_3} D_4^{n_4} D_5^{n_5} D_6^{n_6} D_{1,2,3,4,5,6}$

$\mathcal{E}_2^6 \mid D_1^{n_1-1} D_2^{n_2-1} D_3^{n_3-1} D_4^{n_4-1} D_5^{n_5-1} D_6^{n_6-4} D_{1,2,3,4,5} D_{1,6} D_{2,6} D_{3,6} D_{4,6} D_{5,6}$

$\mathcal{E}_3^6 \mid D_1^{n_1-2} D_2^{n_2-2} D_3^{n_3-2} D_4^{n_4-1} D_5^{n_5-3} D_6^{n_6-3} D_{1,2,3,4} D_{1,5} D_{1,6} D_{2,5} D_{2,6} D_{3,5} D_{3,6} D_{4,5,6}$

$\mathcal{E}_4^6 \mid D_1^{n_1-2} D_2^{n_2-2} D_3^{n_3-2} D_4^{n_4-2} D_5^{n_5-4} D_6^{n_6-4} D_{1,2,3,4} D_{1,5} D_{1,6} D_{2,5} D_{2,6} D_{3,5} D_{3,6} D_{4,5} D_{4,6} D_{5,6}$

$\mathcal{E}_5^6 \mid D_1^{n_1-2} D_2^{n_2-2} D_3^{n_3-2} D_4^{n_4-2} D_5^{n_5-2} D_6^{n_6-2} D_{1,2,3} D_{1,4} D_{1,5,6} (D_{5,6}^{-1} D_{2,4,6} D_{5,6}) D_{2,5}$
$(D_{4,5,6}^{-1} D_{3,6} D_{4,5,6}) D_{3,4,5}$

$\mathcal{E}_6^6 \mid D_1^{n_1-2} D_2^{n_2-3} D_3^{n_3-2} D_4^{n_4-3} D_5^{n_5-2} D_6^{n_6-3} D_{1,2,3} D_{1,4} D_{1,5,6} (D_{5,6}^{-1} D_{2,4} D_{2,6} D_{4,6} D_{5,6})$
$D_{2,5} (D_{4,5,6}^{-1} D_{3,6} D_{4,5,6}) D_{3,4,5}$

$\mathcal{E}_7^6 \mid D_1^{n_1-2} D_2^{n_2-3} D_3^{n_3-3} D_4^{n_4-4} D_5^{n_5-3} D_6^{n_6-3} D_{1,2,3} D_{1,4} D_{1,5,6} (D_{5,6}^{-1} D_{2,4} D_{2,6} D_{4,6} D_{5,6})$
$D_{2,5} (D_{4,5,6}^{-1} D_{3,6} D_{4,5,6}) D_{3,4} D_{3,5} D_{4,5}$

$\mathcal{E}_8^6 \mid D_1^{n_1-3} D_2^{n_2-3} D_3^{n_3-3} D_4^{n_4-4} D_5^{n_5-4} D_6^{n_6-4}$
$D_{1,2,3} D_{1,4} D_{1,5} D_{1,6} D_{2,4} D_{2,5} D_{2,6} D_{3,4} D_{3,5} D_{3,6} D_{4,5} D_{4,6} D_{5,6}$

$\mathcal{E}_9^6 \mid D_1^{n_1-4} D_2^{n_2-4} D_3^{n_3-4} D_4^{n_4-4} D_5^{n_5-4} D_6^{n_6-4}$
$D_{1,2} D_{1,3} D_{1,4} D_{1,5} D_{1,6} D_{2,3} D_{2,4} D_{2,5} D_{2,6} D_{3,4} D_{3,5} D_{3,6} D_{4,5} D_{4,6} D_{5,6}$

These factorizations are all equal in the mapping class group. The second factorization is related to the first by a daisy relation (equation 2.3.2) with five petals, the fourth is related to the second by a daisy relation with four petals, the eighth is related to the fourth by a three petal daisy relation, and the ninth is related to the eighth by a lantern relation (equation 2.3.1). The fifth is related to the ninth by the following lemma, and the sixth and seventh are related to the fifth by lantern relations.

Lemma 4.4.1. *The following two elements are equal in the mapping class group of the disk*

with six holes:

$$\phi = D_{1,2}D_{1,3}D_{1,4}D_{1,5}D_{1,6}D_{2,3}D_{2,4}D_{2,5}D_{2,6}D_{3,4}D_{3,5}D_{3,6}D_{4,5}D_{4,6}D_{5,6}$$

and

$$\psi = D_1^2D_2^2D_3^2D_4^2D_5^2D_6^2D_{1,2,3}D_{1,4}D_{1,5,6}(D_{5,6}^{-1}D_{2,4,6}D_{5,6})D_{2,5}(D_{4,5,6}^{-1}D_{3,6}D_{4,5,6})D_{3,4,5}$$

Proof. Starting with ψ, use the lantern relation and the boundary parallel curves to split all of the Dehn twists about curves containing three holes into Dehn twists about curves containing two holes.

$$D_{1,2}D_{1,3}D_{2,3}D_{1,4}D_{1,5}D_{1,6}D_{5,6}D_{5,6}^{-1}D_{2,4}D_{2,6}D_{4,6}D_{5,6}D_{2,5}D_{5,6}^{-1}D_{4,6}^{-1}D_{4,5}^{-1}D_{3,6}D_{4,5}D_{4,6}D_{5,6}$$

$$\cdot D_{3,4}D_{3,5}D_{4,5}$$

By the conjugation relation, $D_{5,6}D_{2,5}D_{5,6}^{-1}$ is a positive Dehn twist about the image of the curve convexly containing 2 and 5 under a negative Dehn twist about $D_{5,6}$, and this image is disjoint from the curve convexly containing 4 and 6 so $D_{5,6}D_{2,5}D_{5,6}^{-1}$ commutes with $D_{4,6}$. Also $D_{4,5}$ and $D_{3,6}$ commute. Performing these commutations and cancelling inverse pairs we get the following.

$$D_{1,2}D_{1,3}D_{2,3}D_{1,4}D_{1,5}D_{1,6}D_{2,4}D_{2,6}D_{5,6}D_{2,5}D_{5,6}^{-1}D_{3,6}D_{4,6}D_{5,6}D_{3,4}D_{3,5}D_{4,5}$$

Commuting Dehn twists about disjoint curves, and cyclically permuting lantern relation triples we can simplify this to

$$D_{1,2}D_{1,3}D_{1,4}D_{1,5}D_{1,6}D_{2,3}D_{2,4}D_{2,5}D_{2,6}D_{3,6}D_{4,6}D_{5,6}D_{4,5}D_{3,4}D_{3,5}$$

A final cyclic permutation of a lantern triple gives

$$D_{1,2}D_{1,3}D_{1,4}D_{1,5}D_{1,6}D_{2,3}D_{2,4}D_{2,5}D_{2,6}D_{3,6}D_{4,5}D_{4,6}D_{5,6}D_{3,4}D_{3,5}$$

The last six Dehn twists form a generalized lantern product (the right hand side of equation 2.3.3) and can thus be cyclically permuted to give ϕ. □

Remark 4.4.2. When all of the n_j are at least $k-2$, these factorizations are all positive, and are all related through sequences of lantern or daisy relations which pass through only positive factorizations. However, when some of the n_j are less than $k-2$ then some of the above factorizations will not be positive. In such a situation, it is possible that the remaining positive factorizations could be related only through sequences of lantern and daisy relations which necessarily pass through non-positive factorizations. The fillings which always come from sequences of Fintushel-Stern rational blow-downs of the plumbing include $\mathcal{E}_2^4, \mathcal{E}_3^4, \mathcal{E}_2^5, \mathcal{E}_4^5, \mathcal{E}_5^5, \mathcal{E}_2^6, \mathcal{E}_4^6, \mathcal{E}_8^6$, and $\mathcal{E}_9^6$. Fillings corresponding to monodromy substitutions given by the relations arising in section 4.3 include $\mathcal{E}_3^5$ and $\mathcal{E}_3^6$. The filling $\mathcal{E}_5^6$ is the most interesting of the examples in this section because when $n_j = 2$ for all $j \in \{1, \cdots, 6\}$, this is the only filling other than the plumbing. This implies that when all $n_j = 2$, any sequence of lantern or daisy relations between the factorizations corresponding to $\mathcal{E}_1^6$ and that for $\mathcal{E}_5^6$ must pass through negative factorizations.

4.5 A family whose dual graphs have long arms

In the examples we have considered, the dual graphs all have arms consisting of a single vertex. Another restrictive condition on the possibilities for homology is to require that the spheres of the dual plumbing have small self-intersection numbers. If we

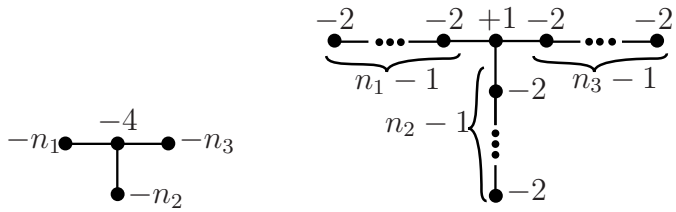

(a) Graphs (b) Dual graphs

Figure 4.21: Another simple family of graphs and their dual graphs ($n_1, n_2, n_3 \geq 1$).

look at three-armed dual graphs where every sphere except the central vertex has self-intersection number -2 as in figure 4.21b, we can understand fillings of Seifert fibered spaces $Y(-4; -n_1, -n_2, -n_3)$ that bound plumbings according to the graphs in figure 4.21a. Note that when $n_1 = n_2 = n_3 = 2$, we are back in example 1. Therefore we can assume at least one of the arms in the dual graph has length at least 2.

Theorem 4.5.1. *If (Y, ξ_{pl}) is the boundary of a dually positive plumbing of spheres, where the star-shaped graph has exactly three arms, the central vertex has self-intersection coefficient -4, and each arm has length one, and each sphere in each arm has self-intersection coefficient strictly less than -4 then (Y, ξ_{pl}) has exactly two minimal strong symplectic fillings up to diffeomorphism, given by the original symplectic plumbing and the manifold obtained by rationally blowing down the central -4 sphere.*

Proof. We consider what each sphere in the dual graph can represent in $H_2(X_M; \mathbb{Z})$. The central vertex, and its adjacent vertices must represent one of two possible homology choices,

as in section 4.1.

Case A			Case B		
$[C_0]$	$=$	ℓ	$[C_0]$	$=$	ℓ
$[C_1^1]$	$=$	$\ell - e_1 - e_2 - e_3$	$[C_1^1]$	$=$	$\ell - e_1 - e_2 - e_4$
$[C_1^2]$	$=$	$\ell - e_1 - e_4 - e_5$	$[C_1^2]$	$=$	$\ell - e_1 - e_3 - e_5$
$[C_1^3]$	$=$	$\ell - e_1 - e_6 - e_7$	$[C_1^3]$	$=$	$\ell - e_2 - e_3 - e_6$

The remaining spheres in the concave cap have the form $e_{i_1} - e_{i_2}$. By lemma 3.3.4, the exceptional class in $[C_2^j]$ with coefficient 1 has coefficient -1 in $[C_1^j]$. Therefore in case A, up to relabelling, $[C_2^1] = e_2 - e_8$ (if e_1 appeared in $[C_2^1]$ it would be impossible to cancel the algebraic intersection of C_4 with both C_2 and C_3 since only two e_i's can appear with nonzero coefficient in $[C_2^1]$). By lemmas 3.3.5 and 3.3.7 which are simple consequences of the intersection relations, $[C_3^1] = e_8 - e_9$ or $[C_3^1] = e_3 - e_2$. However if there is another sphere C_4^1 adjacent to C_3^1 then we cannot have $[C_3^1] = e_3 - e_2$, because there is no way to write $[C_4^1] = e_{i_1} - e_{i_2}$ such that $[C_4^1] \cdot (e_3 - e_2) = 1$, $[C_4^1] \cdot [C_1^1] = 0$, and $[C_4^1] \cdot [C_1^2] = 0$. The homology of the spheres in the other arms is determined independently in the same way. Therefore if we are in case A, and each arm in the dual graph has length at least four (i.e. $n_1, n_2, n_3 > 4$), the homology of the spheres is unique up to relabeling the e_i.

If the first four spheres are configured as in case B, then lemma 3.3.4 implies $[C_2^1] = e_4 - e_7$ or $[C_2^1] = e_1 - e_5$ (up to symmetric relabeling). If we have another sphere C_3^1 adjacent to C_2^1, then we cannot have $[C_2^1] = e_1 - e_5$. This is because it is not possible to find $[C_3^1] = e_{i_1} - e_{i_2}$ such that $[C_3^1] \cdot (e_1 - e_5) = 1$, $[C_3^1] \cdot [C_1^1] = 0$, and $[C_3^1] \cdot [C_1^2] = 0$. Therefore if C_3^1 is adjacent to C_2^1, $[C_2^1] = e_4 - e_7$. Furthermore $[C_3^1] = e_7 - e_8$, since if $[C_3^1] = e_i - e_4$ it is not possible to ensure $[C_3^1] \cdot [C_1^1] = 0$ and $[C_3^1] \cdot [C_1^2] = [C_3^1] \cdot [C_1^3] = 0$ simultaneously. In conclusion, if then lengths of all of the arms in the dual graph is at least three, (i.e.

$n_1, n_2, n_3 > 3$), the homology of all of the spheres are determined, up to obvious symmetries, by the choice that the first four spheres are as in case B.

This implies that when $n_1, n_2, n_3 > 4$, there are at most two diffeomorphism types of strong symplectic fillings of the Seifert fibered space arising as the boundary of the plumbing in figure 4.21a. It is clear from the previous analysis in section 4.1 that the diffeomorphism types obtained from case A and case B differ by a rational blow-down of the central -4 sphere. Furthermore, we know that the original symplectic plumbing and the rational blow-down of the -4 sphere provide two non-diffeomorphic symplectic fillings. □

When some of n_1, n_2, and n_3 take values 3 or 4, some more interesting fillings can appear as similar homological analysis shows. The most interesting case is when $n_1 = n_2 = n_3 = 3$, which will be the first Seifert fibered space in the family discussed in the next section. When some of the $n_j = 4$, one can perform rational blow-downs of any disjoint collection of -4 spheres. If only one or two of the $n_j = 3$, nothing new appears.

4.6 The family $\mathcal{W}_{p,q,r}$

There is a family of dually positive symplectic plumbings of spheres that can be completely rationally blown down, given by the graphs in figure 4.22a. This is the only family of dually positive graphs which has a symplectic rational blowdown (of the entire configuration) due to the classifications in [BS11] and [SSW08].

We can classify the convex symplectic fillings completely for these graphs. Let $Y(\mathcal{W}_{p,q,r})$ denote the boundary of the plumbing of spheres according to the graph $\mathcal{W}_{p,q,r}$.

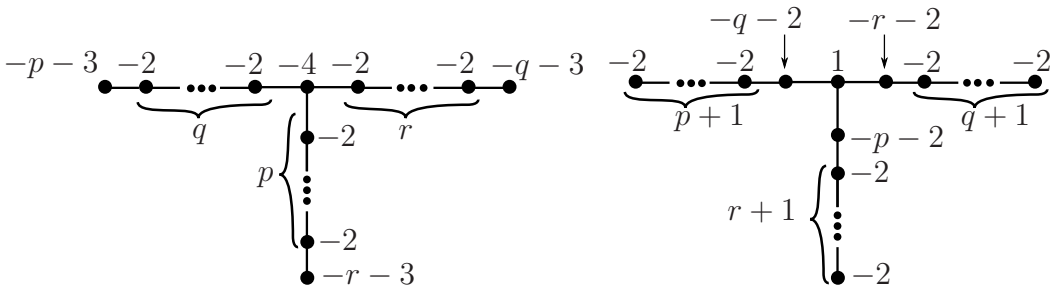

(a) Graphs $\mathcal{W}_{p,q,r}$ (b) Dual graphs

Figure 4.22: $\mathcal{W}_{p,q,r}$ and dual graphs.

Theorem 4.6.1. *The convex symplectic fillings of $(Y(\mathcal{W}_{p,q,r}), \xi_{pl})$ are of the following diffeomorphism types:*

1. *The original symplectic plumbing of spheres according to the graph $\mathcal{W}_{p,q,r}$.*

2. *A rational blow-down of the central -4 sphere in the original plumbing of spheres.*

3. *A rational blow-down of a subset of the spheres in the first arm, the first with square $-p-3$ and the next $(p-1)$ spheres with square -2, (*assuming $p-1 \leq q$*).*

4. *A rational blow-down of a subset of the spheres in the second arm, the first with square $-r-3$ and the next $(r-1)$ spheres with square -2, (*assuming $r-1 \leq p$*).*

5. *A rational blow-down of a subset of the spheres in the third arm, the first with square $-q-3$ and the next $(q-1)$ spheres with square -2, (*assuming $q-1 \leq r$*).*

6. *Any combination of (3),(4), and/or (5) assuming all the necessary hypotheses given above on p, q, r are met. Also, any combination of (3),(4), and (5) with (2), but in that case we require the stronger conditions on (3),(4), and (5) that $p \leq q$, $r \leq p$ and $q \leq r$ respectively (this ensures the rational blow-downs can all be done disjointly).*

7. A rational blow-down of the entire graph.

Proof. First note that all the above diffeomorphism types are realized as convex symplectic fillings of ξ_{pl} because these rational blow-downs are known to be symplectic operations by [Sym98], [SSW08]. Furthermore, all of these rational blow-downs produce non-diffeomorphic manifolds which can be distinguished by their intersection forms (except when there are obvious symmetries of the three arms). Therefore it suffices to provide an upper bound on the number of convex fillings which matches the number of diffeomorphism types provided in the statement of the theorem.

By corollary 3.4.2, an upper bound is given by the number of ways to represent the homology classes of the spheres in the dual graph in terms of a standard basis for $H_2(\mathbb{CP}^2 \# M\,\overline{\mathbb{CP}^2})$ of the form given in section 3.3. The dual graph for $\mathcal{W}_{p,q,r}$ is given in figure 4.22b.

We use our standard notation that C_0 is the central sphere, and C_i^j is the sphere in the j^{th} arm of distance i from the center. There are two possibilities for the homology classes of the four central-most spheres, as in previous computations. Throughout this computation, all e_i^n will be distinct basis elements for $H_2(\mathbb{CP}^2 \# M\,\overline{\mathbb{CP}^2}; \mathbb{Z})$ of square -1.

Case A			Case B		
$[C_0]$	$=$	ℓ	$[C_0]$	$=$	ℓ
$[C_1^1]$	$=$	$\ell - e_1^0 - e_1^1 - \cdots - e_{q+2}^1$	$[C_1^1]$	$=$	$\ell - e_1^0 - e_2^0 - e_1^1 - \cdots - e_{q+1}^1$
$[C_1^2]$	$=$	$\ell - e_1^0 - e_1^2 - \cdots - e_{p+2}^2$	$[C_1^2]$	$=$	$\ell - e_1^0 - e_3^0 - e_1^2 - \cdots - e_{p+1}^2$
$[C_1^3]$	$=$	$\ell - e_1^0 - e_1^3 - \cdots - e_{r+2}^3$	$[C_1^3]$	$=$	$\ell - e_2^0 - e_3^0 - e_1^3 - \cdots - e_{r+1}^3$

The remaining strings of spheres each have two possible configurations that can occur in either case A or B. They can each occur independently of each other, but one of each of

these two choices requires some inequality between p, q, r to be true. The configurations are:

$$\begin{array}{rcl|rcl|rcl}
[C_2^1] & = & e_1^1 - e_1^4 & [C_2^2] & = & e_1^2 - e_1^5 & [C_2^3] & = & e_1^3 - e_1^6 \\
[C_3^1] & = & e_1^4 - e_2^4 & [C_3^2] & = & e_1^5 - e_2^5 & [C_3^3] & = & e_1^6 - e_2^6 \\
 & \vdots & & & \vdots & & & \vdots & \\
\left[C_{p+2}^1\right] & = & e_p^4 - e_{p+1}^4 & \left[C_{r+2}^2\right] & = & e_r^5 - e_{r+1}^5 & \left[C_{q+2}^3\right] & = & e_q^6 - e_{q+1}^6 \\
\hline
\multicolumn{3}{c|}{\text{or}} & \multicolumn{3}{c|}{\text{or}} & \multicolumn{3}{c}{\text{or}} \\
\hline
[C_2^1] & = & e_1^1 - e_1^4 & [C_2^2] & = & e_1^2 - e_1^5 & [C_2^3] & = & e_1^3 - e_1^6 \\
[C_3^1] & = & e_2^1 - e_1^1 & [C_3^2] & = & e_2^2 - e_1^2 & [C_3^3] & = & e_2^3 - e_1^3 \\
 & \vdots & & & \vdots & & & \vdots & \\
\left[C_{p+2}^1\right] & = & e_{p+1}^1 - e_p^1 & \left[C_{r+2}^2\right] & = & e_{r+1}^2 - e_r^2 & \left[C_{q+2}^3\right] & = & e_{q+1}^3 - e_q^3.
\end{array}$$

Note that the bottom choices are only possible if there are enough e_i^n for $n = 1, 2, 3$, namely we need $p + 1 \leq q + 2$, $r + 1 \leq p + 2$, or $q + 1 \leq r + 2$ if we want the bottom choice for the homology classes of $\{C_i^1\}$, $\{C_i^2\}$ or $\{C_i^3\}$ respectively, and the first four spheres represent the homology given by case A. We need $p + 1 \leq q + 1$, $r + 1 \leq p + 1$, or $q + 1 \leq r + 1$ if we want the bottom choice for the homology classes of $\{C_i^1\}$, $\{C_i^2\}$ or $\{C_i^3\}$ respectively, and the first four spheres represent the homology given by case B.

As in previous examples, the effect of choosing the first four spheres to represent the homology in case B versus case A is to rationally blow-down the central -4 sphere. The conditions for when one can choose the lower representation of the homology of the j^{th} arm of the dual graph match up precisely with the conditions for when one can rationally blow down a linear subgraph of the j^{th} arm in the original graph in case A. In case B, these conditions on when we have a second choice for the homology of the j^{th} arm of the dual graph match the conditions needed to rationally blow down a linear subgraph of the j^{th} arm disjointly from the central -4 sphere.

Additionally, the symmetries which make the rational blow-down of one arm diffeo-

morphic to the rational blow-down of another arm, correspond to symmetries in the e_i^j which permute the values of j.

There is one additional way to represent the homology of the arms in the dual graphs, when the first four spheres represent homology given by case B. We know that $[C_2^j] = e_{i_1}^{m_1} - e_{i_2}^{m_2}$ where $e_{i_1}^{m_1}$ must show up with coefficient -1 in $[C_1^j]$. In case A, we cannot have $e_{i_1}^{m_1} = e_1^0$ and still have $[C_2^j] \cdot [C_1^{j'}] = 0$ for $j \neq j' \in \{1,2,3\}$. However, in case B, this can occur but it uniquely determines the remaining homology classes as follows.

$$\begin{array}{rcl|rcl|rcl} [C_2^1] &=& e_1^0 - e_1^2 & [C_2^2] &=& e_3^0 - e_1^3 & [C_2^3] &=& e_2^0 - e_1^1 \\ [C_3^1] &=& e_1^2 - e_2^2 & [C_3^2] &=& e_1^3 - e_2^3 & [C_3^3] &=& e_1^1 - e_2^1 \\ \vdots & & & \vdots & & & \vdots & & \\ \left[C_{p+2}^1\right] &=& e_p^2 - e_{p+1}^2 & \left[C_{r+2}^2\right] &=& e_r^3 - e_{r+1}^3 & \left[C_{q+2}^3\right] &=& e_q^1 - e_{q+1}^1 \end{array}$$

This gives an embedding of the dual configuration of symplectic spheres into $\mathbb{C}\mathrm{P}^2 \#(p+q+r+6)\,\overline{\mathbb{C}\mathrm{P}^2}$. Note that the dual graph has $p+q+r+7$ vertices, so a regular neighborhood P of the corresponding configuration of spheres has $b_2(P) = p+q+r+7 = b_2(\mathbb{C}\mathrm{P}^2 \#(p+q+r+6)\,\overline{\mathbb{C}\mathrm{P}^2})$. The first and second homology of $\partial P = Y(\mathcal{W}_{p,q,r})$ are both torsion, and P and $\mathbb{C}\mathrm{P}^2 \#(p+q+r+6)\,\overline{\mathbb{C}\mathrm{P}^2}$ are simply connected, so their first homologies are zero. Therefore, the Mayer-Vietoris theorem implies that the first and second homologies of the complement of P in this embedding are both torsion. Therefore this is the diffeomorphism type of a rational homology ball. Since this is the unique possible rational homology ball which can strongly symplectically fill its contact boundary, it must be diffeomorphic to the smoothing of the normal surface singularity studied in [SSW08].

Therefore the number of ways to represent the homology of the spheres in the dual graph is in direct correspondence with the diffeomorphism types we can realize by starting

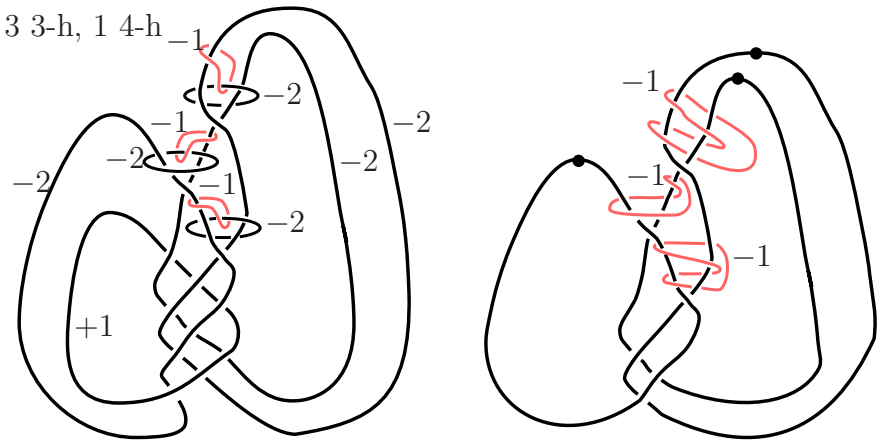

(a) Embedding into $\mathbb{C}\mathrm{P}^2 \# 6\,\overline{\mathbb{C}\mathrm{P}^2}$

(b) Upside down complement of dual configuration

Figure 4.23: The embedding of the concave cap and its complement which is a rational homology ball for $\mathcal{W}_{3,3,3}$.

with the original symplectic plumbing, and rationally blowing down a subgraph or the entire graph, so these are all possible convex symplectic fillings of (Y, ξ_{pl}). □

The explicit handlebody diagrams constructed as in section 4.1 for the embedding of the dual graph corresponding to the last case of the theorem and the complement of this embedding are shown in figure 4.23 for the case $\mathcal{W}_{3,3,3}$.

Chapter 5

Comparing to rational blow-down

The rational blow-down operation was first defined by Fintushel and Stern in [FS97], and was subsequently generalized by Park in [Par97] and by Stipsicz, Szabó, and Wahl in [SSW08]. The operations considered by Fintushel and Stern are defined by cutting out a neighborhood of embedded 2-spheres in a 4-manifold which intersect according to a plumbing graph as in figure 5.1 and gluing in a certain rational homology ball with the same boundary: $L(p^2, p-1)$. Fintushel and Stern calculated the effect of this operation on the Seiberg-Witten invariants of the manifold, and Park used this operation to produce the first example of an exotic copy of $\mathbb{C}\mathrm{P}^2 \# 7\,\overline{\mathbb{C}\mathrm{P}^2}$ in [Par05]. Although the original operation was defined in the smooth category, the phenomena observed with the Seiberg-Witten invariants suggested that this operation may be done symplectically. This was proven by Symington in [Sym98] in the case that the 2-spheres are symplectic, by showing that both the neighborhood of the 2-spheres and the rational homology ball have convex symplectic boundary inducing the same contact structures. All of these results were extended to a generalized family where the plumbing of spheres and the rational ball both have boundary $L(p^2, pq-1)$. For these lens

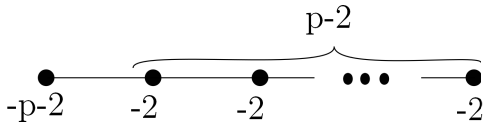

Figure 5.1: The plumbing graph for the Fintushel and Stern rational blow-down.

space boundary cases, the 2-spheres intersect according to a linear graph, but more general negative definite plumbings can be symplectically cut out and replaced by symplectic rational homology balls. A list of all such graphs was proposed in [SSW08] and eventually proven to be a complete list (see [BS11, GS07, PSS13]). Similar operations can be defined using convex symplectic fillings of Seifert fibered spaces with the canonical contact structure, in the sense that we can cut out a symplectic plumbing of spheres and glue in an alternate symplectic filling. The examples of Stipsicz, Szabó, and Wahl are a special case of this, but in greater generality, the symplectic filling being glued in need not be a rational homology ball. Because the plumbings being cut out and replaced with Seifert-fibered boundary are plumbed according to star-shaped graphs, these more general cut and paste operations were called *star surgery* in [KS]. Star surgery was shown to be effective at producing exotic copies of $\mathbb{C}\mathrm{P}^2 \# N\,\overline{\mathbb{C}\mathrm{P}^2}$ for $N = 6, 7, 8$ in [KS].

There are two important properties of the rational blow-down which make them effective operations for producing small exotic 4-manifolds.

1. Rational blow-down operations decrease the Euler characteristic of the 4-manifold by killing off generators of second homology.

2. The Seiberg-Witten (or Donaldson) invariants of the rationally blown-down manifold can be calculated in terms of the Seiberg-Witten (or Donaldson) invariants of the original manifold along with some homological computations.

Michalogiorgaki [Mic07] proved a theorem which implies that property (2) holds more generally for any star surgery operation which removes a dually positive star-shaped plumbing of spheres. In the first part of this chapter we will prove that property (1) also holds for

all dually positive star surgeries. In other words, the dually positive plumbing of spheres has the largest Euler characteristic amongst all symplectic fillings of the Seifert fibered boundary with the canonical contact structure. In the second part of this chapter, we will show that star surgery operations are strictly more general than sequences of rational blow-downs.

5.1 Euler characteristic upper bounds

The main goal of this section is to prove the following theorem.

Theorem 5.1.1. *Let Γ be a dually-positive star-shaped graph. Let X be the corresponding symplectic plumbing of spheres with convex boundary inducing the canonical contact structure, and let $(Y, \xi) = \partial(X, \omega)$. Then the Euler characteristic of any minimal convex symplectic filling of (Y, ξ) is bounded above by the Euler characteristic of X.*

The Euler characteristic is additive under gluing two pieces along their odd dimensional boundaries. Therefore, if a symplectic filling appears as the complement of an embedding of the dual plumbing into $\mathbb{C}\mathrm{P}^2 \# N\,\overline{\mathbb{C}\mathrm{P}^2}$, its the Euler characteristic is $2 + N - |\Gamma'|$. Here $|\Gamma'|$ indicates the number of vertices in the dual graph. Assuming the filling is minimal, by lemma 3.4.4, all N exceptional homology classes appear with non-zero coefficient in at least one of the homology classes of the dual graph spheres. The homology classes of the embedded dual graph spheres, written in terms of the standard basis for $H_2(\mathbb{C}\mathrm{P}^2 \# N\,\overline{\mathbb{C}\mathrm{P}^2})$, are restricted by the lemmas of section 3.3. With all of these restrictions on the homology embeddings, the different possibilities for the Euler characteristics of the corresponding fillings are determined by the varying ways that exceptional classes appear with non-zero coefficients in the homology classes of distinct spheres.

Note that the subtle additional hypotheses from section 3.4 needed to obtain complete classifications are not needed for this theorem, because the Euler characteristic is determined simply by the homological embedding data.

Proof of theorem 5.1.1. To understand fillings of (M, ξ_{can}) we want to understand symplectic embeddings of the dual plumbing into $\mathbb{C}\mathrm{P}^2 \# N\,\overline{\mathbb{C}\mathrm{P}^2}$. The dual graph construction of section 3.1 provides one such embedding, where the complement is the original plumbing. The homological embedding corresponding to this embedding can be easily computed.

The spheres adjacent to the central $+1$ sphere represent the class $h - e_1 - e_{i_1} - \cdots - e_{i_n}$. They all share e_1 with coefficient -1, but the other e_x's that appear with nonzero coefficient are all distinct. After blowing up enough times, the most recently introduced exceptional sphere in each singular fiber becomes the next sphere in the arm of the dual graph (instead of becoming part of the corresponding arm in the plumbing graph). Then we blow up at points at its intersection with the subsequent sphere until its proper transform has the necessary self-intersection number, so that its proper transform represents $e_i - e_{x_1} - \cdots - e_{x_n}$. Repeating this process, the spheres in the j^{th} arm represent homology classes as follows.

$$h - e_1 - e_1^{1,j} - \cdots - e_{n_{1,j}}^{1,j}$$

$$e_{n_{1,j}}^{1,j} - e_1^{2,j} - \cdots - e_{n_{2,j}}^{2,j}$$

$$e_{n_{2,j}}^{2,j} - e_1^{3,j} - \cdots - e_{n_{3,j}}^{3,j}$$

$$\vdots$$

$$e_{n_{m-1,j}}^{m-1,j} - e_1^{m,j} - \cdots - e_{n_{m,j}}^{m,j}$$

Here all $e_x^{i,j}$ are exceptional classes distinct from each other and from e_1. There are no exceptional sphere classes which appear with nonzero coefficient in more than one arm because the blow-ups are all done in distinct singular fibers which each correspond to distinct arms. The only exceptional classes besides e_1 that appear with nonzero coefficient in two different spheres are in adjacent spheres, and appear with coefficient -1 in the inner-more sphere and with coefficient $+1$ in the outer-more sphere.

It suffices to show that any other homological embedding of the dual graph uses no more distinct exceptional classes than this embedding.

By lemma 3.3.3, each pair of spheres adjacent to the central $+1$ sphere in the dual graph, must have exactly one shared e_i appearing with -1 coefficient in both. In the plumbing embedding, they all share the same class, e_1. If they did not all share the same class, there would necessarily be at least one sphere C_1^j in which two exceptional classes e_x and e_y appear with -1 coefficient, where e_x appears with -1 coefficient in $C_1^{j_1}, \cdots, C_1^{j_n}$ and e_y appears with -1 coefficients in a disjoint set of spheres $C_1^{j_{n+1}}, \cdots, C_1^{j_m}$. There is a third exceptional class e_z which appears with -1 coefficient in $C_1^{j_1}$ and $C_1^{j_{n+1}}$. Now consider the homology embedding where $C_1^j, C_1^{j_1}, \cdots, C_1^{j_m}$ all share the same e_x with non-zero coefficient. Then in order to keep the squares of the homology classes of C_1^j, $C_1^{j_1}$, and $C_1^{j_{n+1}}$ the same, there must be three new distinct exceptional classes e_a, e_b, e_c, with one appearing with coefficient -1 in each of these classes. Therefore decreasing the number of distinct e_i's which are shared between the spheres adjacent to the central vertex, increases the total number of distinct exceptional classes appearing with nonzero coefficients in the embedding.

By lemma 3.3.5, spheres which are adjacent in the same arm must share at least one exceptional class with nonzero coefficients. In the plumbing embedding, the only sharing

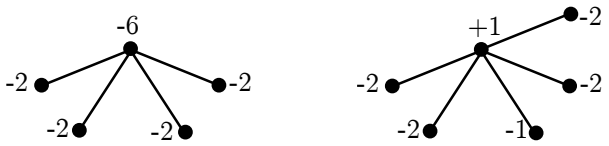

(a) Plumbing graph (b) Dual graph

Figure 5.2

of exceptional classes (other than e_1 which was discussed in the previous paragraph) is a single exceptional class shared between consecutive spheres within an arm. Therefore this homology embedding has the minimal possible amount of sharing of exceptional classes away from the central vertex. If more of these exceptional classes were shared amongst multiple different spheres, the total number of exceptional classes appearing with non-zero coefficient would decrease. This implies that the plumbing homology embedding maximizes the number of exceptional classes which appear with nonzero coefficient.

Therefore, the original plumbing has the maximal Euler characteristic of any minimal convex filling, since all convex fillings appears as the complement of the symplectic embedding of the dual graph into a blow-up of $\mathbb{C}\mathrm{P}^2$. □

5.2 Star surgeries unobtainable from rational blow-downs

Initially, one might ask whether every symplectic filling of a dually positive Seifert fibered spaces with its canonical contact structure can be obtained from the plumbing by some sequence of already understood symplectic rational blow-down operations. In fact, this result was shown to be true when the boundary is a lens space with its canonical contact structure in [BO]. Here, we show that this is not the case for Seifert fibered spaces with an explicit example. In particular, we will show that the plumbing according to the graph in

figure 5.2a has a star-surgery operation which is not equivalent to any sequence of symplectic rational blow-downs (where here symplectic rational blow-down includes Fintushel and Stern's original family, Park's generalization, as well as the further negative definite examples classified in [SSW08] and [BS11]). This example is a special case of those considered in section 4.3.

Theorem 5.2.1. *The boundary (Y, ξ_{can}) of the plumbing of spheres P, plumbed according to the graph in figure 5.2a, has exactly two minimal strong symplectic fillings. One is the plumbing itself and the other has Euler characteristic 2. The filling of Euler characteristic 2 cannot be obtained from the plumbing by any single symplectic rational blow-down, or any sequence of symplectic rational blow-downs.*

Proof. The dual graph is given in figure 5.2b. The only possible homological embeddings allowed by lemma 3.3.8 and the restrictions of the squares of the dual graph spheres are given below.

	C_1	C_2	C_3	C_4	C_5
Emb 1	$h-e_1-e_2-e_3$	$h-e_1-e_4-e_5$	$h-e_1-e_6-e_7$	$h-e_1-e_8-e_9$	$h-e_1-e_{10}$
Emb 2	$h-e_1-e_3-e_4$	$h-e_1-e_5-e_6$	$h-e_2-e_3-e_5$	$h-e_2-e_4-e_6$	$h-e_1-e_2$

There is at most one isotopy class of smooth embeddings for each of these two homological embeddings, by corollary 3.4.2. Therefore there are at most two diffeomorphism types of convex symplectic fillings of the canonical contact boundary of this plumbing.

The Euler characteristic of the two potential complementary fillings is

$$\chi(\mathbb{C}\mathrm{P}^2 \# N\,\overline{\mathbb{C}\mathrm{P}^2}) - \chi(\text{Dual Graph}) = 3 + N - 7 = N - 4.$$

Thus, here we see there are at most two minimal strong symplectic fillings, one of Euler characteristic 6 and the other of Euler characteristic 2. The first homological embedding is

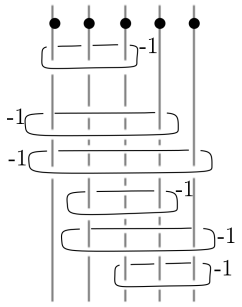

Figure 5.3: The Lefschetz fibration for the filling of Euler characteristic two.

that of the dual graph construction, so the original plumbing graph is realized as a complementary filling to such an embedding. The second filling of Euler characteristic two is realized by a Lefschetz fibration as shown in figure 5.3. The fact that the boundary open book supports the correct contact structure ξ_{pl} follows from lemma 4.3.2.

Any sequence of symplectic rational blow-downs of spheres contained inside the plumbing P would produce a sequence of symplectic fillings of the same contact boundary (since the rational blow-downs are symplectic operations that are performed on the interior). There are only two minimal symplectic fillings of this particular contact manifold, the plumbing and the smaller filling. Therefore, the only way it would be possible to obtain the smaller filling from the plumbing by a sequence of rational blow-downs is by a single rational blow-down; there can be no intermediate steps. A rational blow-down replaces a neighborhood of a set of embedded symplectic spheres (whose union is simply connected), by a rational homology ball. Therefore the change in the Euler characteristic of a manifold before and after a rational blowdown, is precisely the number of spheres in the rational blow-down. The Euler characteristic of the smaller filling in this case is 2, and the Euler characteristic of the plumbing is 6. Therefore we need to check which plumbing graphs with

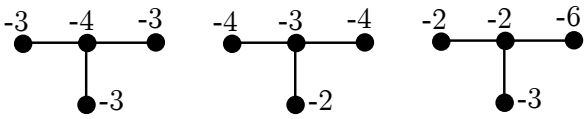

Figure 5.4: Non-linear graphs with four vertices which can be rationally blown down [BS11].

4 vertices can be rationally blown down.

Such graphs are either linear, or have three arms of length one. The classification in [BS11] describes explicitly which graphs with three arms can be rationally blown down. The three of these where each arm has length one are shown in figure 5.4. The linear graphs which can be rationally blown include the examples of Fintushel and Stern and the more general examples of Park, where the continued fraction expansion of the weights is $-\frac{p^2}{pq-1}$ for $gcd(p,q) = 1$. There is an inductive procedure to build all such plumbings (described in [SSW08] section 4), where the induction increases the length of the plumbing by one each time. This shows there are four different linear plumbings of length 4 which have rational homology ball fillings. The self-intersection numbers of the spheres in the plumbings are: $(-7,-2,-2,-2)$ (the original Fintushel-Stern rational blow-down with $p = 5$), $(-3,-5,-3,-2)$ (Park's generalization with $p = 8$, $q = 3$), $(-2,-2,-5,-4)$ (Park's generalization with $p = 7$, $q = 5$), and $(-2,-6,-2,-3)$ (Park's generalization with $p = 7$, $q = 4$).

If the plumbing P could be symplectically rationally blown down to obtain the smaller filling, that would mean that there exist four symplectic spheres in P whose intersection data is specified by one of these seven graphs. We can use the adjunction formula to rule out this possibility. Note that $H_2(P;\mathbb{Z})$ is generated by the five spheres which are the cores of the disk bundles that are plumbed together. We denote the sphere corresponding to

the central vertex by C_0, and the spheres corresponding to the vertices in the four arms by C_1, C_2, C_3, and C_4. The C_i are a symplectic spheres, so the adjunction formula holds: $\langle c_1(\omega), C_i\rangle = C_i^2 + 2$. Therefore, $\langle c_1(\omega), [C_0]\rangle = -4$ and $\langle c_1(\omega), [C_i]\rangle = 0$ for $i = 1, 2, 3, 4$. Now for any other symplectic sphere S embedded in P, we can write $[S] = \sum_{i=0}^{4} a_i[C_i]$. Then $[S]^2 + 2 = \langle c_1(\omega), [S]\rangle = -4a_0$. In particular, $[S]^2 + 2$ must be divisible by 4 since a_0 must be an integer. All of the graphs with four vertices representing plumbings that can be rationally blown down contain at least one sphere whose self-intersection number $+2$ is not divisible by 4. Therefore none of these symplectic plumbings which can be rationally blown down, can embed into P. □

Remark 5.2.2. In fact none of these rational blow-downs can be done smoothly either because the spheres to be rationally blown down have odd intersection form whereas P has even intersection form. However, it is not clear that there is no sequence of smooth (but not symplectic) rational blow-downs/ups which results in the diffeomorphism type of the smaller filling, since the intermediate steps need not be symplectic in this case. However, this result shows that as a symplectic operation, star surgery is strictly more general than rational blowdowns.

Chapter 6

Translating to monodromy substitutions

Because each of the dually positive Seifert fibered spaces with their canonical contact structures are supported by planar open books, Wendl's theorem (theorem 2.4.2) implies that every minimal symplectic filling corresponds to a Lefschetz fibration, or equivalently, a positive factorization of the monodromy of the canonical planar open book that supports the contact structure. Two different positive factorizations of the same monodromy element yield two different minimal symplectic fillings of the same contact manifold, and an example of such a pair of factorizations is called a *monodromy substitution*. Thus one could classify symplectic fillings of Seifert fibered spaces by studying all different positive factorizations of the monodromy elements for the open books supporting ξ_{pl} coming from theorem 2.4.1. The methods used for classification in chapter 3 take a rather different perspective on this classification problem so it is nontrivial to work out the relationship between these two methods. While the homological embedding classifications used in section 3 are easy to carry out, the monodromy substitutions are often easier to work with in applications to 4-manifold topology. In this chapter, we work to explain these translations in order to utilize the strengths of both methods.

6.1 Translations for the canonical plumbing fillings

We begin the translation project with the fillings that we know exist for all Seifert fibered spaces with their canonical contact structure: the convex star-shaped plumbings. The goal of the translation is to demonstrate a process that starts with the data of the embedding of the dual graph into $\mathbb{C}\mathrm{P}^2 \# N\,\overline{\mathbb{C}\mathrm{P}^2}$ which is complementary to the plumbing filling and ends with the data of the positive monodromy factorization corresponding to the Gay-Mark Lefschetz fibration of theorem 2.4.1.

We will see that this process yields a correspondence between the vertices of the dual graph and the boundary components of the planar fibers of the Lefschetz fibration. Moreover, the vanishing cycles of the canonical Lefschetz fibration can be determined via the self-intersection number markings on the vertices of the dual graph. Because the canonical Lefschetz fibration is determined by the graph for the convex plumbing, and the dual graph for the concave plumbing is determined by the graph, it is obvious that there is some way to determine the canonical Lefschetz fibration from the dual graph. What is most interesting about this correspondence, is that it provides a model indicating the correspondence between the embedded spheres of the concave plumbing and the monodromy substitutions. We state the correspondence first and then explain how this relates to the embedding of the concave plumbing in the dual graph construction of section 3.1.

Let Γ' denote the dual graph of a dually positive star-shaped graph Γ. Label each of the non-central vertices in the dual graph v_i^j such that j specifies the arm that the vertex is in, and i specifies the distance (number of edges) between v_i^j and the central vertex. The canonical Lefschetz fibration for the convex plumbing for Γ is then given by the following procedure using the data of Γ'.

Start with a disk with a single boundary parallel vanishing cycle. For each arm of the dual graph choose a subdisk such that these subdisks are all disjoint from each other and the boundary parallel vanishing cycle. In arm j, start with v_1^j (which is adjacent to the central vertex), and suppose it has weight $-n_1^j \leq -1$. Place n_1^j vanishing cycles on concentric curves which are parallel to the boundary of the subdisk and place a hole at the center of the disk labelled h_1^j. If there are more vertices in the dual graph in arm j, choose a subdisk which lies between the two innermost vanishing cycles just added (or if only one vanishing cycle was added, in a neighborhood just outside of it). If the weight of v_2^j is $-n_2^j$, place $n_2^j - 1$ concentric vanishing cycles parallel to the boundary of this new subdisk. Add a new hole labelled h_2^j at the center. If there are more vertices in arm j, identify a subdisk between the two innermost vanishing cycles just added (or just outside of the single vanishing cycle just added if $n_2^j = 2$) and repeat the procedure for v_3^j (adding $n_3^j - 1$ vanishing cycles and a hole), and so on until all the vertices in arm j of the dual graph have been assigned a corresponding hole. After doing this procedure for all arms of the dual graph Γ', we obtain the canonical Lefschetz fibration for the plumbing corresponding to the graph Γ. The reader can convince him/herself that the combinatorial procedure for producing the canonical Gay-Mark Lefschetz fibration in this case matches up with the combinatorial procedure for producing the dual graph. Figure 6.1 shows a demonstrative example.

Now we show how this correspondence grows naturally out of a sequence of handle-body diagrams for the embedding of the concave dual plumbing into $\mathbb{C}\mathrm{P}^2 \# N\,\overline{\mathbb{C}\mathrm{P}^2}$ and the complement of the embedding. Suppose Γ' has central vertex marked $+1$, d arms, and the marking for the vertex in the j^{th} arm of distance i from the center is $-n_i^j$. To exhibit the embedding of the corresponding plumbing into $\mathbb{C}\mathrm{P}^2 \# N\,\overline{\mathbb{C}\mathrm{P}^2}$ such that the complement is

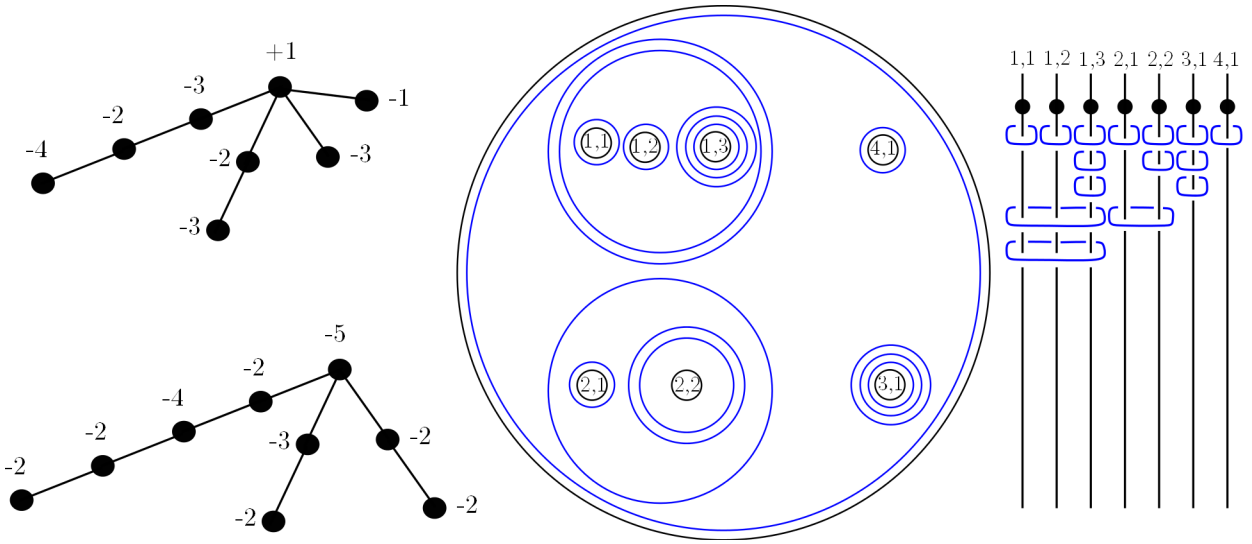

Figure 6.1: An example of a dual graph (top left), its corresponding graph (bottom left), and the corresponding canonical Lefschetz fibration for the plumbing of the lower graph, represented by the fiber with vanishing cycles drawn in blue in the center, and as a handlebody on the right (complete the braid trivially).

the convex plumbing, we start with a handlebody diagram for $\mathbb{C}\mathrm{P}^2$ with $(d+1)$ 2-handles attached along unknots linked together with a full $+1$ twist and with $+1$ framings. To make this a diagram for $\mathbb{C}\mathrm{P}^2$ we cancel d 2-handles with d 3-handles, and attach a 4-handle to close off the manifold. The attaching circles represent the equators of $d+1$ complex projective lines in $\mathbb{C}\mathrm{P}^2$. Then we blow-up according to the dual graph construction of section 3.1. First blow-up at the common intersection point of d of the complex projective lines, which in the diagram corresponds to introducing a new -1 framed 2-handle which links with, untwists, and reduces the framings on d of the original 2-handles. This results in figure 6.2a without the x_j boxes, assuming the vertical strands have the tops and bottoms identified and have 0-framing. The vertical strands represent the equators for the plumbing spheres $C_1^1, \cdots, C_1^d$ (the first sphere in each arm of the dual plumbing). We blow-up along each of these spheres

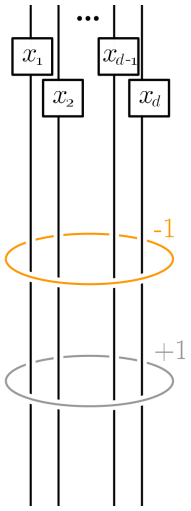

(a) Embedding of dual graph. Include d 3-handles and one 4-handle.

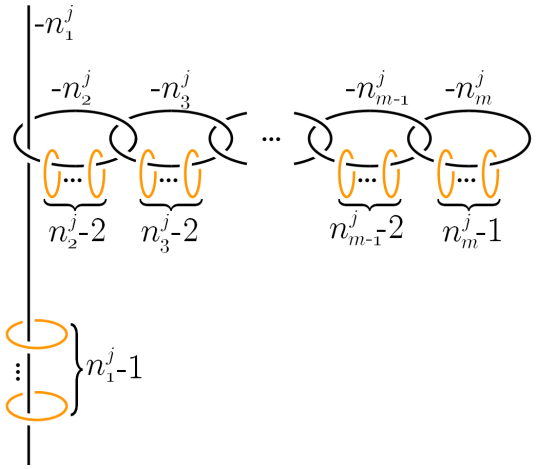

(b) Figure for box x_j. The value of m also depends on j despite the notation. All orange curves have framing -1.

Figure 6.2: Embedding the dual plumbing into $\mathbb{C}\mathrm{P}^2 \# N\,\overline{\mathbb{C}\mathrm{P}^2}$ via the canonical embedding given by the dual graph construction.

n_1^j times to adjust the framing down to $-n_1^j$, and then if the arm has length greater than one, the last of these exceptional spheres becomes the next sphere in the arm. Then blow-up along this chosen exceptional sphere $n_2^j - 1$ times to adjust its framing to $-n_2^j$, and use the last of these exceptional spheres for the next sphere in the arm (if it exists). Continue until the entire arm is built. At the end of this process, we have an embedding of the dual plumbing which is represented by the handlebody of figure 6.2 with the x_j boxes as indicated.

Now we will show how this particular handlebody for $\mathbb{C}\mathrm{P}^2 \# N\,\overline{\mathbb{C}\mathrm{P}^2}$, which displays the embedding explicitly, can be used to produce the canonical Gay-Mark Lefschetz fibration structure. First we cut out the embedded dual plumbing by removing the 0-handle and the 2-handles whose cores are parts of the core spheres of the plumbing. Then turn the resulting manifold with boundary upside-down. This results in figure 6.3. After simplifying

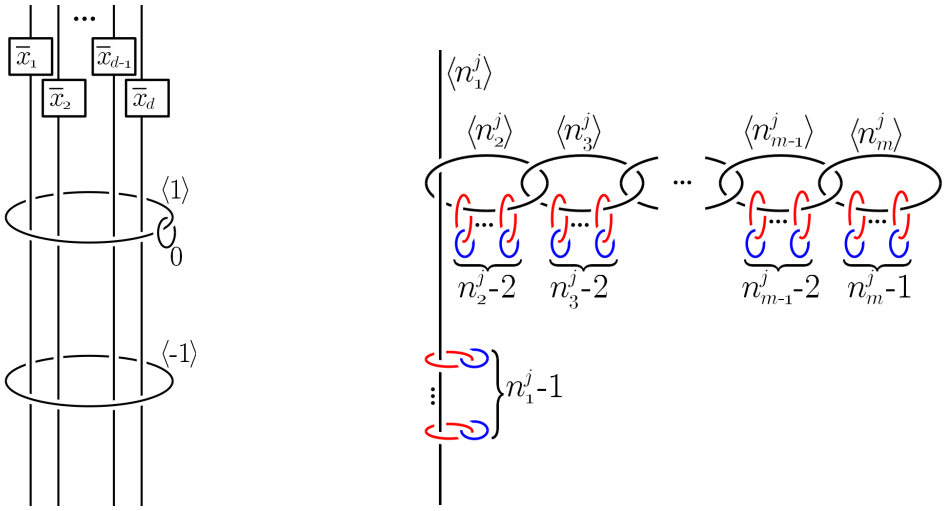

(a) (b) Figure for box $\bar{x}_j$. Color framings: ⟨1⟩, 0

Figure 6.3: The complement of the dual plumbing upside-down.

the surgery diagram by Kirby calculus blow-downs, we get figure 6.4.

Further Kirby calculus moves are performed within the boxed region in figure 6.5. Our goal is to reach a handlebody diagram for a planar Lefschetz fibration, so we want a trivial braid of dotted circles representing 1-handles. This braid lies in a solid torus fibered by meridional disks that are pierced by the braid strands. The 2-handles should have -1-framed attaching circles which lie in these transverse meridional disks. We must stabilize the diagram by introducing a canceling 1-2-handle pair for each vertex in the dual graph beyond the first in each of the d arms (figure 6.5b). Recall that the number of 1-handles in the Lefschetz fibration diagram is equal to the number of holes in the disk which makes up its fibers and this is equal to the number of vertices in the arms of the dual graph. There are of course many ways to stabilize, so knowing what type of stabilization works to produce a Lefschetz fibration in the complement of the canonical embedding is useful as a clue for

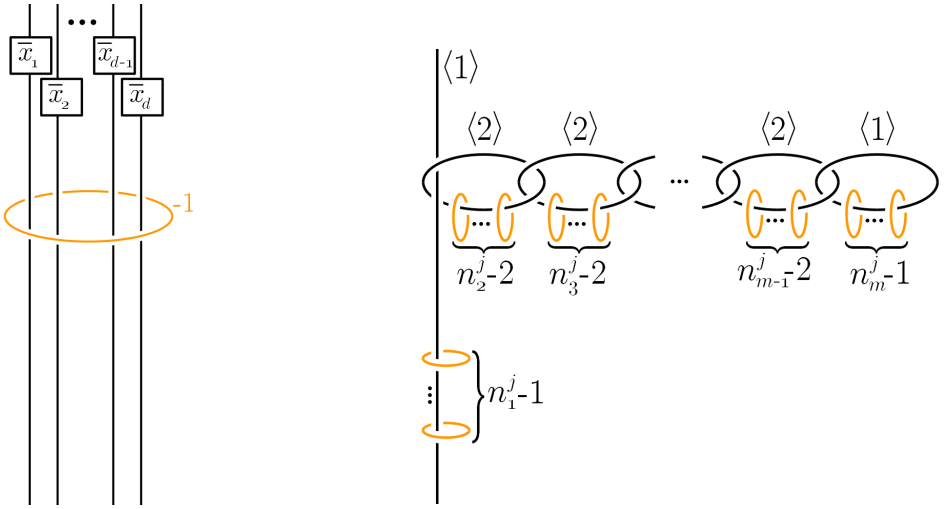

(a) (b) Figure for box $\bar{x}_j$. Color framings: -1

Figure 6.4: The complement of the dual plumbing upside-down, continued.

repeating this process for more complicated embeddings. We then perform a sequence of 1-handle slides, in order to arrange the 1-handles so that they are all components of the same trivial braid which runs transversally to the Seifert disks of the -1-framed attaching circles (figure 6.5c). The key pieces of this handle calculus sequence to remember for future use are the stabilizations and these 1-handle slides.

Examining the piece of the Lefschetz fibration given by figure 6.6c, which gives the piece for a single arm, we see that this gives the vanishing cycles and holes described on the subdisk for the chosen arm as described above in terms of the dual graph. The pieces for the various arms fit together into figure 6.6a which provides a handlebody diagram for the canonical Lefschetz fibration on the convex plumbing.

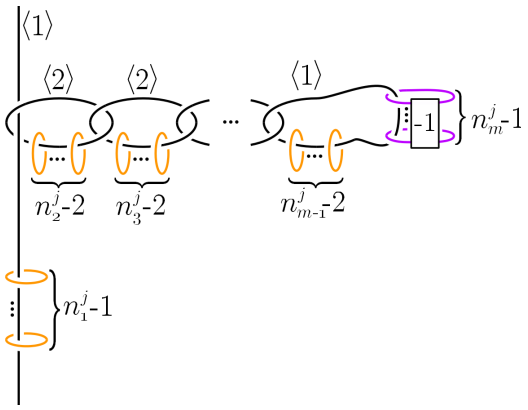

(a) Blow-down ⟨1⟩ from figure 6.4b. Color framings: −1, −2

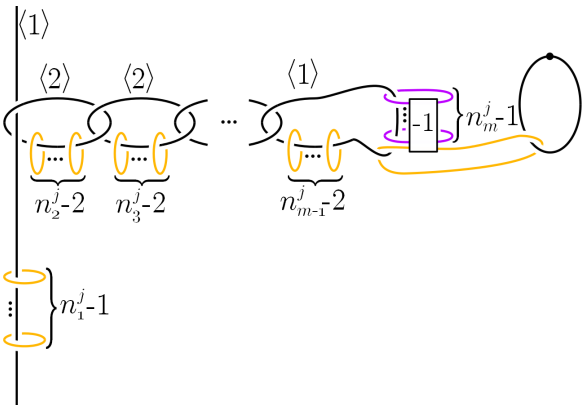

(b) Stabilize. Color framings: −1, −2

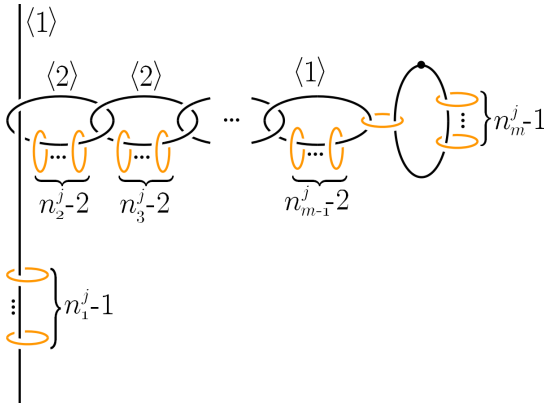

(c) Handleslide. Color framings: −1

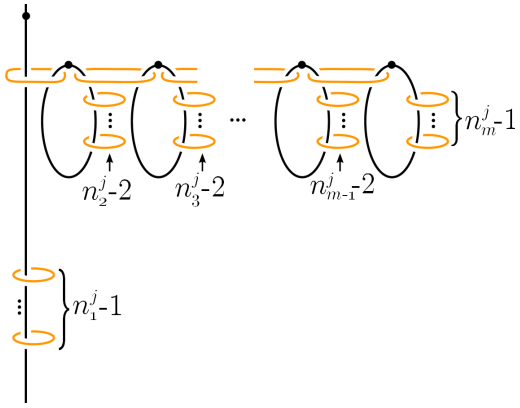

(d) Repeat. Color framings: −1

Figure 6.5: The complement of the dual plumbing upside-down, focusing on the portion corresponding to one arm.

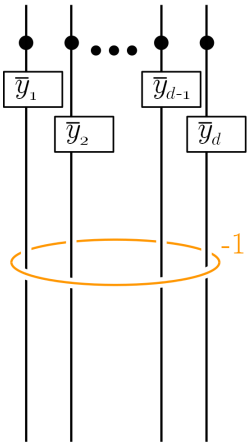

(a) Fit figure 6.6c into the $\overline{y}_j$ boxes for the complete Lefschetz fibration. The new dotted circles in the $\overline{y}_j$ boxes run through the displayed -1 curve.

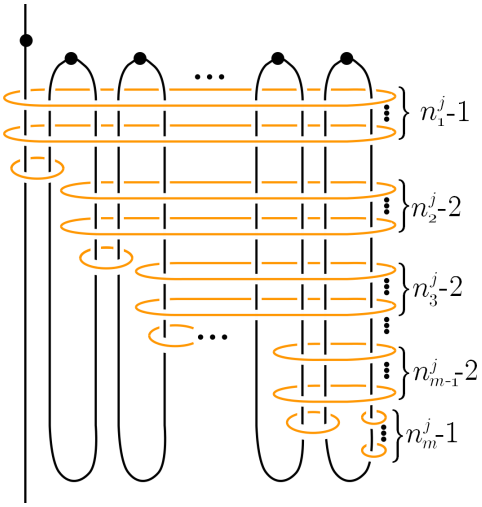

(b) Isotopy from figure 6.5d. Color framings: -1

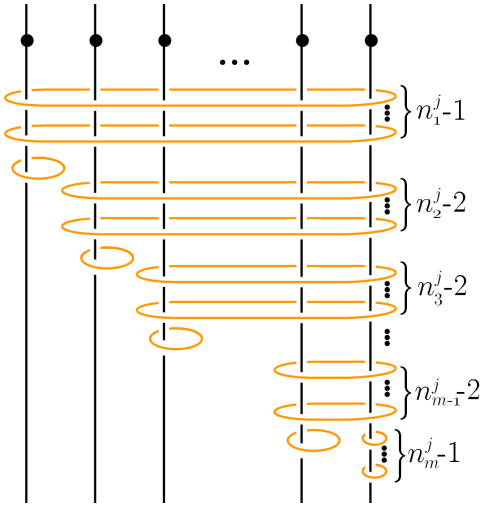

(c) Box y_j. From previous diagram, slide 1-handles over each other. Color framings: -1

Figure 6.6: Handle moves to produce a Lefschetz fibration.

6.2 Translating homological embeddings of the C_1^j

In the canonical embedding of the dual graph, the homology classes of $C_1^1, \cdots, C_1^d$ all share a single exceptional class (e_1) with coefficient -1. We saw in section 4.4 that more interesting homological embeddings can be realized subject to the constraint that every pair of $[C_1^1], \cdots, [C_1^d]$ shares a single exceptional class with coefficient -1 (lemma 3.3.3). In the case where the dual graph has at most six arms, each of length one, all homological possibilities allowed by lemma 3.3.3 were realized by symplectic embeddings obtained by blowing up a configuration of complex projective lines. We found a Lefschetz fibration corresponding to each embedding, and we will go through here the translation of the most complicated embedding of that section (figure 4.19b repeated here as figure 6.7a). Then we will discuss some limitations on extending the examples of section 4.4 to a larger number of arms.

6.2.1 A particularly interesting six arm embedding

To translate the embedding of a dual graph with six arms each consisting of a single sphere into $\mathbb{C}\mathrm{P}^2 \# N\,\overline{\mathbb{C}\mathrm{P}^2}$ shown in the handle structure of figure 6.7a to a handlebody for the complement with a visible Lefschetz fibration structure, we follow the same sorts of steps as were followed in the simple examples of section 4.1, with some minor additional complications that we discuss here. Recall that this embedding represents the homological embedding:

	$\mathcal{E}_5^6$
$[C_1^1] =$	$\ell - e_1 - e_3 - e_5 - e_\cdot - \cdots - e_\cdot$
$[C_1^2] =$	$\ell - e_1 - e_4 - e_6 - e_\cdot - \cdots - e_\cdot$
$[C_1^3] =$	$\ell - e_1 - e_2 - e_7 - e_\cdot - \cdots - e_\cdot$
$[C_1^4] =$	$\ell - e_2 - e_4 - e_5 - e_\cdot - \cdots - e_\cdot$
$[C_1^5] =$	$\ell - e_2 - e_3 - e_6 - e_\cdot - \cdots - e_\cdot$
$[C_1^6] =$	$\ell - e_3 - e_4 - e_7 - e_\cdot - \cdots - e_\cdot$

Note that the embedding of figure 6.7a was produced by starting with six strands braided according to a full positive twist. Then we isotope the braid slightly to bring together triples of crossings between strands corresponding to three spheres which share an exceptional class. Finally blow-up to reverse the crossings in the upper half of the twist, thus unlinking the six strands from each other.

A diagram for the complement of the embedded dual plumbing is given by figure 6.7b. This simplifies to figure 6.7c. Rotating the plane of projection by 90° so that we take the perspective from the left side of figure 6.7c, we get the Lefschetz fibration handlebody of figure 6.8. The only additional tricky part is that once we fix our identification of the fibers with a six holed disk, some of the vanishing cycles do not enclose the holes convexly. Instead, these curves are the image of the curve that encloses the same holes convexly under a Dehn twist about some other curve. More specifically, the fourth vanishing cycle from the top is the image of the curve convexly enclosing holes 2, 4, and 6, under a a right handed (positive) Dehn twist about the curve convexly enclosing holes 5 and 6, as shown in figure 6.9. Similarly the second to last vanishing cycle is the image of the curve convexly enclosing holes 3 and 6 under a right handed Dehn twist about the curve convexly enclosing holes 4, 5, and 6. Using the conjugation relation we can write the monodromy of the open book on

the boundary of this Lefschetz fibration as follows, as claimed in section 4.4.

$$D_1^{n_1-2}D_2^{n_2-2}D_3^{n_3-2}D_4^{n_4-2}D_5^{n_5-2}D_6^{n_6-2}D_{1,2,3}D_{1,4}D_{1,5,6}(D_{5,6}^{-1}D_{2,4,6}D_{5,6})D_{2,5}(D_{4,5,6}^{-1}D_{3,6}D_{4,5,6})D_{3,4,5}$$

6.2.2 Translating more general embeddings of the C_1^j

This procedure for obtaining a Lefschetz fibration is repeatable for more general braids which can become unlinked by sequences of blow-ups. The homological configuration determines how the exceptional spheres intersect the dual graph spheres, or equivalently the linking of the -1-framed blow-up curves with the strands of the braid. While many homological configurations can be realized by blow-ups that unlink the strands of the braid, it may not always be possible. Here we provide some examples of homological data for the C_1^j which can always be realized in this way, and an example which we have been unable to realize and have reason to suspect it is not realizable.

Consider the homological configuration where $[C_1^1], \cdots, [C_1^{j_0}]$ all share a single exceptional class, and all pairs of $[C_1^j]$ which are not a subset of this collection have a unique distinct exceptional class in common. Then we can realize this embedding symplectically by starting with a collection of j_0 complex projective lines through a single point p, together with $d - j_0$ generic lines, and one additional distinguished generic line. Then blow-up once at p and once at each of the intersection points between pairs of non-distinguished lines. Blow-up additional times at points on the proper transforms of the non-distinguished lines until their self-intersection numbers agree with the dual graph. In terms of the handlebody braid picture, this embedding can be realized by starting with the standard form for the braid made of a full twist of d strands. Then blow-up at p, introducing a new -1 curve

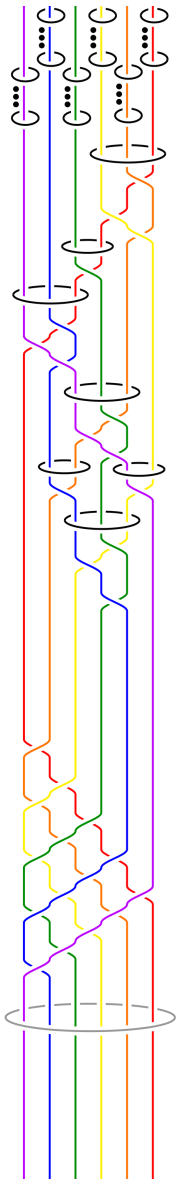

(a) $\mathcal{E}_5^6$: $+1$, $-n_1$, $-n_2$, $-n_3$, $-n_4$, $-n_5$, $-n_6$, -1

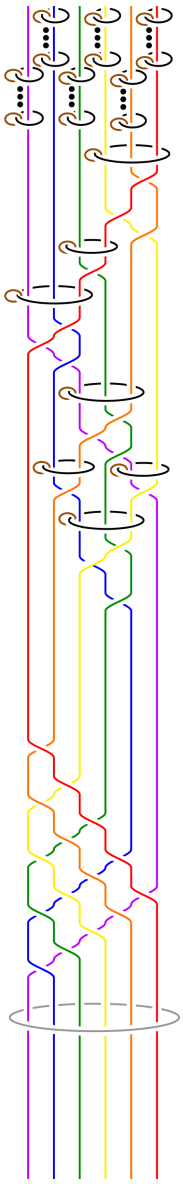

(b) Complement upside-down. $\langle -1\rangle$, $\langle n_1\rangle$, $\langle n_2\rangle$, $\langle n_3\rangle$, $\langle n_4\rangle$, $\langle n_5\rangle$, $\langle n_6\rangle$, $\langle 1\rangle$, 0

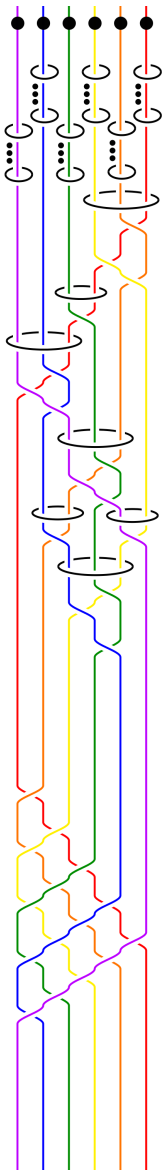

(c) Complement upside-down. 2-handles are black attached with framing -1

Figure 6.7

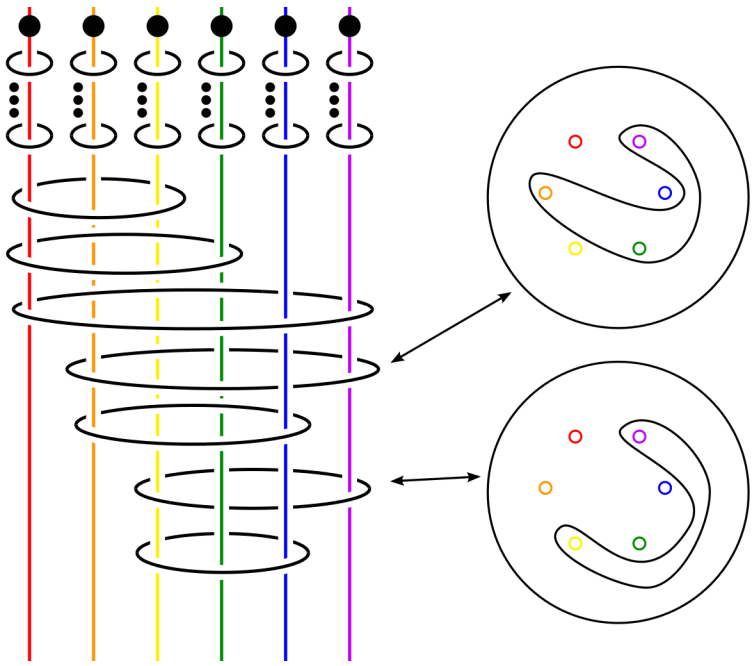

Figure 6.8: Lefschetz fibration obtained by rotating the projection plane of figure 6.7c. The non-convex curves are shown in the fibers. Recall our convention that the outward normal to the disk points downward in the direction of the trivial braid of dotted circles.

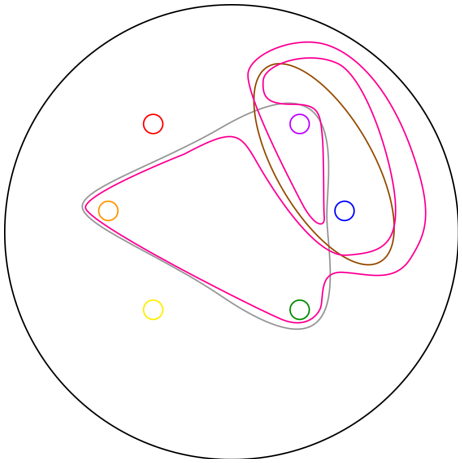

Figure 6.9: Applying a positive right handed Dehn twist about the curve convexly enclosing holes 5 and 6 to the curve convexly enclosing holes 2, 4 and 6.

into the picture, which links with the right-most j_0 strands and reverses all of the crossings between them in the upper half of the twist. Blow-up additional times to introduce -1 curves linking pairs of strands and reversing the remaining crossings in the upper half of the full twist. Because all of the crossings in the upper half of the twist have been reversed and no isotopy was performed on the diagram introducing new crossings, the remaining braid of d strands is unlinked. Blowing up additional times introducing -1 curves which only link a single strand modifies the framings without changing the braid. Cutting out the plumbing and turning the result upside down as we have done in previous examples yields a Lefschetz fibration whose fibers are d-holed disks. The first vanishing cycle is a curve convexly enclosing the first j_0 holes. The remaining vanishing cycles enclose the other pairs of holes and are ordered as $\{1, j_0+1\}, \cdots, \{1,d\}, \{2, j_0+1\}, \cdots, \{2,d\}, \cdots, \{j_0, j_0+1\}, \cdots, \{j_0,d\}, \{j_0+1, j_0+2\}, \cdots, \{j_0+1,d\}, \{j_0+2, j_0+3\}, \cdots, \{j_0+2,d\} \cdots \{d-1,d\}$. Note that when $j_0 = d$, we are in the case of the canonical embedding so the complement is the convex plumbing with the Gay-Mark Lefschetz fibration. The following lemma shows that the monodromies of the open books bounding the Lefschetz fibrations for all values of j_0 are all equal, and in fact are related by a sequence of daisy relations, each of which corresponds to a Fintushel-Stern rational blow-down.

Lemma 6.2.1. *On the d-holed disk, with holes labeled counter-clockwise $\{1, \cdots, d\}$, the elements ϕ_j given by the products*

$D_1^{j-2} \cdots D_j^{j-2} D_{1,\cdots,j}(D_{1,j+1} \cdots D_{1,d}) \cdots (D_{j,j+1} \cdots D_{j,d})(D_{j+1,j+2} \cdots D_{j+1,d})$

$\cdot(D_{j+2,j+3} \cdots D_{j+2,d}) \cdots (D_{d-1,d})$

for $2 \leq j \leq d$ are all equal and ϕ_{j+1} is related to ϕ_j by a daisy relation (equation 2.3.2) and commutation.

Proof. The equality statement follows from the daisy relation statement.

First we claim that

$$(D_{1,j+1}\cdots D_{1,d})\cdots(D_{j,j+1}\cdots D_{j,d}) = (D_{1,j+1}\cdots D_{j,j+1})(D_{1,j+2}\cdots D_{1,d})\cdots(D_{j,j+2}\cdots D_{j,d})$$

by commuting Dehn twists about disjoint curves. Indeed, we can commute $D_{2,j+1}$ past $D_{1,y}$ for $j+2 \leq y \leq d$ because the holes 2 and $j+1$ lie outside the convex hull of the holes 1 and $j+2, \cdots, d$. Similarly $D_{3,j+1}$ can commute past $D_{x,y}$ for $1 \leq x \leq 2$ and $j+2 \leq y \leq d$, and so on. This shows that ϕ_j can be equivalently written as

$$D_1^{j-2}\cdots D_j^{j-2} D_{1,\cdots,j}(D_{1,j+1}\cdots D_{j,j+1})(D_{1,j+2}\cdots D_{1,d})\cdots(D_{j,j+2}\cdots D_{j,d})\cdot$$

$$\cdot(D_{j+1,j+2}\cdots D_{j+1,d})(D_{j+2,j+3}\cdots D_{j+2,d})\cdots(D_{d-1,d})$$

Applying the daisy relation to $D_{1,\cdots,j}(D_{1,j+1}\cdots D_{j,j+1})$ we get

$$D_1^{j-2}\cdots D_j^{j-2}(D_{j+1}^{j-1} D_1\cdots D_j D_{1,\cdots,j,j+1})(D_{1,j+2}\cdots D_{1,d})\cdots(D_{j,j+2}\cdots D_{j,d})\cdot$$

$$\cdot(D_{j+1,j+2}\cdots D_{j+1,d})(D_{j+2,j+3}\cdots D_{j+2,d})\cdots(D_{d-1,d})$$

which we observe is equal to ϕ_{j+1}. □

Note that when $d = 2$, this is the case where each pair of spheres shares a distinct exceptional class, and the corresponding Lefschetz fibration gives one side of the generalized lantern relation (equation 2.3.3).

The examples of section 4.3 provide another family of translations which can be demonstrated through handlebody diagrams in the same way.

More general homological configurations do not always work out as nicely. For example consider a dual graph with seven arms, each consisting of a single sphere. There is a homological configuration where seven triples share an exceptional class, and every pair is in exactly one of these seven triples. The triples are specified by the Fano plane (figure 6.10). To find a symplectic representative of this embedding, we would like to take a configuration of pseudoholomorphic spheres in $\mathbb{C}\mathrm{P}^2$ which intersect as do the lines of the Fano plane and blow up at their intersections. It is relatively straightforward to prove algebraically that there is no collection of seven complex projective lines in $\mathbb{C}\mathrm{P}^2$ intersecting as specified by the Fano plane. It is unclear whether a pseudoholomorphic line arrangement with this combinatorial intersection data exists. On the one hand, for a given almost complex structure J on $\mathbb{C}\mathrm{P}^2$, the J-holomorphic lines satisfy many similar properties to genuine complex projective lines and the space of J-holomorphic lines is diffeomorphic to the space of complex projective lines (they are both $\mathbb{C}\mathrm{P}^2$). However, it is possible that there is a dependence on J in the topology of the space of J-holomorphic line arrangements with certain combinatorial intersection data. Hoping that such a pseudoholomorphic arrangment exists, we could try to proceed directly with the handle calculus of the braid to find a smooth embedding which has a Lefschetz fibration in its complement. However, attempts to do this by the author have failed. The issue is that it seems impossible to arrange the crossings of the braid in the upper half of the full twist so that all seven triples of strands have their crossings grouped together, without introducing additional crossings between the strands. These additional crossings can prevent the blow-ups from unlinking the braid. One attempt by the author to realize such a configuration had the blow-ups change the 1 full twisted braid into a seven component link with four unlinked components together with a copy of the Borromean rings.

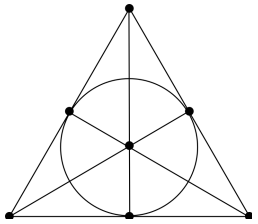

Figure 6.10: The Fano Plane: an arrangement of seven lines which intersect in seven triple points, which can be realized as projective lines over a field of characteristic 2 but not over $\mathbb{C}$.

The Borromean rings are not slice so the attaching circles for the 2-handles that are part of the braid could not provide equators of disjointly embedded spheres. Still it remains an open question as to whether the desired embedding exists, and whether any line arrangement which cannot be realized by complex projective lines can be realized by J-holomorphic lines in $\mathbb{C}\mathrm{P}^2$ for some almost complex structure J.

A final important note is that any homological configuration affecting only the C_1^j which can be realized in the absence of C_i^j for $i > 1$, can also be realized when the dual graph arms are longer. To obtain a Lefschetz fibration in these cases, use the series of stabilizations described in section 6.1 for the longer parts of the arm, and combine this (independently) with the braid moves on the full twist of strands, and their translation to a Lefschetz fibration. Other types of embeddings of the longer parts of the arms which are independent of the C_1^j, can also be combined with these examples (see the next section for examples). This implies that the examples of section 4.4 can generalize to translations for fillings of Seifert fibered spaces of a more general family where the value of e_0 and number of arms remains the same as one of the examples of section 4.4, but the coefficients on the vertices in the arms can vary instead of necessarily all being -2.

6.3 Translating homological embeddings of the C_i^j for $i > 1$

In this section we focus on translating dual graph embeddings to Lefschetz fibrations when the homological embedding differs from the canonical one in at least one sphere which is not adjacent to the center. One case of this is when the homological embedding of the dual plumbing differs from the canonical one only within a single arm. In this case, the complementary filling will be obtained by the following process. Start with the convex plumbing, and consider a neighborhood of the spheres in the corresponding arm together with the central sphere. This neighborhood has convex boundary which is a lens space with its canonical contact structure. The filling which is complementary to the described embedding of the dual graph is obtained by replacing this neighborhood of spheres with an alternate filling of the lens space. Such fillings were classified by Lisca [Lis08]. Bhupal and Ozbagci [BO] took Lisca's Stein handlebodies and showed how to turn them into handlebodies which exhibit Lefschetz fibrations. Therefore translations in this case have essentially been covered (though the language in [BO] is slightly different). There are similar translations for fillings obtained from the convex plumbing by replacing multiple linear strings of spheres within various arms by alternate fillings of the lens space boundary. In this case the condition on the homological embedding is that the exceptional classes which appear with non-zero coefficient in $[C_i^j]$ for $i > 1$ do not appear in $[C_i^{j'}]$ for any $j' \neq j$ and any i.

Now we move onto some examples of homological embeddings which make use of the non-linear structure of the plumbing graphs. The fillings which are created using lens space fillings come from homological embeddings where the longer parts of the arms do not interact with each other. Here we will consider how exceptional classes can appear with non-zero coefficient in multiple arms beyond the required sharing between the spheres adjacent

to the center. For the simplest of these examples, we can provide a full translation from the homological embedding to a Lefschetz fibration. We can combinatorially describe all of the symplectically realizable homological embeddings involving the spheres away from the center, so we do not run into the same limitations as in section 6.2. However, the Kirby calculus becomes more involved for increasingly complicated homological possibilities.

First we recall from section 3.4.1 how the spheres in the dual plumbing which are not adjacent to the center arise. The spheres adjacent to and in the center are proper transforms of pseudoholomorphic lines in $\mathbb{C}\mathrm{P}^2$, but the outer spheres are proper transforms of exceptional spheres. We can recover the homological configuration by keeping track of the original pseudoholomorphic lines, all of the newly introduced exceptional spheres during the blow-up sequence, and which of these spheres pass through the blow-up points at each stage.

In the canonical embedding, for $i > 1$, C_i^j is the proper transform of an exceptional sphere obtained by blowing up at a point on C_{i-1}^j which is not on any other sphere that we are tracking. Other than the blow-up which separates the intersection of the d pseudoholomorphic lines, all the blow-ups are done at points which lie on a single tracked sphere. If we want to build an embedding where the outer parts of different arms interact, we need to build some of the arms from exceptional spheres which intersect more than one C_1^j. Depending on the intersection configuration of the pseudoholomorphic lines, such exceptional spheres will intersect somewhere between 2 and d of the C_1^j's.

Some examples of blow-up sequences and the corresponding homological embeddings are shown schematically in figures 6.11, 6.12, and 6.13.

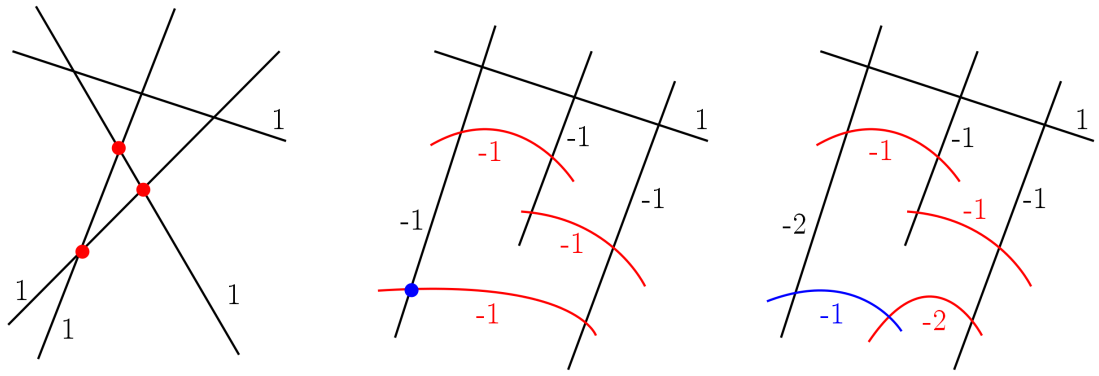

Figure 6.11: Blowing-up schematic. In the final configuration we have an embedding of a star-shaped plumbing with homological data $[C_0] = \ell$, $[C_1^1] = \ell - e_1 - e_2 - e_4$, $[C_1^2] = \ell - e_1 - e_3$, $[C_1^3] = \ell - e_2 - e_3$, $[C_2^3] = e_2 - e_4$.

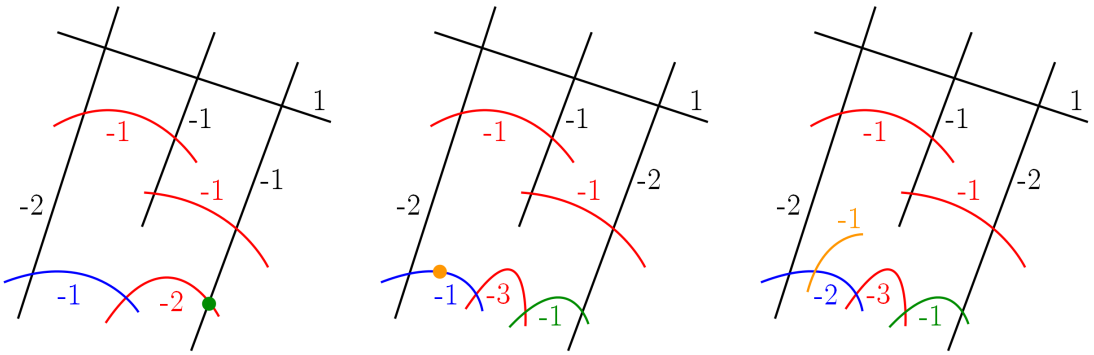

Figure 6.12: Blowing-up schematic continued from figure 6.11. Final homological embedding: $[C_0] = \ell$, $[C_1^1] = \ell - e_1 - e_2 - e_4$, $[C_2^1] = e_4 - e_6$, $[C_3^1] = e_2 - e_4 - e_5$, $[C_1^2] = \ell - e_1 - e_3$, $[C_1^3] = \ell - e_2 - e_3 - e_5$.

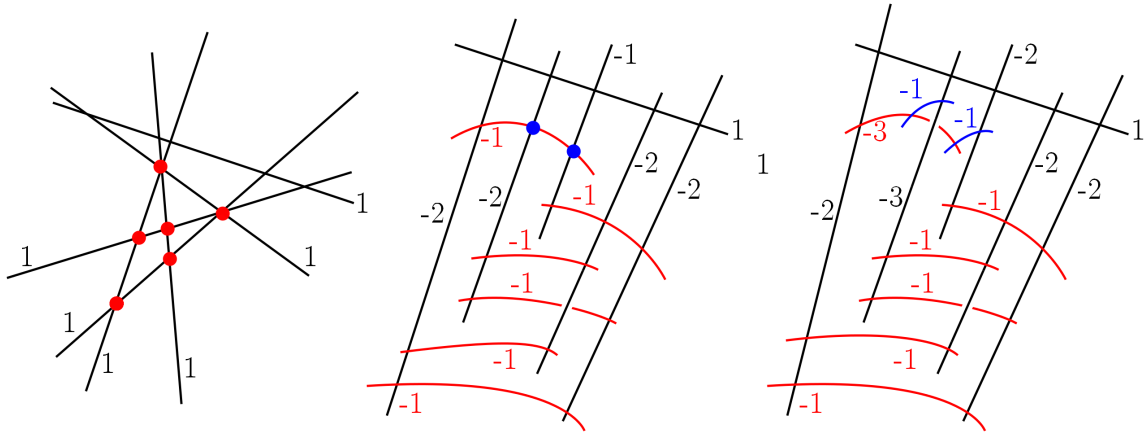

Figure 6.13: Blowing-up schematic. Final homological embedding:
$[C_0] = \ell$, $[C_1^1] = \ell - e_1 - e_2 - e_3$, $[C_2^1] = e_1 - e_7 - e_8$ $[C_1^2] = \ell - e_1 - e_4 - e_5 - e_7$, $[C_1^3] = \ell - e_1 - e_6 - e_8$, $[C_1^4] = \ell - e_2 - e_4 - e_6$, $[C_1^5] = \ell - e_3 - e_5 - e_6$.

We will start by translating embeddings in which some C_2^j is the proper transform of an exceptional sphere which was introduced by blowing up at the intersection of two of the pseudoholomorphic lines. In order to include this sphere into one of these arms, we need to blow-up at its intersection with the other arm so that it is disjoint from the other arm. An example of this is represented schematically in figure 6.11, and the local picture of the relevant portion of the embedding is exhibited through a handle structure in figure 6.14.

We would like to see how adding in this sphere to the arm via the additional blow-up modifies the Lefschetz fibration for the complementary filling. To avoid making assumptions about the rest of the embedding, we do this translation locally. We assume that the entire diagram has a translation if we replaced the embedding of the dual plumbing with the extra -2 sphere shown on the right of figure 6.14 with the embedding of the dual plumbing without this extra sphere and blow-up as shown in the center of figure 6.14. This translation will

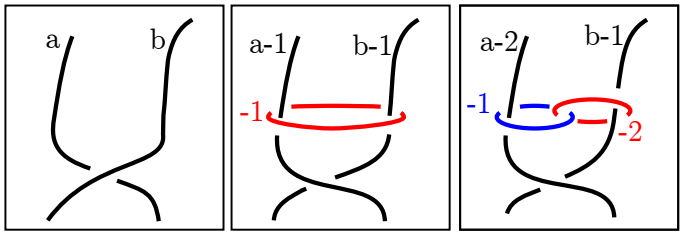

Figure 6.14: Handle structure for an embedding where an exceptional sphere intersecting two other spheres is included into one of the arms.

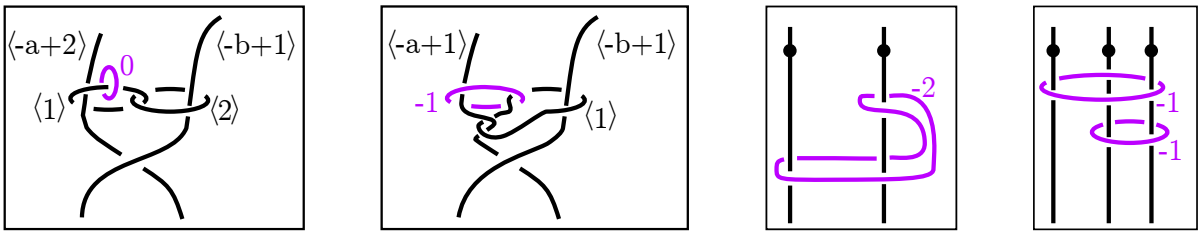

(a) (b) (c) (d)

Figure 6.15: Local translation for the embedding of figure 6.14.

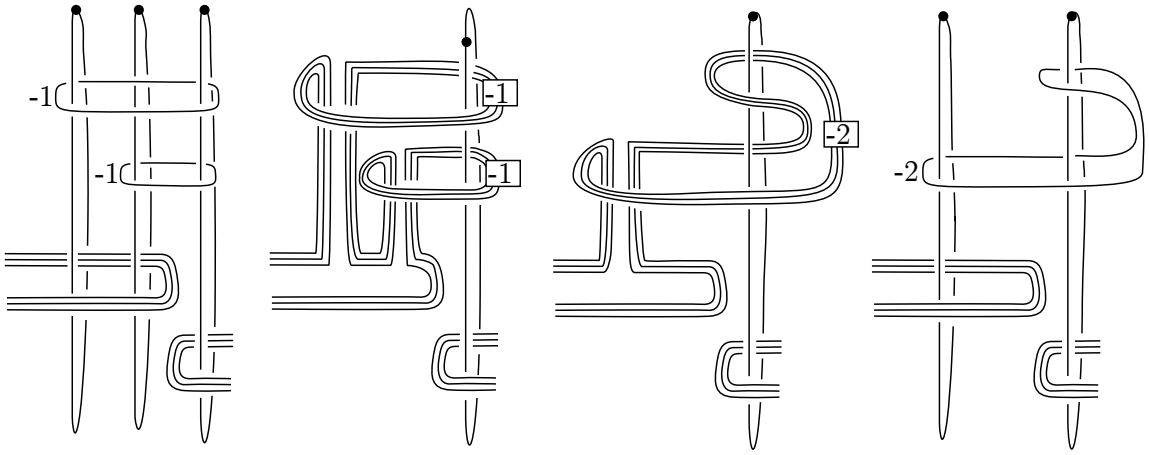

Figure 6.16: Proof of equivalence of the local diagrams in figures 6.15c and 6.15d.

involve rotating the projection plane when the upside-down diagram is simplified so that the bracketed surgery curves are eliminated and we can use dotted circle notation for all of the one handles. We will continue the convention that the rotation is done by 90° clockwise about the vertical axis, meaning we take the new projection to be the point of view of a person standing on the left-hand side of the diagram. Note this is the convention that was used for all our previous examples so this local move can be combined with others (the convention was significant in the examples of sections 6.2, 4.3, and 4.4).

First we consider the diagram for the upside-down complement to the embedded dual spheres (figure 6.15a and 6.15b). We assume the rest of the diagram can be translated with a 90° rotation of the projection plane to get from figure 6.15b to figure 6.15c. In order to give this the right Lefschetz fibration, we expect to need to stabilize once since we are adding one extra sphere into the dual graph. The required stabilization is performed from figure 6.15c to figure 6.15d. The equivalence of these two diagrams is shown in figure 6.16.

Now we discuss how the monodromy substitution is affected by the additional blow-up that allows us to include the exceptional sphere into an arm of the dual graph (e.g. the final blow-up in figure 6.11 indicated in blue which creates the exceptional class e_4.) This means we will consider the canonical Lefschetz fibration and an alternate Lefschetz fibration and how each of these changes under the additional blow-up and inclusion of the additional sphere into the graph. We assume that the original monodromy substitution before blowing up has the form

$$\phi_x\phi_y\alpha = \beta\phi_{x,y}\gamma$$

where α, β, and γ are products of positive Dehn twists, and $\phi_x\phi_y\alpha$ is the monodromy factorization for the canonical Lefschetz fibration (up to commutative equivalence). The

additional blow-up changes the dual graph by reducing by one the framing on the vertex in one arm (the y arm) and adding a new vertex for a sphere of square -2 into the other arm (the x arm). The effect on the canonical Lefschetz fibration is to add an extra vanishing cycle in the collection around the hole y, and to add an extra hole (labelled x') just outside the inner-most vanishing cycle around x along with one vanishing cycle boundary parallel to the new x' hole. So if $\phi_x\phi_y\alpha$ is the factorization for the canonical Lefschetz fibration for the dual graph before the additional blow-up, then the new canonical Lefschetz fibration is $\phi_x\phi_{x'}\phi_y^2\widetilde{\alpha}$ where $\widetilde{\alpha}$ is the same set of positive Dehn twists as α, just now it is on the disk with an extra hole x', and every curve which went around x in α, now goes around x and x' in $\widetilde{\alpha}$.

The monodromy substitution $\phi_x\phi_y\alpha = \beta\phi_{xy}\gamma$ on the disk without the x' hole induces a relation on the disk with the x' hole.

$$\phi_{x,x'}\phi_y\widetilde{\alpha} = \widetilde{\beta}\phi_{x,x',y}\widetilde{\gamma}$$

Using this relation we find the following.

$$\phi_x\phi_{x'}\phi_y^2\widetilde{\alpha} = \widetilde{\beta}\phi_{x,x'}^{-1}\phi_x\phi_{x'}\phi_y\phi_{x,x',y}\widetilde{\gamma}$$

Applying a lantern relation to the right hand side gives the following new monodromy substitution.

$$\phi_x\phi_{x'}\phi_y^2\widetilde{\alpha} = \widetilde{\beta}\phi_{x,y}\phi_{x',y}\widetilde{\gamma}$$

This monodromy substitution corresponds to the local picture we obtained via the handle-body decomposition in figure 6.15d. On the right hand side, the curve enclosing x and y is

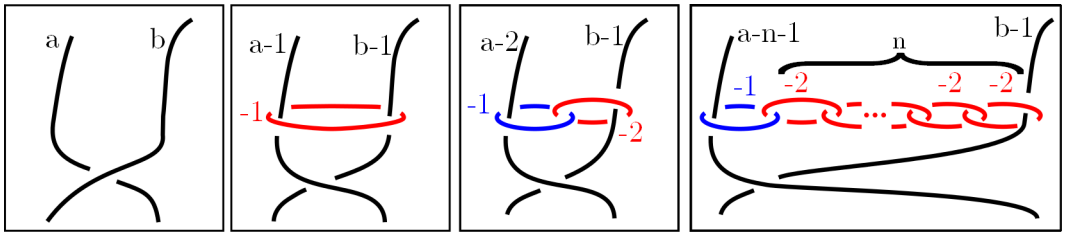

Figure 6.17: Handle structure for an embedding where n exceptional spheres are included into one of the arms generalizing figure 6.14.

replaced by a curve enclosing x and y and a curve enclosing x' and y, where x' is a newly introduced hole corresponding to the newly introduced 1-handle.

This move generalizes to families parameterized by the natural numbers in two ways. Next, we will explain each of these generalizations and their translations.

6.3.1 Iterating blow-ups at the same point

The first way to generalize is to iterate the blow-ups. Start with two pseudoholomorphic lines (technically proper transforms of pseudoholomorphic lines) and the first exceptional sphere which intersects these two lines and no others in the configuration. Blowing-up once at one of the intersections allowed us to include the proper transform of the first exceptional sphere into the dual graph configuration. Blowing-up additional times at the same intersection point with the other pseudoholomorphic line allows us to include the proper transform of each previous exceptional sphere into the dual graph. The local picture of the embedding for this generalization is in figure 6.17.

The translation to a Lefschetz fibration proceeds as before by turning the figure upside-down as in figure 6.18, and simplifying the diagrams. Assuming a translation exists outside of the local area which rotates the projection by 90° as usual, we get from figure

6.18d to 6.18e. The stabilizations are done in figure 6.18f and the equivalence of figures 6.18e and 6.18f is shown by the diagrams of figure 6.19.

The effect on the monodromy substitution is similar to the $n = 1$ case discussed earlier. We assume as before that the original monodromy substitution before blowing up n times has the form $\phi_x\phi_y\alpha = \beta\phi_{x,y}\gamma$. The additional blow-ups change the dual graph by reducing the framing on the vertex in the y arm by n and adding n new vertices corresponding to spheres of square -2 in the x arm. The canonical Lefschetz fibration for the modified dual graph has n new holes in its fiber $x^1, \cdots, x^n$. If $\phi_x\phi_y\alpha$ is the factorization for the canonical Lefschetz fibration for the dual graph before the additional blow-up, then the new canonical Lefschetz fibration is $\phi_x\phi_{x^1}\cdots\phi_{x^n}\phi_y^{n+1}\widetilde{\alpha}$ where $\widetilde{\alpha}$ is the same set of positive Dehn twists as α, but now on the disk with n additional holes $x^1, \cdots, x^n$, and every curve which went around x in α, now goes around x and $x^1, \cdots, x^n$ in $\widetilde{\alpha}$.

The monodromy substitution $\phi_x\phi_y\alpha = \beta\phi_{xy}\gamma$ induces the relation $\phi_{x,x^1,\cdots,x^n}\phi_y\widetilde{\alpha} = \widetilde{\beta}\phi_{x,x^1,\cdots,x^n,y}\widetilde{\gamma}$.

Using this relation we find the following.

$$\phi_x\phi_{x^1}\cdots\phi_{x^n}\phi_y^{n+1}\widetilde{\alpha} = \widetilde{\beta}\phi^{-1}_{x,x^1,\cdots,x^n}\phi_x\phi_{x^1}\cdots\phi_{x^n}\phi_y^n\phi_{x,x^1,\cdots,x^n,y}\widetilde{\gamma}$$

Applying a daisy relation with $n+1$ petals to the right hand side gives the following new monodromy substitution.

$$\phi_x\phi_{x^1}\cdots\phi_{x^n}\phi_y^{n+1}\widetilde{\alpha} = \widetilde{\beta}\phi_{x,y}\phi_{x^1,y}\cdots\phi_{x^n,y}\widetilde{\gamma}$$

This monodromy substitution agrees with the handlebody decomposition in figure 6.18f.

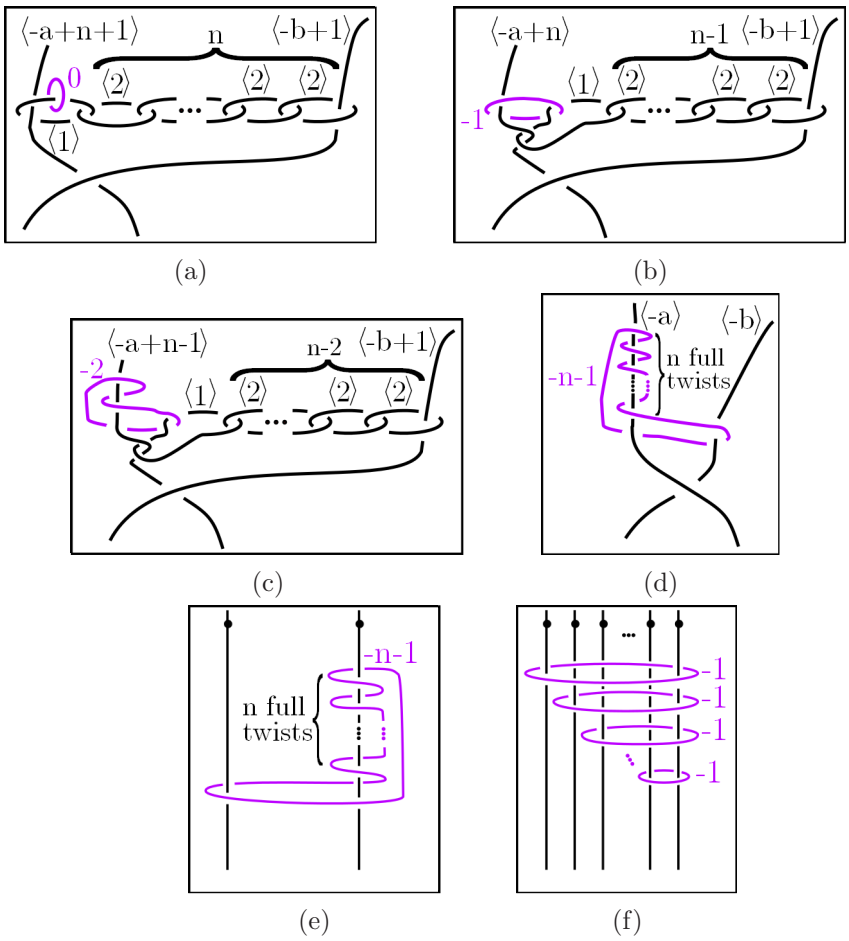

Figure 6.18: Local translation for the embedding of figure 6.17. The projection is rotated in the last two figures. The last two diagrams are equivalent by figure 6.19.

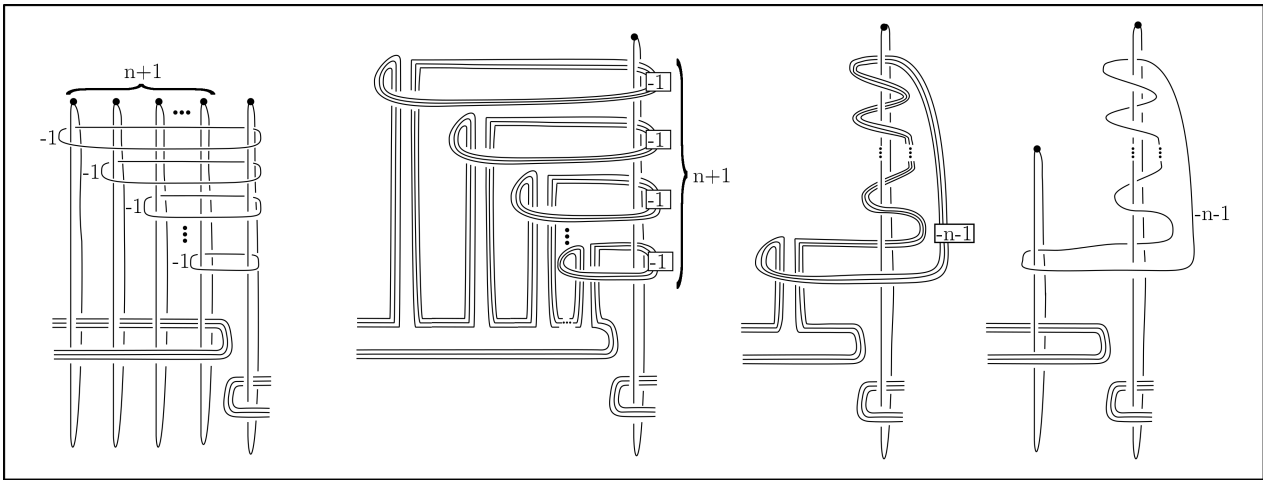

Figure 6.19: Generalization of figure 6.16. Proves the equivalence of diagrams 6.18e and 6.18f.

6.3.2 Including exceptional spheres intersecting m lines

The second way to generalize is to include onto the end of an arm the proper transform of an exceptional sphere which intersects more than two of the pseudoholomorphic lines. Start with a diagram of the relevant m pseudoholomorphic lines and the exceptional sphere intersecting it. Blowing-up once at each one of the intersections allows us to include the proper transform of this exceptional sphere into the dual graph configuration. The local diagrams for these embeddings are in figure 6.20.

The translation to a Lefschetz fibration proceeds as before by turning the figure upside-down as in figure 6.21, and simplifying the diagrams. Once all of the surgery curves with bracketed labels have been eliminated from the local diagram, we assume a global translation can be made which rotates the projection plane as usual.

The effect on the monodromy substitution is similar to the previous case, though con-

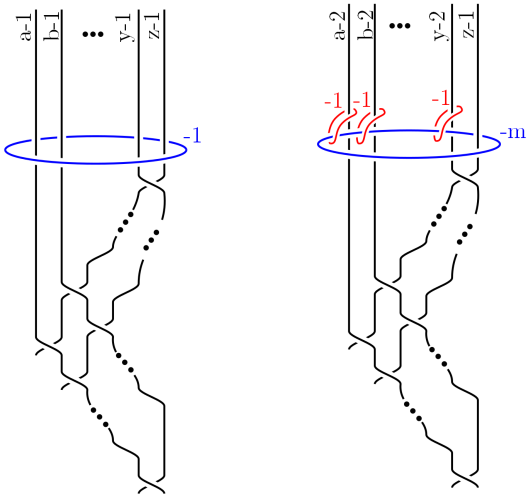

(a) (b)

Figure 6.20: Handle structure for an embedding where we include an exceptional sphere that intersected m lines into one of the arms.

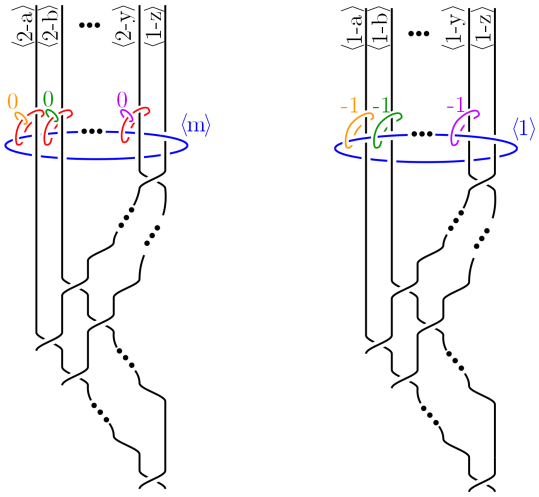

(a) Unlabelled framings are ⟨1⟩ (b)

Figure 6.21: The complement of the embedding of figure 6.20.

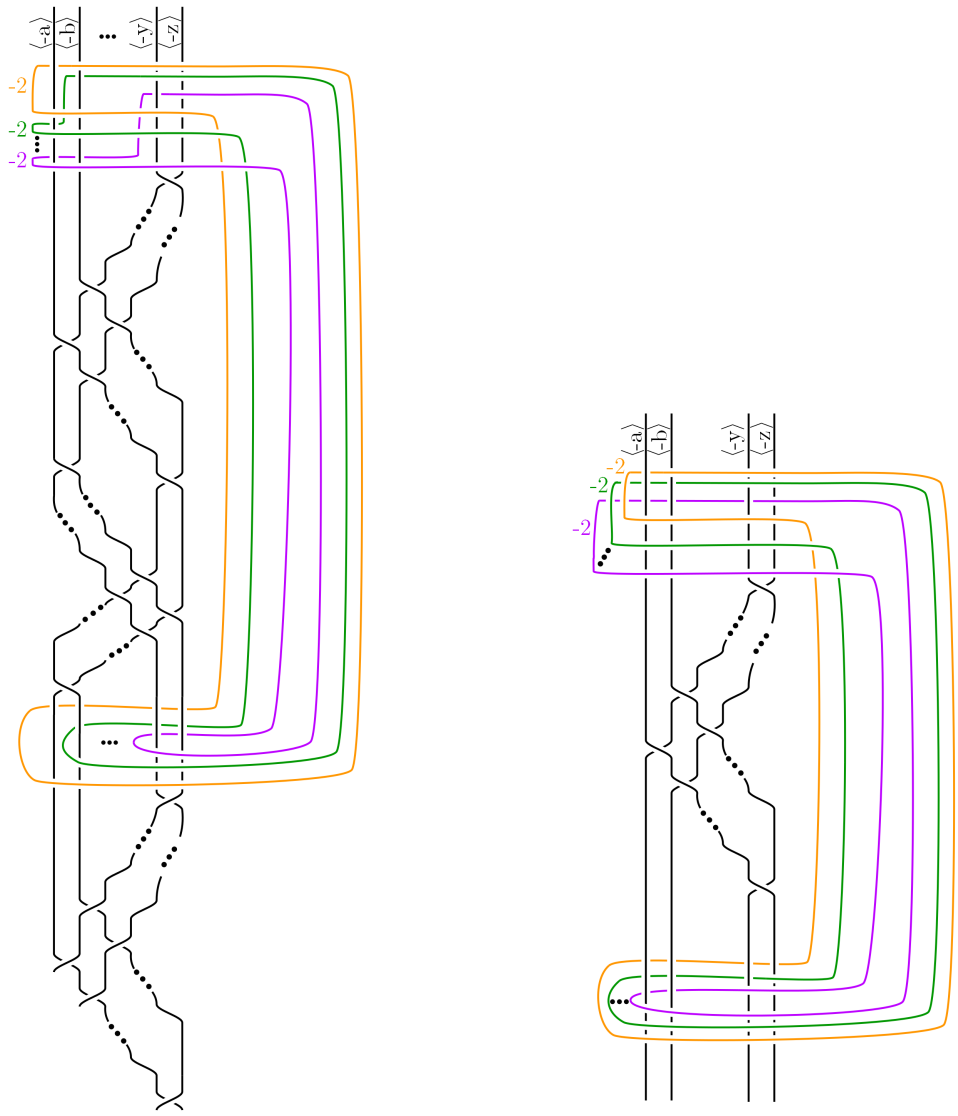

(a) (b)

Figure 6.22: Applying Kirby calculus moves to figure 6.21.

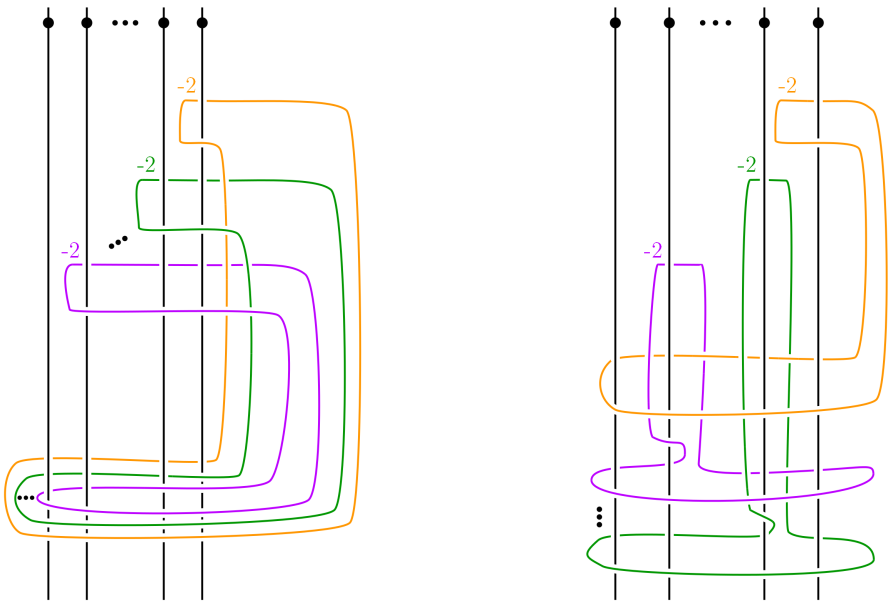

(a) (b)

Figure 6.23: Obtained by rotating the projection plane from figure 6.22, assuming the rest of the diagram has a translation.

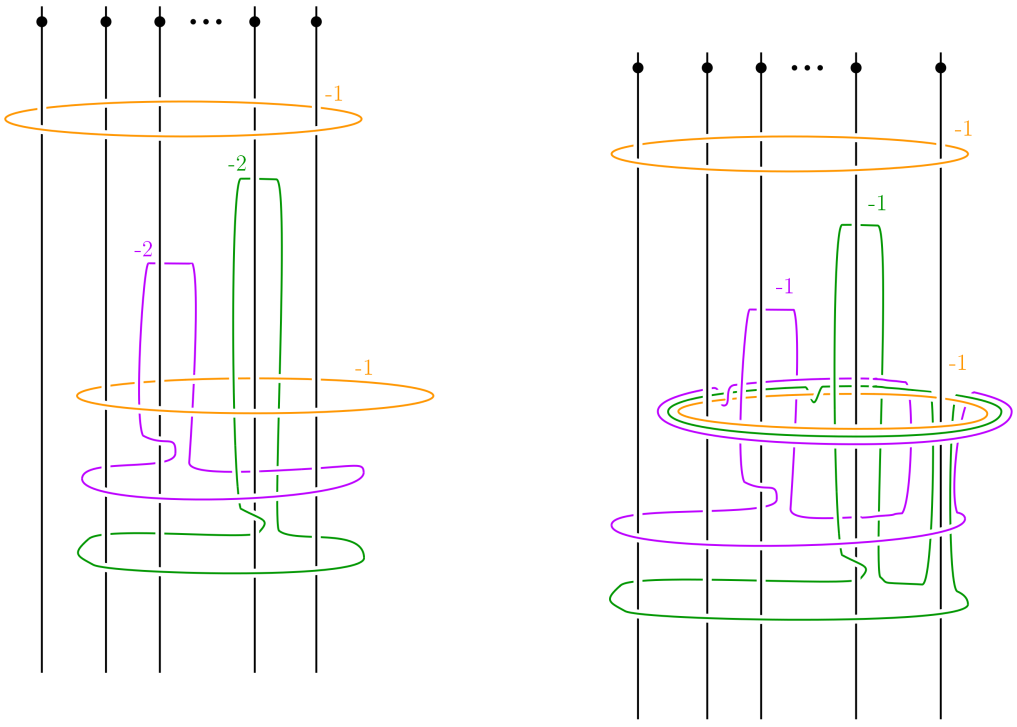

(a) (b)

Figure 6.24: The first diagram is related to figure 6.23b by the move in figure 6.16. The second is related to the first by handle slides.

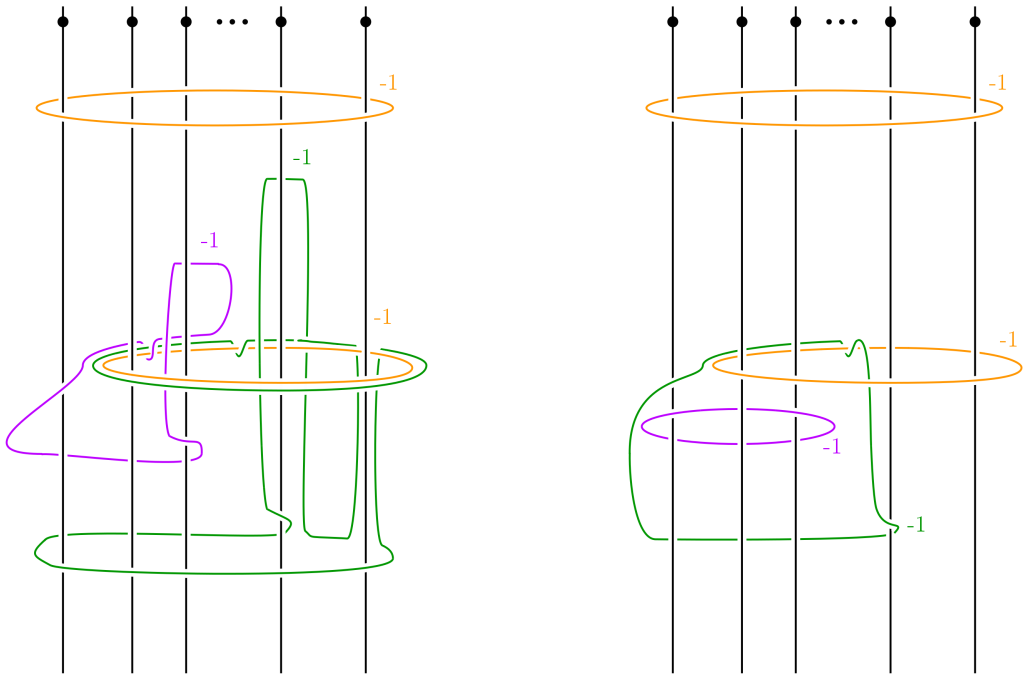

(a) (b)

Figure 6.25: These diagrams are isotopy equivalent to those in figure 6.24. The goal is to reach a Lefschetz fibration picture.

jugation makes it trickier to write down. The appropriate assumption is that before blowing up $m-1$ times and including an extra sphere in the dual graph, the original monodromy substitution has the form $\phi_{x_1}\cdots\phi_{x_m}\alpha = \beta\phi_{x_1,\cdots,x_m}\gamma$ where the left side corresponds to the canonical Lefschetz fibration. The additional blow-ups change the dual graph by reducing by one the framing on the vertices in $x_2,\cdots,x_m$ arms and adding one new vertex corresponding to spheres of square $-m$ in the x_1 arm. The canonical Lefschetz fibration for the modified dual graph has one new hole in its fiber x_0. The new canonical Lefschetz fibration is $\phi_{x_0}^{m-1}\phi_{x_1}\phi_{x_2}^2\cdots\phi_{x_m}^2\widetilde{\alpha}$ (in $\widetilde{\alpha}$ every Dehn twist about a curve which went around x_1, now goes around x_1 and x_0). The monodromy substitution $\phi_{x_1}\cdots\phi_{x_m}\alpha = \beta\phi_{x_1,\cdots,x_m}\gamma$ induces the relation

$$\phi_{x_0,x_1}\phi_{x_2}\cdots\phi_{x_m}\widetilde{\alpha} = \widetilde{\beta}\phi_{x_0,x_1,x_2\cdots,x_m}\widetilde{\gamma}.$$

Using this relation we find the following.

$$\phi_{x_0}^{m-1}\phi_{x_1}\phi_{x_2}^2\cdots\phi_{x_m}^2\widetilde{\alpha} = \widetilde{\beta}\phi_{x_0,x_1}^{-1}\phi_{x_0}^{m-1}\phi_{x_1}\phi_{x_2}\cdots\phi_{x_m}\phi_{x_0,x_1,x_2,\cdots,x_m}\widetilde{\gamma}$$

The right hand side is related to a positive factorization corresponding to the Lefschetz fibration in figure 6.26a by a daisy relation which has been conjugated, as is visible in figure 6.26b.

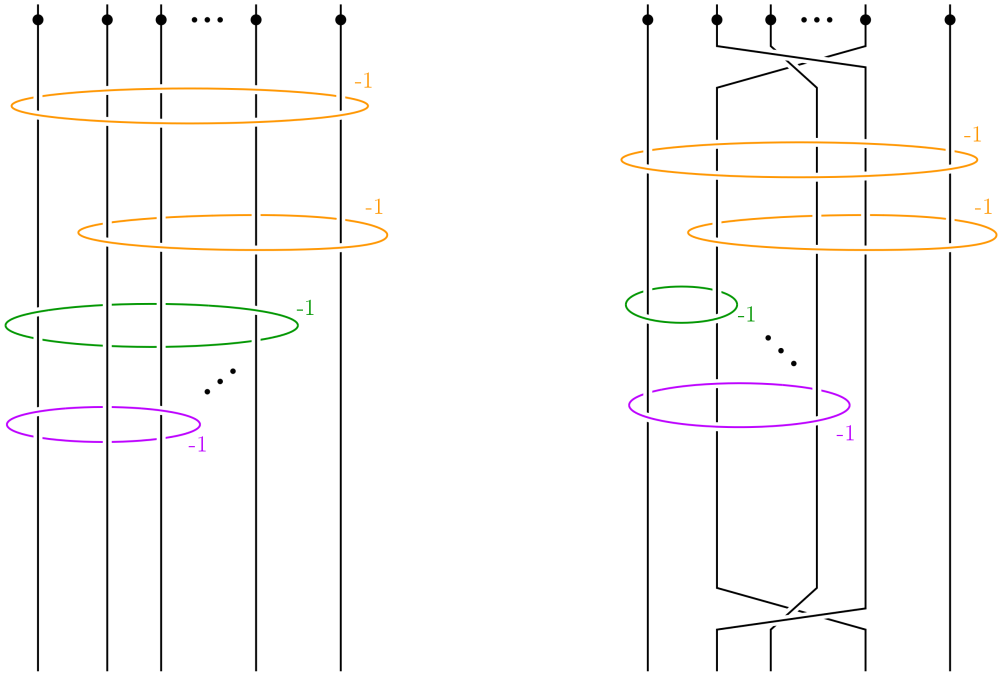

(a) (b)

Figure 6.26: Finally, we reach the Lefschetz fibration on the complement of the embedding. The second figure shows how this is related to $\phi_{x_0,x_1}^{-1}\phi_{x_0}^{m-1}\phi_{x_1}\phi_{x_2}\cdots\phi_{x_m}\phi_{x_1',x_1,x_2,\cdots,x_m}$ by a conjugated daisy relation.

Bibliography

[ABK+94] B. Aebischer, M. Borer, M. Kälin, Ch. Leuenberger, and H. M. Reimann. *Symplectic geometry*, volume 124 of *Progress in Mathematics*. Birkhäuser Verlag, Basel, 1994. An introduction based on the seminar in Bern, 1992.

[AO01] Selman Akbulut and Burak Ozbagci. Lefschetz fibrations on compact Stein surfaces. *Geom. Topol.*, 5:319–334 (electronic), 2001.

[AO02] Selman Akbulut and Burak Ozbagci. On the topology of compact Stein surfaces. *Int. Math. Res. Not.*, (15):769–782, 2002.

[BO] Mohan Bhupal and Burak Ozbagci. Symplectic fillings of lens spaces as lefschetz fibrations. arxiv:1307.6935.

[Bow12] Jonathan Bowden. Exactly fillable contact structures without Stein fillings. *Algebr. Geom. Topol.*, 12(3):1803–1810, 2012.

[BS11] Mohan Bhupal and András I. Stipsicz. Weighted homogeneous singularities and rational homology disk smoothings. *Amer. J. Math.*, 133(5):1259–1297, 2011.

[EH02a] John B. Etnyre and Ko Honda. On symplectic cobordisms. *Math. Ann.*, 323(1):31–39, 2002.

[EH02b] John B. Etnyre and Ko Honda. Tight contact structures with no symplectic fillings. *Invent. Math.*, 148(3):609–626, 2002.

[Eli90a] Yakov Eliashberg. Filling by holomorphic discs and its applications. In *Geometry of low-dimensional manifolds, 2 (Durham, 1989)*, volume 151 of *London Math. Soc. Lecture Note Ser.*, pages 45–67. Cambridge Univ. Press, Cambridge, 1990.

[Eli90b] Yakov Eliashberg. Topological characterization of Stein manifolds of dimension > 2. *Internat. J. Math.*, 1(1):29–46, 1990.

[Eli96] Yasha Eliashberg. Unique holomorphically fillable contact structure on the 3-torus. *Internat. Math. Res. Notices*, (2):77–82, 1996.

[Eli04] Yakov Eliashberg. A few remarks about symplectic filling. *Geom. Topol.*, 8:277–293, 2004.

[Etn98] John B. Etnyre. Symplectic convexity in low-dimensional topology. *Topology Appl.*, 88(1-2):3–25, 1998. Symplectic, contact and low-dimensional topology (Athens, GA, 1996).

[FS97] Ronald Fintushel and Ronald J. Stern. Rational blowdowns of smooth 4-manifolds. *J. Differential Geom.*, 46(2):181–235, 1997.

[Gay02] David T. Gay. Explicit concave fillings of contact three-manifolds. *Math. Proc. Cambridge Philos. Soc.*, 133(3):431–441, 2002.

[Ghi05] Paolo Ghiggini. Strongly fillable contact 3-manifolds without Stein fillings. *Geom. Topol.*, 9:1677–1687 (electronic), 2005.

[Gir02] Emmanuel Giroux. Géométrie de contact: de la dimension trois vers les dimensions supérieures. In *Proceedings of the International Congress of Mathematicians, Vol. II (Beijing, 2002)*, pages 405–414. Higher Ed. Press, Beijing, 2002.

[GL14] Marco Golla and Paolo Lisca. On Stein fillings of contact torus bundles, 2014. arXiv:1412.0828[math.GT].

[GM13] David Gay and Thomas E. Mark. Convex plumbings and Lefschetz fibrations. *J. Symplectic Geom.*, 11(3):363–375, 2013.

[Gom95] Robert E. Gompf. A new construction of symplectic manifolds. *Ann. of Math. (2)*, 142(3):527–595, 1995.

[Gom98] Robert E. Gompf. Handlebody construction of Stein surfaces. *Ann. of Math. (2)*, 148(2):619–693, 1998.

[Gra58] Hans Grauert. On Levi's problem and the imbedding of real-analytic manifolds. *Ann. of Math. (2)*, 68:460–472, 1958.

[Gro85] M. Gromov. Pseudoholomorphic curves in symplectic manifolds. *Invent. Math.*, 82(2):307–347, 1985.

[GS99] Robert E. Gompf and András I. Stipsicz. 4-*manifolds and Kirby calculus*, volume 20 of *Graduate Studies in Mathematics*. American Mathematical Society, Providence, RI, 1999.

[GS07] David T. Gay and András I. Stipsicz. Symplectic rational blow-down along Seifert fibered 3-manifolds. *Int. Math. Res. Not. IMRN*, (22):Art. ID rnm084, 20, 2007.

[GS09] David T. Gay and András I. Stipsicz. Symplectic surgeries and normal surface singularities. *Algebr. Geom. Topol.*, 9(4):2203–2223, 2009.

[Kal13] Amey Kaloti. Stein Fillings of Planar Open Books, 2013. arXiv:1311.0208[math.GT].

[KL13] Amey Kaloti and Youlin Li. Stein Fillings of contact 3-manifolds obtained as Legendrian surgeries, 2013. arXiv:1307.4726[math.GT].

[KS] Çağrı Karakurt and Laura Starkston. Surgery along star shaped plumbings and exotic smooth structures on 4-manifolds. arxiv:1402.0801.

[Lis08] Paolo Lisca. On symplectic fillings of lens spaces. *Trans. Amer. Math. Soc.*, 360(2):765–799 (electronic), 2008.

[LL11] Ana G. Lecuona and Paolo Lisca. Stein fillable Seifert fibered 3-manifolds. *Algebr. Geom. Topol.*, 11(2):625–642, 2011.

[LP01] Andrea Loi and Riccardo Piergallini. Compact Stein surfaces with boundary as branched covers of B^4. *Invent. Math.*, 143(2):325–348, 2001.

[McD90] Dusa McDuff. The structure of rational and ruled symplectic 4-manifolds. *J. Amer. Math. Soc.*, 3(3):679–712, 1990.

[McD91] Dusa McDuff. Symplectic manifolds with contact type boundaries. *Invent. Math.*, 103(3):651–671, 1991.

[Mic07] Maria Michalogiorgaki. Rational blow-down along Wahl type plumbing trees of spheres. *Algebr. Geom. Topol.*, 7:1327–1343, 2007.

[MNW13] Patrick Massot, Klaus Niederkrüger, and Chris Wendl. Weak and strong fillability of higher dimensional contact manifolds. *Invent. Math.*, 192(2):287–373, 2013.

[NW11] Klaus Niederkrüger and Chris Wendl. Weak symplectic fillings and holomorphic curves. *Ann. Sci. Éc. Norm. Supér. (4)*, 44(5):801–853, 2011.

[OO05] Hiroshi Ohta and Kaoru Ono. Simple singularities and symplectic fillings. *J. Differential Geom.*, 69(1):1–42, 2005.

[Par97] Jongil Park. Seiberg-Witten invariants of generalised rational blow-downs. *Bull. Austral. Math. Soc.*, 56(3):363–384, 1997.

[Par05] Jongil Park. Simply connected symplectic 4-manifolds with $b_2^+ = 1$ and $c_1^2 = 2$. *Invent. Math.*, 159(3):657–667, 2005.

[Pla04] Olga Plamenevskaya. Contact structures with distinct Heegaard Floer invariants. *Math. Res. Lett.*, 11(4):547–561, 2004.

[PS14] Heesang Park and András I. Stipsicz. Smoothings of singularities and symplectic surgery. *J. Symplectic Geom.*, 12(3):585–597, 2014.

[PSS13] Heesang Park, András I. Stipsicz, and Dongsoo Shin. Normal complex surface singularities with rational homology disk smoothings, 2013. arXiv:1311.1929v2 [math.AG].

[PVHM10] Olga Plamenevskaya and Jeremy Van Horn-Morris. Planar open books, monodromy factorizations and symplectic fillings. *Geom. Topol.*, 14(4):2077–2101, 2010.

[SSW08] András I. Stipsicz, Zoltán Szabó, and Jonathan Wahl. Rational blowdowns and smoothings of surface singularities. *J. Topol.*, 1(2):477–517, 2008.

[Sym98] Margaret Symington. Symplectic rational blowdowns. *J. Differential Geom.*, 50(3):505–518, 1998.

[Sym01] Margaret Symington. Generalized symplectic rational blowdowns. *Algebr. Geom. Topol.*, 1:503–518 (electronic), 2001.

[TW75] W. P. Thurston and H. E. Winkelnkemper. On the existence of contact forms. *Proc. Amer. Math. Soc.*, 52:345–347, 1975.

[Wei79] Alan Weinstein. On the hypotheses of Rabinowitz' periodic orbit theorems. *J. Differential Equations*, 33(3):353–358, 1979.

[Wen10] Chris Wendl. Strongly fillable contact manifolds and J-holomorphic foliations. *Duke Math. J.*, 151(3):337–384, 2010.